

AD/A-004 087

DEVELOPMENT OF SLED STRUCTURAL DESIGN  
PROCEDURES

Gilbert A. Greenbaum, et al

Mechanics Research Incorporated

Prepared for:

Air Force Special Weapons Center  
Test Group (6585th)

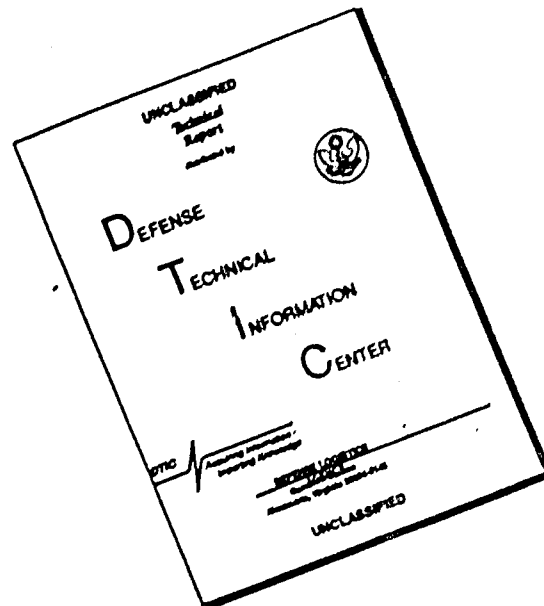
July 1973

DISTRIBUTED BY:

**NTIS**

National Technical Information Service  
U. S. DEPARTMENT OF COMMERCE

# DISCLAIMER NOTICE



THIS DOCUMENT IS BEST QUALITY AVAILABLE. THE COPY FURNISHED TO DTIC CONTAINED A SIGNIFICANT NUMBER OF PAGES WHICH DO NOT REPRODUCE LEGIBLY.

## DOCUMENT CONTROL DATA - R &amp; D

RD/A-004087

(Security classification of title, body of abstract and indexing annotation must be entered when the overall report is classified)

1. ORIGINATING ACTIVITY (Corporate author) Mechanics Research Incorporated 9841 Airport Boulevard Los Angeles, California 90045		2a. REPORT SECURITY CLASSIFICATION Unclassified	
		2b. GROUP NA	
3. REPORT TITLE  Development of Sled Structural Design Procedures			
4. DESCRIPTIVE NOTES (Type of report and inclusive dates) Final Report 30 June 1972 - 17 June 1973			
5. AUTHOR(S) (First name, middle initial, last name) Gilbert A. Greenbaum Terry N. Gardner David L. Platus			
6. REPORT DATE July 1973	7a. TOTAL NO. OF PAGES 169	7b. NO. OF REFS 9	
8a. CONTRACT OR GRANT NO. F29601-72-A-0113-0006	9a. ORIGINATOR'S REPORT NUMBER(S) MRI-2544-TR-2		
b. PROJECT NO.			
c.	9b. OTHER REPORT NO(S) (Any other numbers that may be assigned this report)		
d.	AFSWC-TR-73-22		
10. DISTRIBUTION STATEMENT  Distribution of this document is unlimited.			
11. SUPPLEMENTARY NOTES  NA		12. SPONSORING MILITARY ACTIVITY 6585th Test Group Air Force Special Weapons Center (AFSC) Holloman AFB, New Mexico 88330	
13. ABSTRACT <p>The major objective of this study was to establish improved design analysis procedures for the design of dual rail and monorail rocket sleds. The work included reviewing and evaluating past analytical studies of rocket sleds and experimental test data for two dual rail and two monorail sleds. Studies were undertaken to identify the major sources of dynamic excitation of rocket sleds. Three major sources of dynamic excitation were identified; rail roughness, unsteady aerodynamic forces and oscillating axial and lateral rocket thrust forces. Rail roughness was found to be the prime source of dynamic excitation during the coast portion of the rocket sled trajectory. During the thrust stage of the trajectory, and especially at burnout, oscillating axial and lateral thrust forces were found to produce sled dynamic loads which were the same order of magnitude as those produced by rail roughness.</p> <p>The analytical work performed in this study concentrated on predicting the dynamic response of sleds due to rail roughness. Acceptable correlation between analytical and test results were obtained during coast. Lack of experimental data on unsteady aerodynamic forces and oscillating thrust forces precluded performing comprehensive analytical evaluation of these excitation sources. However, the magnitude of their effects were quantified and scale factors were established to account for their contribution to sled dynamic response during thrust and burnout.</p>			

DD FORM 1 NOV 65 1473

Reproduced by  
NATIONAL TECHNICAL  
INFORMATION SERVICE  
US Department of Commerce  
Springfield, VA. 22151

PRICES SUBJECT TO CHANGE  
UNCLASSIFIED  
Security Classification

14. KEY WORDS	LINK A		LINK B		LINK C	
	ROLE	WT	ROLE	WT	ROLE	WT
Structural Dynamics Rocket Sleds Aerodynamics Mathematical Modeling Computer Simulations Rail Roughness Nonlinear Vibrations Instrumentation Force Transducers						



AFSWC-TR-73-22

DEVELOPMENT OF SLED STRUCTURAL  
DESIGN PROCEDURES

by

Gilbert A. Greenbaum  
Terry N. Garner  
David L. Platus

Mechanics Research Incorporated  
Los Angeles, California

TECHNICAL REPORT AFSWC-TR-73-22

Test Track Division  
6585th Test Group  
Holloman Air Force Base, New Mexico

16

FOREWORD

CONTRACT NUMBER: F29601-72-A-0113-0006

CONTRACTOR: Mechanics Research Incorporated  
9841 Airport Boulevard  
Los Angeles, California 90045

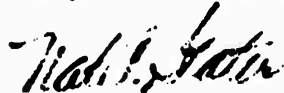
PROGRAM MONITOR: Dr. Larry C. Mixon, TKF

DATES OF RESEARCH: 30 June 1972 to 23 May 1973

DATE REPORT SUBMITTED: 23 May 1973

ACKNOWLEDGEMENTS: Acknowledgement is made to Dr. L. C. Mixon,  
Air Force Project Officer, for his helpful  
guidance and assistance.

Publication of this report does not  
constitute Air Force approval of the report's  
findings or conclusions. It is published  
only for the exchange and stimulation of ideas.



NAT A. STATER, Colonel, USAF  
Chief, Test Track Division

Item 13, Abstract (Cont'd)

The objectives of the study were accomplished. New design analysis procedures for dual rail sleds and monorail sleds were developed. However, more experimental data is required to verify the accuracy of these procedures, over the wide range of sled configurations and trajectories for which they are intended to be applicable.

## ABSTRACT

The major objective of this study was to establish improved design analysis procedures for the design of dual rail and monorail rocket sleds. The work included reviewing and evaluating past analytical studies of rocket sleds and experimental test data for two dual rail and two monorail sleds. Studies were undertaken to identify the major sources of dynamic excitation of rocket sleds. Three major sources of dynamic excitation were identified; rail roughness, unsteady aerodynamic forces and oscillating axial and lateral rocket thrust forces. Rail roughness was found to be the prime source of dynamic excitation during the coast portion of the rocket sled trajectory. During the thrust stage of the trajectory, and especially at burnout, oscillating axial and lateral thrust forces were found to produce sled dynamic loads which were the same order of magnitude as those produced by rail roughness.

The analytical work performed in this study concentrated on predicting the dynamic response of sleds due to rail roughness. Acceptable correlation between analytical and test results were obtained during coast. Lack of experimental data on unsteady aerodynamic forces and oscillating thrust forces precluded performing comprehensive analytical evaluation of these excitation sources. However, the magnitude of their effects were quantified and scale factors were established to account for their contribution to sled dynamic response during thrust and burnout.

The objectives of the study were accomplished. New design analysis procedures for dual rail sleds and monorail sleds were developed. However, more experimental data is required to verify the accuracy of these procedures, over the wide range of sled configurations and trajectories for which they are intended to be applicable.

## TABLE OF CONTENTS

Section		Page
I	INTRODUCTION AND SUMMARY .....	1
	1.1 Background .....	1
	1.2 Purpose and Scope .....	1
	1.3 Approach and Summary of Results .....	2
	1.3.1 Literature Survey and Review of Existing Sled Test Data .....	2
	1.3.2 Development of Analytical Methods of Analysis .....	4
	1.3.3 Development of Design Analysis Procedure for Dual Rail and Monorail Sleds .....	5
II	INTERPRETATION OF SLED TEST DATA .....	6
	2.1 Background .....	6
	2.2 Dual Rail Sleds .....	7
	2.2.1 Single Mod Sled .....	7
	2.2.2 Gnu Sled (6208) .....	10
	2.2.3 Summary of Conclusions from Dual Rail Test Data .....	15
	2.3 Monorail Sleds .....	18
	2.3.1 Modular Monorail .....	18
	2.3.2 Instrumented Monorail .....	23
	2.3.3 Summary of Conclusions from Monorail Test Data .....	23
III	FORMULATION OF MATHEMATICAL MODELS .....	28
	3.1 Nonlinear Dynamic Simulation of Dual and Monorail Sleds .....	28
	3.1.1 Nonlinear Structural Response Theory .....	28
	3.1.2 Description of SLEDYNE .....	33

# TABLE OF CONTENTS (continued)

Section		Page
	3.1.3 Comparison of Analytical and Test Results .....	36
	3.2 Simplified Impact Model for Monorail Sled .....	39
	3.2.1 Procedure A .....	39
	3.2.2 Procedure B .....	46
	3.2.3 Determination of Sled-Rail Impact Velocity .....	46
	3.2.4 Examples and Comparison with Flight Data ...	54
IV	INVESTIGATION OF OTHER EXCITATION SOURCES .....	62
	4.1 Dynamic Interaction of Pusher and Forebody .....	62
	4.1 Dynamic Interaction of Sled and Test Track .....	62
V	DEVELOPMENT OF DESIGN AND ANALYSIS PROCEDURES .....	66
	5.1 Introduction .....	66
	5.2 Factors Used with Quasi-Steady Loads for Dual and Monorail Sleds .....	66
	5.3 Dynamic Load Prediction for Design of Dual Rail Sleds .....	67
	5.4 Dynamic Load Prediction for Design of Monorail Sleds .....	69
VI	SLED STRUCTURAL DESIGN ANALYSIS PROCEDURES .....	72
	6.1 Dual Rail Sled Structural Design Procedure .....	72
	6.1.1 Dual Rail Sled -- Quasi-Steady Loads .....	72
	6.1.2 Dual Rail Sled -- Dynamic Loads .....	75
	6.1.2.1 Preliminary Dynamic Loads .....	77
	6.1.2.2 Final Dynamic Loads .....	80
	6.2 Monorail Sled Structural Design Procedure .....	84
	6.2.1 Monorail Sled -- Quasi-Steady Loads .....	84

# TABLE OF CONTENTS (continued)

Section		Page
	6.2.2 Monorail Sled -- Dynamic Loads .....	86
	6.2.2.1 Preliminary Dynamic Loads .....	86
	6.2.2.2 Final Dynamic Loads .....	101
VII	RECOMMENDATIONS .....	104
	7.1 Measurement of Additional Sled Test Track Data .....	104
	7.2 Rail Roughness Measurements .....	104
	7.2.1 Survey .....	104
	7.2.2 Test Vehicle for Measuring Rail Profile and/or Rail Roughness Excitations .....	105
	7.3 Sled Impact Tests .....	114
	7.4 Soft Metal Slippers for Reducing Dynamic Loads .....	114
VIII	CONCLUSIONS .....	119
	REFERENCES .....	120
	APPENDIX I -- SLEDYNE User's Guide .....	121
	APPENDIX II -- Development of Simulation Equations .....	137
	APPENDIX III -- Basis of Sled Impact Parameter .....	143
	APPENDIX IV -- Simplified Pitch-Bounce Response Spectra Model for Dual Rail Sleds .....	145

# LIST OF ILLUSTRATIONS

Figure No.		Page
2.1	Single Mod Sled, Slipper Force Measurements at Burnout, Run 24X-D1 .....	8
2.2	Effect of Slipper Gap on Single Mod Sled Apparent Natural Frequency .....	9
2.3	Single Mod Sled, Force in Slippers Induced by Sinusoidal Load at Engine Mount, 3% Damping .....	11
2.4	Single Mod Sled Slipper Forces, Motor On, Transonic Velocity, 24X-C1 Run .....	12
2.5	Single Mod Sled, Force in Slippers Induced by Sinusoidal Force Above Forward Slipper Beam .....	13
2.6	Single Mod Sled Slipper Forces, Typical Data from Coast Phase, 24X-D1 Run .....	14
2.7	Gnu (6208) Slipper Forces .....	16
2.8a	Dual Rail Test Track Data vs SIMP .....	17
2.8b	Peak Slipper Beam Dynamic Force vs Slipper Beam Stiffness, Dual Rail Sleds .....	19
2.9	Installation of Force Transducer in Monorail Sled .....	20
2.10	Modular Monorail Sled .....	21
2.11	Modular Monorail, 53X-B2, Measured Forward Slipper Dynamic Forces .....	24
2.12	Modular Monorail, 53X-B2, Front Slipper Force Measurements at Burnout .....	25
2.13	Instrumented Monorail with Pusher .....	26
2.14	Instrumented Monorail Slipper Force Measurements, 44X-E2, E8, Source: Reference (2) .....	27
3.1a	Restraints Applied to Dual Rail Sled for Calculation of SLEDYNE Modes .....	30
3.1b	Restraints Applied to Monorail Sled for Calculation of SLEDYNE Modes .....	30
3.2	Displacement Functions Used in Nonlinear Dynamic Response Simulation .....	31



# LIST OF ILLUSTRATIONS (continued)

Figure No.		Page
3.3	Percent Error in Calculated Results Compared with Test Data -- Instrumented Monorail 4000 fps ( $M=3.6$ ) .....	34
3.4	Section of Sample Rail Height Measurements .....	35
3.5	Comparison of SLEDYNE Results with Test Track Data Dual Rail Sleds .....	37
3.6	Time History of Vertical Force from SLEDYNE Modular Monorail -- Forward Slipper, 3400 fps .....	40
3.7	Impact Model for Monorail Sleds .....	41
3.8	Models for Computing Slipper and Support Structure Stiffness .....	43
3.9	Distributions of Sled Weight and Lift Force .....	44
3.10	Distribution of Impact Acceleration .....	45
3.11	Typical Result of Impact Analysis of Multi-Degree-of-Freedom Model .....	47
3.12	Single-Degree-of Freedom Model Used for Design Curves ....	48
3.13	Impact Velocity for Monorail Sleds .....	49
3.14	Finite Element Model -- Forward Slipper Impact .....	55
3.15	Forward Slipper Vertical Force Time History for Unit Step Velocity .....	55
3.16	Instrumented Monorail Forward Slipper Vertical Force .....	57
3.17	Modular Monorail Finite Element Model .....	58
3.18	Forward Slipper Vertical Force Time History for Unit Velocity Impact .....	58
3.19	Modular Monorail Sled -- Weight and Lift Distributions ...	59
4.1	Single DOF on Beam-On-Elastic Foundation of Model of Sled on Test Track Bed .....	64
4.2	Dynamic Amplification of Single DOF on Beam on an Elastic Foundation .....	65
5.1	SIMP Line for Design of Dual Rail Sleds .....	68

# LIST OF ILLUSTRATIONS (continued)

Figure No.		Page
5.2	Magnitude of Lateral Loads for Monorail Sleds .....	71
6.1	Equilibrium of Thrust Induced Loads .....	74
6.2	Application of Quasi-Steady Braking Forces .....	76
6.3		78
6.4		78
6.5	Dynamic Slipper Beam Force vs SIMP, Dual Rail Sleds .....	79
6.6	Distribution of Preliminary Dynamic Loads Case 1 .....	81
6.7	Design Factors vs SIMP .....	83
6.8	Equilibrium of Thrust-Induced Loads .....	87
6.9	Application of Quasi-Steady Braking Forces .....	87
6.10	Model for Computing Vertical Stiffness of a Slipper and Support Structure .....	89
6.11	Model for Computing Lateral Stiffness of a Slipper and Support Structure .....	89
6.12	Distribution of Sled Weight and Lift Force .....	91
6.13	Impact Velocity for Monorail Sleds .....	92
6.14	Distribution of Case FV Preliminary Dynamic Loads .....	98
6.15	Slipper Force Time History .....	100
6.16	Magnitude of Lateral Loads for Monorail Sleds .....	103
7.1a	Establishment of Longitudinal and Vertical References ....	106
7.1b	Establishment of Longitudinal and Vertical References ....	107
7.2	Tooling Bar .....	108
7.3	Measuring Device for Vertical Heights of the Rail Underside .....	109
7.4	Measuring Device for Vertical Heights of the Rail Top ....	110
7.5	Optical Micrometer .....	111

LIST OF ILLUSTRATIONS (continued)

Figure No.		Page
7.6	Rail Roughness Measurement Sled Concept .....	113
7.7	Sled Drop Test Approaches -- Direct Rail Impact .....	115
7.8	Sled Drop Test Approaches -- Indirect Rail Impact .....	116

# LIST OF TABLES

Table No.		Page
I	Modular Monorail, 53X - B2, Vertical Front Slipper Force .....	22
II	Comparison of SLEDYNE Model Representation with "Exact" STARDYNE Modes .....	32
III	Comparison of SLEDYNE Results with Test Track Data Monorail Sleds - Vertical Force During Coast (lbs) .....	38
IV	Summary of Dual Rail Sled Design Conditions .....	73
V	Summary of Monorail Sled Design Conditions .....	85

## SECTION I

### INTRODUCTION AND SUMMARY

#### 1.1 Background

The proper design of high speed dual rail and monorail sleds requires an understanding of the forces acting on the sled due to thrust, aerodynamics, braking and sled/track dynamic interaction. The quasi-steady-state thrust, aerodynamic and braking forces are fairly well-known and can normally be calculated. However, determination of the dynamic transient forces is much more indefinite. The major sources of sled dynamic excitation are rail roughness, oscillating aerodynamics and oscillating axial and lateral thrust forces. Each of these sources may induce large dynamic response of the sled. The problem is complicated by the gap between sleepers and the rail which makes analytical methods nonlinear.

Prior to the present work, the only accepted published design analysis methods for high speed dual and monorail sleds were contained within the ISTRACON Handbook (1). This handbook contains procedures for applying quasi-steady-state aerodynamic, thrust and braking force to sled designs and also  $\lambda$  (g-load) factors. The  $\lambda$  factors are intended to account for rail roughness induced dynamic behavior but are far from adequate and needed to be improved. For example, they do not account for the dynamic properties of the sled such as inertia, stiffness and damping. Furthermore, these accelerations are assumed to be constant over the sled length, and hence, do not account for variations in maximum accelerations encountered by the various components of the sled. Consequently, the calculated internal forces in the sled could be far from those actually experienced in test. Despite these shortcomings, there is one fact that cannot be denied. Over the years a great many sleds have been designed, built and successfully run on the Holloman test track. Evidently, the loads to which they were designed were equal to or greater than those imposed by the environment. Nonetheless, it is important that the dynamic behavior of high speed sleds be better understood in order to improve the performance and reliability of future sleds.

#### 1.2 Purpose and Scope

The purpose of this program was to evaluate current design analysis practice for high speed sleds, and in light of available test data, to establish new procedures for a wide range of monorail and dual rail sled configurations. More specifically, the objectives were to:

- Review prior analytical work and theories concerning the dynamic behavior of high speed sleds
- Review available high speed sled test data for both monorail and dual rail sleds

- investigate the major theories concerning sled/track dynamic interaction and attempt to determine the importance of rail roughness, aerodynamic and thrust oscillating loads and aerodynamic feedback on transient dynamic response of rocket sleds
- Evaluate the effects of sled parameters, such as mass, stiffness, geometry, etc., on the magnitude of dynamic sled forces
- Determine if simplified analysis techniques for the design of rocket sleds could be obtained, and, if so, to establish these design/analysis procedures for a wide range of sled configurations

### 1.3 Approach and Summary of Results

To accomplish the program objectives the following major tasks were undertaken:

- Literature survey and review of existing sled test data
- Development of nonlinear analytical methods for predicting dynamic response of rocket sleds and correlation of analytical results and test data
- Development of design analysis procedures for dual rail and monorail sleds

#### 1.3.1 Literature Survey and Review of Existing Sled Test Data

A review of the existing literature revealed three plausible theories as to why sleds experience large dynamic accelerations. In addition, a fourth theory based on a review of test data was added. The four theories are classified as follows:

- Rail roughness
- Unsteady aerodynamic forces
- Aerodynamic feedback (aeroelasticity)
- Oscillating axial and lateral thrust

##### Rail Roughness

Mixon (2) presents a rather extensive investigation of sled dynamic response to rail roughness for monorail sleds, and contributes significantly to an understanding of this phenomenon. No other source of dynamic excitation was considered. Mixon predicted the vertical and lateral response of a sled to rail roughness using a nonlinear model. His sled model is a rigid body supported by massless linear springs and dampers. A rail roughness forcing function was introduced by modulating the nominal

slipper gap with the rail displacement distance profile. Quasi-steady-state aerodynamic forces were also introduced. Fair correlation was obtained between measured and predicted peak slipper forces in the vertical direction, although significant differences occurred in the lateral direction. However, test data from only one monorail sled was examined (the instrumented monorail) and this sled did not have any on-board thrusting motors. The present investigation showed that on-board thrusting motors had a significant effect on the dynamic response of sleds, especially around burnout.

Fisher, et al (3), and Oliver, et al (4), also considered rail roughness as the only source of excitation for both dual and monorail sleds. However, both references deal only with soft suspension system in which the slipper gap is assumed to be unimportant. This assumption is fairly good for dual rail sleds which have natural frequencies in the 20 Hz range, but not monorail sleds whose frequencies are usually in the 150 to 250 Hz range. Moreover, our investigation of soft suspension dual rail sleds showed that the effects of oscillating aerodynamic forces in the transonic range and on-board thrusting motors produced the same order of magnitude dynamic loads as rail roughness.

#### Unsteady Aerodynamic Forces

The review of available sled test data was hindered by a lack of information on unsteady aerodynamic pressure forces. One theory is that they are caused by separated flow being shed by protrusions from the sled body or behind corners such as the cone-cylinder junctions. This type of excitation should be random except for perhaps a periodic disturbance to the flow, such as passing of rail supports. Hasse (5) points out that sound pressure measurements on top of the sled reveal such a periodic disturbance.

Another explanation is based on choking effects under the forward part of the sled. Some inferences were drawn about this mechanism during this study. A dual rail sled showed increased response levels as it accelerated through the transonic velocity range. The nature of the response strongly suggests that the exciting force was acting at the forward end of the sled. Such response was not observed during deceleration through the same velocities nor was it observed at any time for monorail sleds.

Assessment of the precise nature of unsteady aerodynamic excitation will require pressure measurements which have not yet been made.

#### Aerodynamic Feedback (Aeroelasticity)

Another possible source of excitation for which no experimental data are available is aerodynamic forces which depend on the sled's angle-of-attack and/or angular rate. Braun and Melkus (6) performed a study on a large sled where they included linear aerodynamics and gaps at the slippers. They obtained a limit cycle type behavior for all the studied combinations of parameters, although it is not clear what was driving the motion. Despite a positive static margin (cp behind cg) and positive damping, both of which out to be stabilizing, the results showed unstable behavior.

McIntyre's work (7) is a linear analysis leading to flutter envelopes depending on velocity and supporting spring characteristics. This approach probably is not useful for explaining the monorail data because there is no experimental evidence of the precipitous sort of response that characterizes flutter.

Neither Mixon nor the present study considered aerodynamic feedback in the analytical investigation. Yet, both studies achieved acceptable correlation during the coast phase of the trajectory. Thus, we believe that aerodynamic feedback is not an important phenomenon for high speed sleds, most likely because of the relatively small variations in angle-of-attack.

#### Oscillating Axial and Lateral Thrust Loads

The review of test data showed significantly higher slipper dynamic loads during thrust and at motor burnout than during the coast phase of the trajectory. Apparently, motor thrust loads are dynamically exciting the sled. To analytically predict this phenomenon would require experimental data on the oscillating thrust characteristics of the on-board motors. Little of this type of data was available for the motors used on the test sleds. Therefore, it was not possible to fully assess this potential source of excitation. However, one liquid motor and the dynamic responses it caused were investigated to the point of thorough understanding.

#### 1.3.2 Development of Analytical Methods of Analysis

Upon completion of the literature survey and review of test data, an analytical investigation of the dynamic behavior of sleds was undertaken. This study was primarily concerned with predicting the dynamic response of sleds to rail roughness and correlating these results with test data. It was felt that acceptable correlation during the coast phase of the trajectory could be obtained since unsteady aerodynamics and oscillating thrust loads are unimportant during coast. It was also felt that if acceptable correlation during coast could be obtained, the analytical methods could serve as a basis for establishing sled design procedures with scale factors to account for unsteady aerodynamics and oscillating thrust forces, since analytical models were not available for either mechanism. Analytical investigation of the latter two excitation sources required experimental data on the magnitude and nature of these sources; these data were not available.

The analytical method developed under this task included a non-linear dynamic simulation computer program (SLEDYNE) which considers the flexibility of the sled and the gap between slipper and rail. This program calculates the dynamic behavior of the sled as it bounces along the rough rail. A deterministic approach is used with a randomly generated rail profile of the Holloman track. The latter is based upon a limited amount of measured track data. The results of this study did indeed show good correlation during the coast phase of the trajectory for both monorail and dual rail sleds.



Upon completion of this study, simplified analysis techniques for high speed sleds were investigated. The results of this study led to the establishment of a design procedure for dual rail and monorail sleds which could be used in preliminary design.

### 1.3.3 Development of Design Analysis Procedure for Dual Rail and Monorail Sleds

The final task of the program was to develop design analysis procedures which could be used for a wide range of sled designs. By necessity, the procedures established were to a large extent based upon estimates, assumptions and judgements. It is hoped that further experimental and analytical work will be performed to verify these proposed design analysis procedures. The development design analysis methods separate the quasi-steady-state loads from the dynamic loads. Dynamic loads are those inertia loads associated with bouncing and pitching in the vertical and lateral planes. The proposed dynamic analysis procedures depart significantly from current design procedures and take into consideration many of the parameters (i.e., stiffness, inertia, geometry) which the current design procedures ignore (1).

Preliminary and final design procedures are presented in Section 6.0 of this report for both dual rail and monorail sleds. These procedures were developed by correlating analytical results with a limited amount of test results. Since the analytical effort of this study considered only rail roughness, it was necessary to adjust these results with scale factors to account for the other sources of dynamic excitation. The methods used involved matching analytical peak slipper force prediction with available test data. Only a small amount of test data was available for this study. The proposed procedures should be used with caution until more data are obtained, especially with sleds of unusual configuration or trajectories.

It is hoped that the proposed design analysis procedures will provide a rational base which can be easily refined and expanded to new sled configurations and trajectories as more experimental and analytical work is performed.

## SECTION II

### INTERPRETATION OF SLED TEST DATA

#### 2.1 Background

The plan at the outset of the study was to devote the early period to interpretation and evaluation of the data, and then based on the results, to formulate the design criteria. Interpretation of the test track data proved to be a more elusive task than originally anticipated. This was due to two fundamental difficulties which plagued the work throughout this study: lack of information about the nature of the sources of excitation and limited data on the response of sleds to the sources.

Interpretation of the test track data requires first that possible sources of excitation be identified and then that response of sleds to those sources be characterized. This is necessary so that features such as point of onset in the trajectory, amplitude, frequency, and phase of response may be correlated between flight data and what would be expected from postulated excitation sources. The difficulties in characterizing the excitation sources were the following:

- Rail roughness was considered the principal candidate as an excitation source. The available data consisted of 440 measurements made over a 400 foot section of one rail of the Holloman test track. These were measurements of the height of the center of the rail. There was no information on horizontal roughness, on roughness of the underside of the rail where almost all sleds are supported during the high velocity phases of their runs, or of other sections of the track which may or may not have the same roughness characteristic.
- Oscillating aerodynamic loads were considered another likely source of sled excitation. It is known that in the transonic velocity range aerodynamic choking occurs under the forward part of sleds. The pressure fields are high and unstable, and the resulting oscillations could intuitively be expected to induce large dynamic loads. Buffeting could also be a significant source. There are, however, no direct data to establish either the existence or the magnitude of any aerodynamic forcing functions.
- Large sleds, weighing over 15,000 or 20,000 pounds, exert high loads on the track bed. Loads of such magnitude, moving down the track and oscillating, could reasonably be expected to excite the "beam on an elastic foundation" type of response in the track bed. There is, however, no information on the dynamic characteristic of the track bed, only a static measurement indicating the foundation stiffness -- nothing from which the crucial added mass term can be estimated.

- It is known that high dynamic loads are experienced during engine ignition and burnout. It is likely that they are caused by engine transients, but there is little information which can be used to characterize amplitude or frequency content of thrust transients, either axial or lateral, for the variety of engines used at the track.

The available test track data consist almost entirely of strain gage measurement taken from slipper support structure. For monorail sleds there are data on vertical and horizontal forces and for dual rail sleds, vertical forces only. During the performance of this study, time-history records of these data were available for two dual rail sleds and two monorail sleds. There was also some power spectral density information from two other dual rail sleds.

Despite the lack of quantitative test data, there is one fact which cannot be ignored. Over the years a great many sleds have been designed, built, and operated on the Holloman test track. With rare exceptions, they have survived the environment and in many cases have been used numerous times. Evidently, the loads to which they have been designed have been greater than those imposed by the environment.

In the following sections some observations are made, and certain generalizations are postulated. It is recognized, of course, that generalizations drawn from such extremely limited data will be suspect. It is hoped here not that the generalizations will be conclusive, but that the method of treating the data will serve as a guideline for future observation of additional data, leading to better understanding of the phenomena.

## 2.2 Dual Rail Sleds

### 2.2.1 Single Mod Sled

Time history test track data was analyzed for two runs of the Single Mod sled, 24X-C1 and 24X-D1. The Single Mod sled at burnout weighs 9400 pounds and has a span of 20 feet between the slipper beams. On the C1 and D1 runs it pushed a 3,140 pound forebody to 1860 fps, and a 4000 pound forebody to 1762 fps, respectively. Its first two modes of vibration in the vertical plane have frequencies of 20.2 cps and 27.6 cps.

#### Engine Burnout

Figure 2.1 shows the time history of slipper forces at engine burnout for the D1 Single Mod run. During the D1, D1 and B4 (for which a small amount of data was available), the highest forces felt in the aft slipper beam were experienced at engine burnout. The highest force observed on any of the three runs was seen on the rear port slipper in the D1 run. The dynamic half-amplitude reached 19,600 pounds at 8.1 seconds.

The apparent natural frequency of several of the high amplitude oscillations has been indicated on Figure 2.1. The graph of Figure 2.2 gives the ratio of apparent to natural frequency as a function of the peak force of oscillation. This factor accounts for the nonlinear gap effect

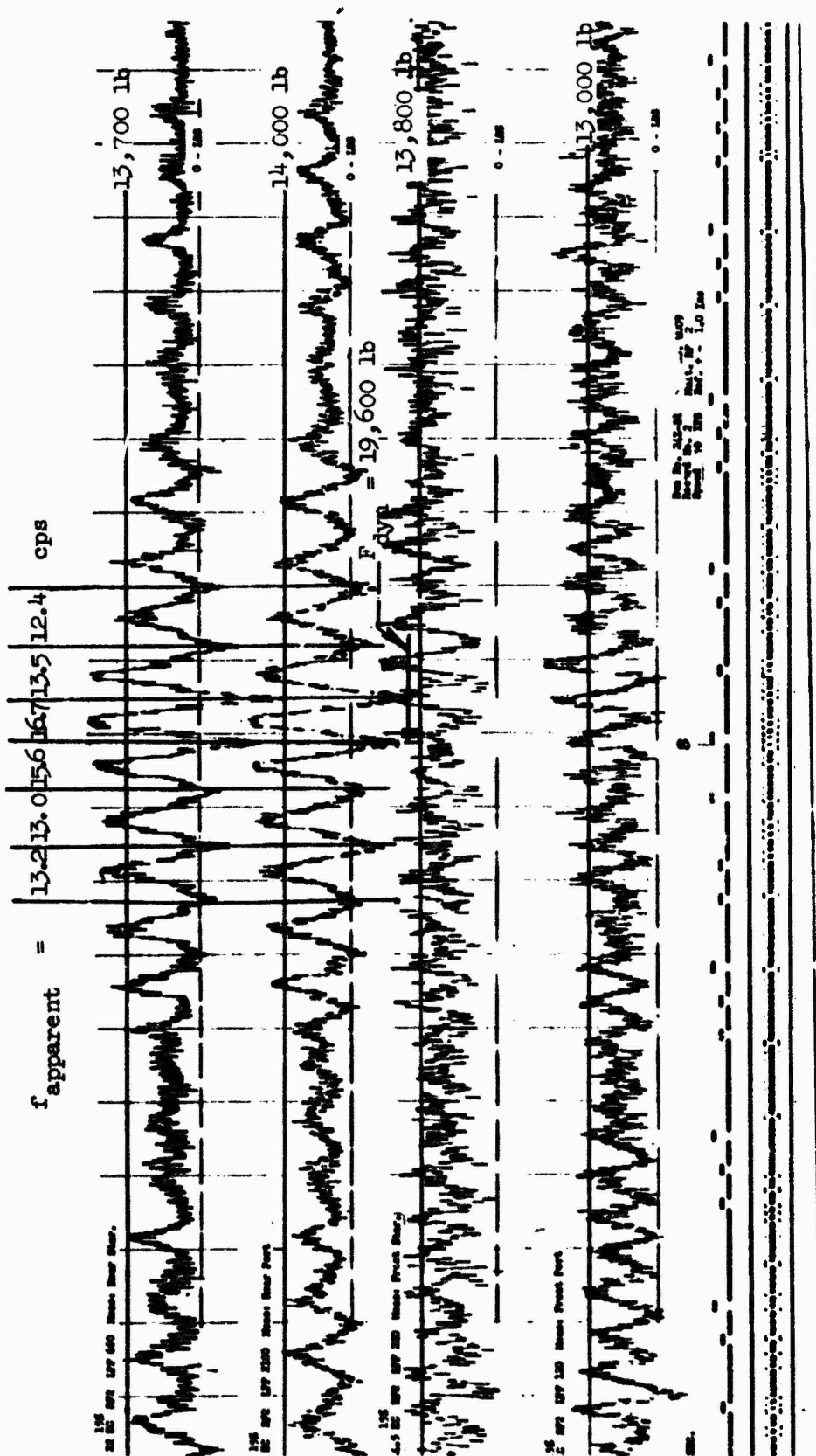


Figure 2.1. Single Mod Sled, Slipper Force Measurements at Burnout, Run 24X-D1

$$\frac{f_{\text{apparent}}}{f_{\text{natural}}} = \frac{1}{\frac{\epsilon K}{\pi F_{\text{max}}} + 1}$$

$\epsilon$  = slipper gap = .125 in

$K$  = slipper stiffness

$F_{\text{max}}$  = peak dynamic slipper force

Single Mod Sled  
Aft Slipper,  $K = 1.3 \times 10^5$  lb/in

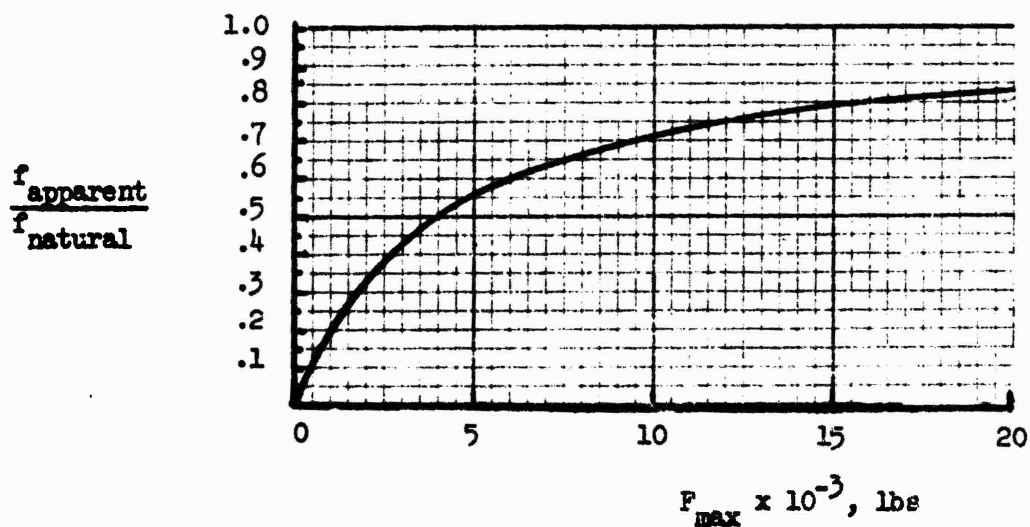


Figure 2.2. Effect of Slipper Gap on Single Mod Sled Apparent Natural Frequency

which lowers the apparent natural frequency. When the observed frequencies of several of the high amplitude cycles are adjusted by this correction factor, depending on the amplitude of the oscillation, the sled is found to be vibrating in its 20 cps first mode.

An 84 dof finite element model was constructed for the Single Mod sled. It was used for a frequency response analysis. Figure 2.3 shows the dynamic force in a single slipper resulting from a vertical 1,000 pound sinusoidal force acting at the engine mount of the Single Mod sled. It is seen that each aft slipper would feel 4.6 times the force applied vertically at the engine mount. Hence, a few percent of the nominal 15,000 pound thrust acting vertically and in the frequency range 13 to 17 cps could be expected to cause a major portion of the loads observed. In fact, the AJ60 engine used on the Single Mod sled is known to develop nozzle flow instabilities during engine shutdown and associated lateral forces with characteristic frequencies in this range. This was verified by telephone conversations with personnel at the Aerojet General Corporation in Sacramento.

#### Aerodynamic Oscillating Loads

It was observed from the test data of both the C1 and D1 Single Mod runs that dynamic amplification, especially in the forward slippers, occurred in the transonic speed range. Figure 2.4 shows the typical sample at 4.0 seconds in the C1 run where the velocity was 950 fps. The front port slipper experienced a peak dynamic load of over 15,000 lbs. The apparent frequency is 20.4 cps and it is observed that the forward and aft slipper beams are out of phase. The natural frequency, as calculated with the factor from Figure 2.2, is slightly over 26 cps. Figure 2.5 shows the results of a frequency analysis done on the same finite-element model described in the previous section. In this case, an oscillatory force was applied to the sled at the station of the forward slipper beam. Peak amplification is for the forward slipper beam at 27.6 cps, and it shows that the forward and aft slippers are out of phase. The disparity in frequency between the flight and the analytical data may be attributed to the additional weight of unburned propellant which was on-board at 4 seconds.

#### Loads During Coast

Figure 2.6 shows a typical sample of flight data from the D1 run after engine burnout. The velocity was about 1500 fps. Peak dynamic loads reach about 10,000 pounds for the aft slippers and 9,000 pounds for the forward slippers. No particular amplification is observed for either of the C1 or D1 sleds in the transonic region during deceleration.

#### 2.2.2 Gnu Sled (6208)

The 6208 sled nicknamed Gnu is boosted to 900 fps and accelerates under its own power to 2,000 fps. It uses several JAV-1 engines and

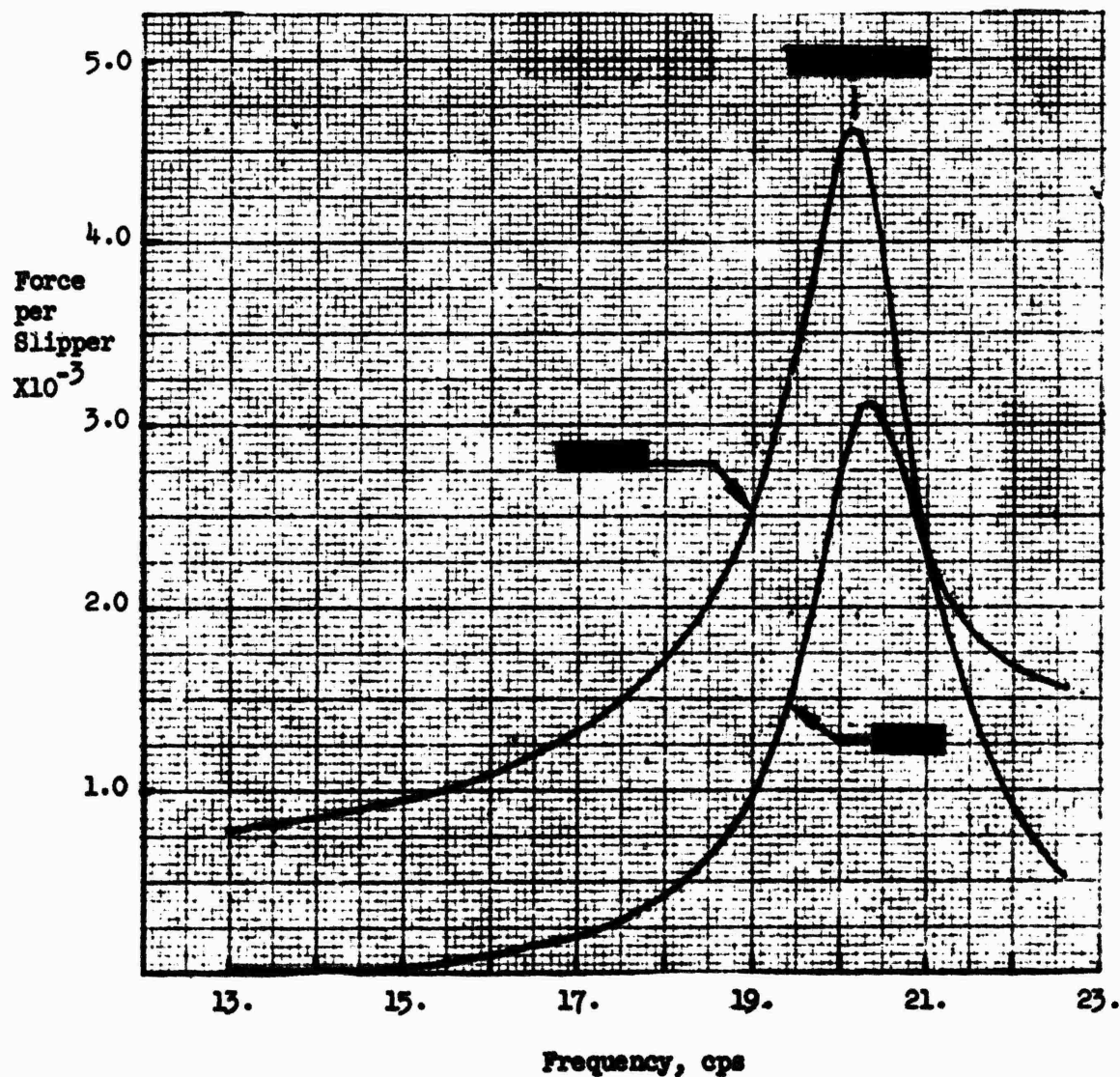
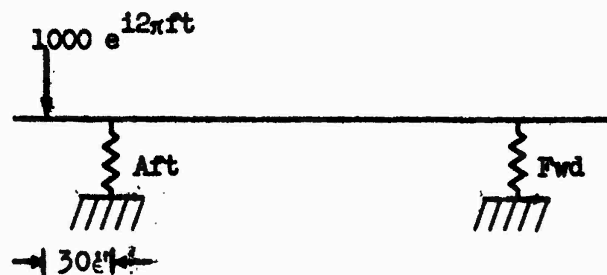


Figure 2.3. Single Mod Sled, Force in Slippers Induced by Sinusoidal Load at Engine Mount, 3% Damping

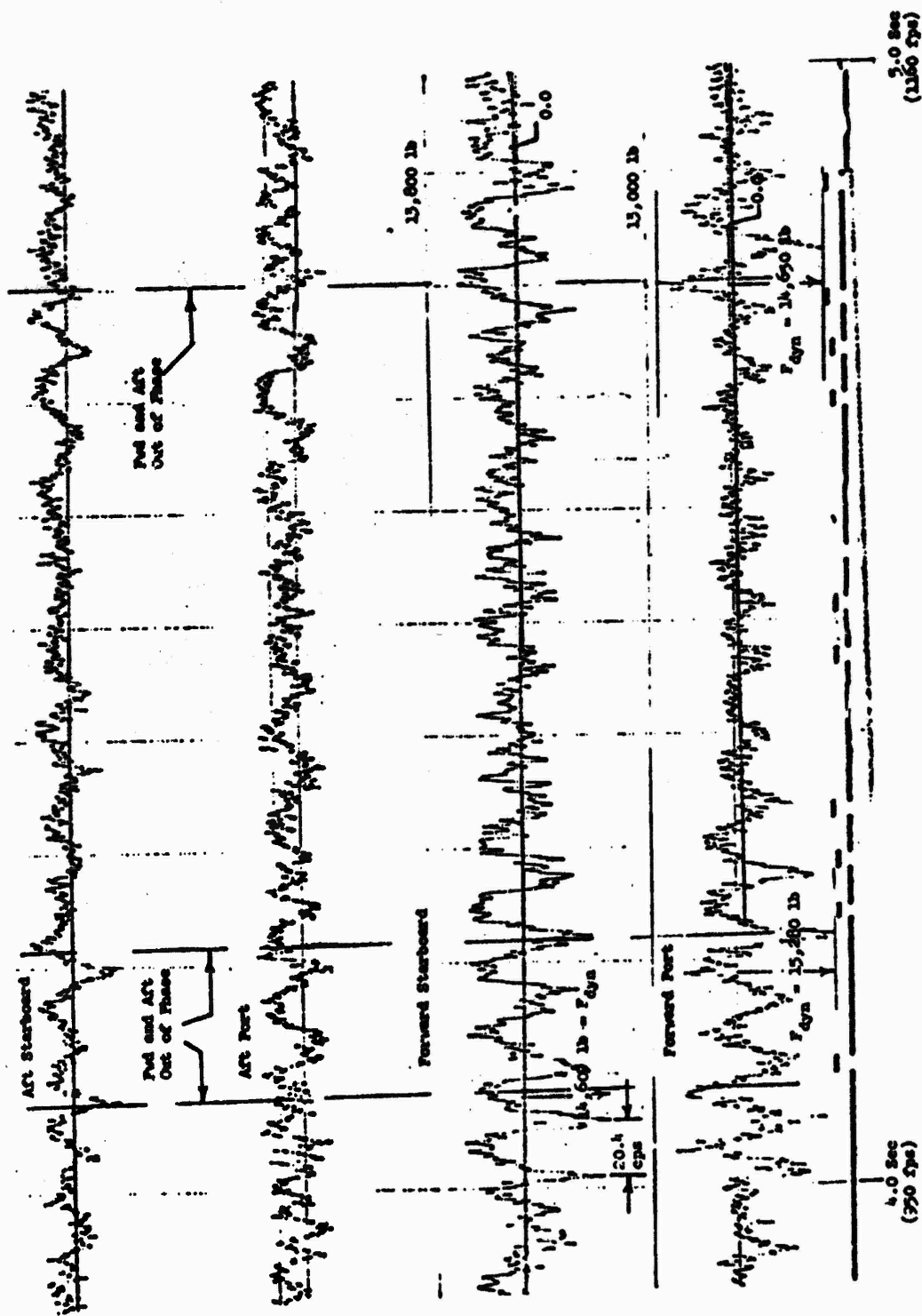


Figure 2.4. Single Mod Sled Slipper Forces  
Motor On, Transonic Velocity, 24X-C1 Run



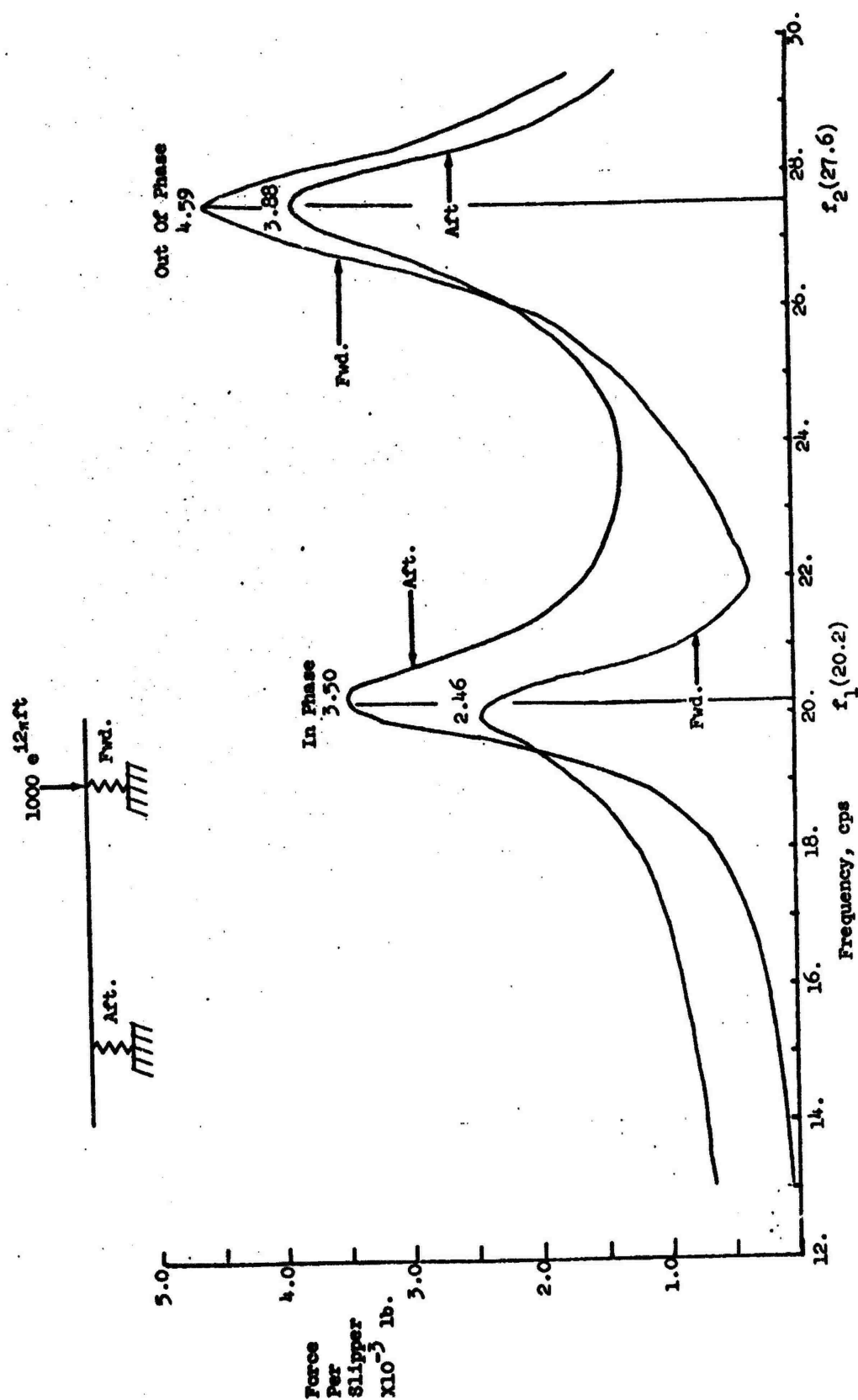


Figure 2.5. Single Mod Sled, Force in Slippers Induced By Sinusoidal Force Above Forward Slipper Beam, 3% Damping

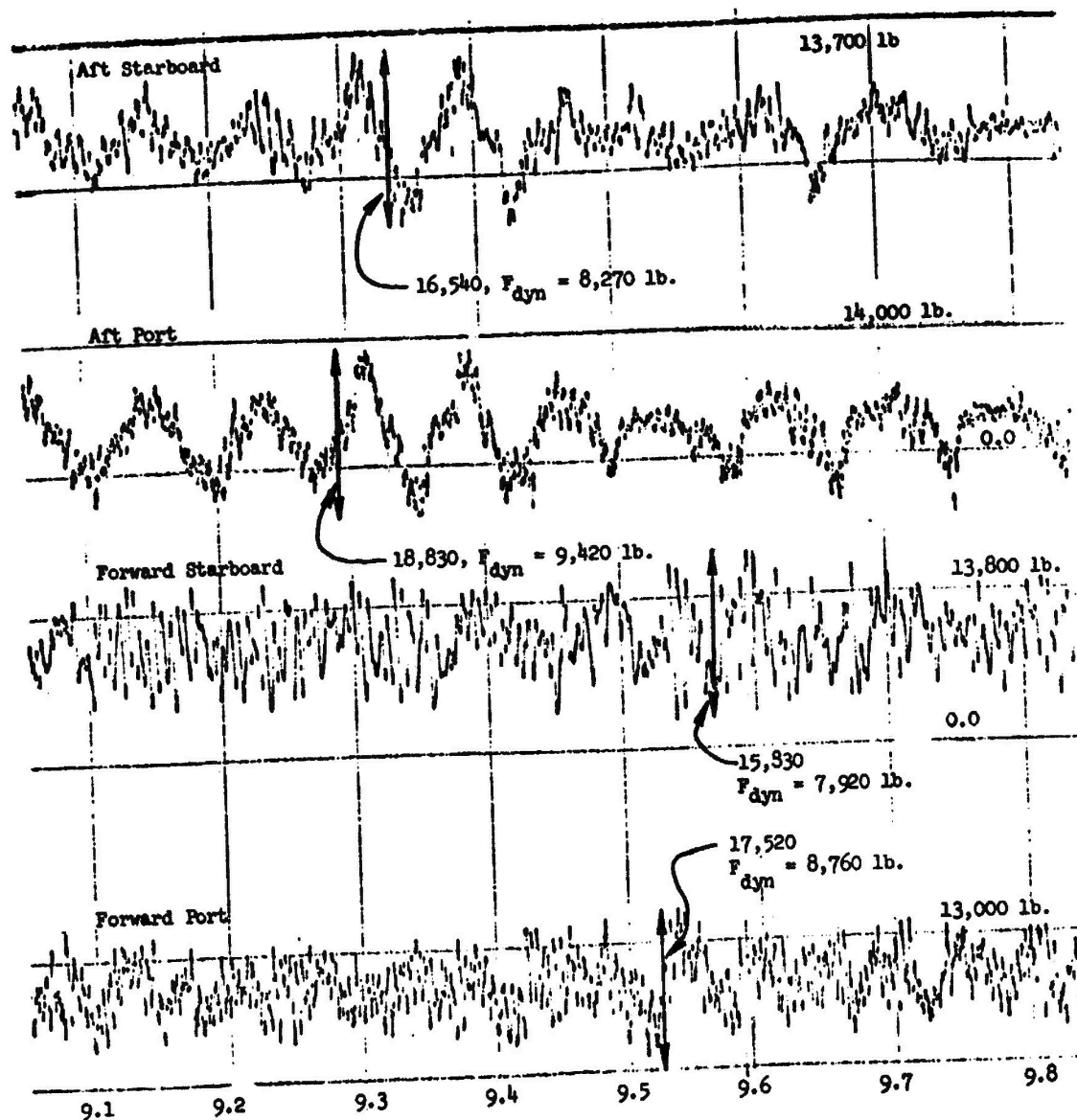


Figure 2.6. Single Mod Sled Slipper Forces, Typical Data from Coast Phase, 24X-D1 Run

weighs 3,180 pounds at burnout. It measures 140 inches between slipper beams, and like the Single Mod sled, has a low cg, barely more than a foot above the rail head.

Figure 2.7 shows what flight data are available. The numbers noted alongside the force history plots are values of dynamic half-amplitude force in each slipper. Front slippers see peaks of about 5,100 pounds during engine burnout and 4,000 pounds during coast. Forces in the aft slipper are higher, with peaks going as high as 7,000 pounds during engine burnout and 5,100 pounds during coast. Because there is an engine ignition occurring during passage through the transonic regime, just before three seconds, no conclusion can be drawn about the effect of oscillating aerodynamic loads.

### 2.2.3 Summary of Conclusions From Dual Rail Test Data

From the foregoing observations, a few very tentative conclusions may be drawn.

- Sources of excitation for dual rail sleds include at least oscillating aerodynamics, engine transients, and rail roughness. For one sled with solid propellant motors (Gnu), engine termination loads were about 40% greater than the rail roughness loads. For another sled with a liquid engine, engine termination loads were 100% greater than rail roughness loads.
- Lateral loads were not measured directly. For the Single Mod sled it was possible to observe the phase relationship between the forces in the two forward and in the two aft slippers. At no point was there a significant difference in those forces which would be necessary if there were large roll response of the sled. Of course, the sled cg is so low (15 inches) that even large lateral forces might not induce significant roll response.
- More or less fortuitously, a parameter was found that tends toward a straight line correlation with test results. The Sled Impact Parameter (SIMP) involves only mass and stiffness properties of the sled<sup>1</sup>. In Figure 2.8a peak dynamic slipper beam loads are plotted against SIMP. Measured peak dynamic slipper forces have been doubled and are now called peak dynamic slipper beam forces. Peak values during coast are differentiated from absolute maxima measured during engine burnout or transonic. The ratio between peak dynamic and coast loads is the basis for amplification factors which have been established for design load predictions. This is discussed in Chapter 5.0.

---

<sup>1</sup>See Appendix III for discussion of SIMP.

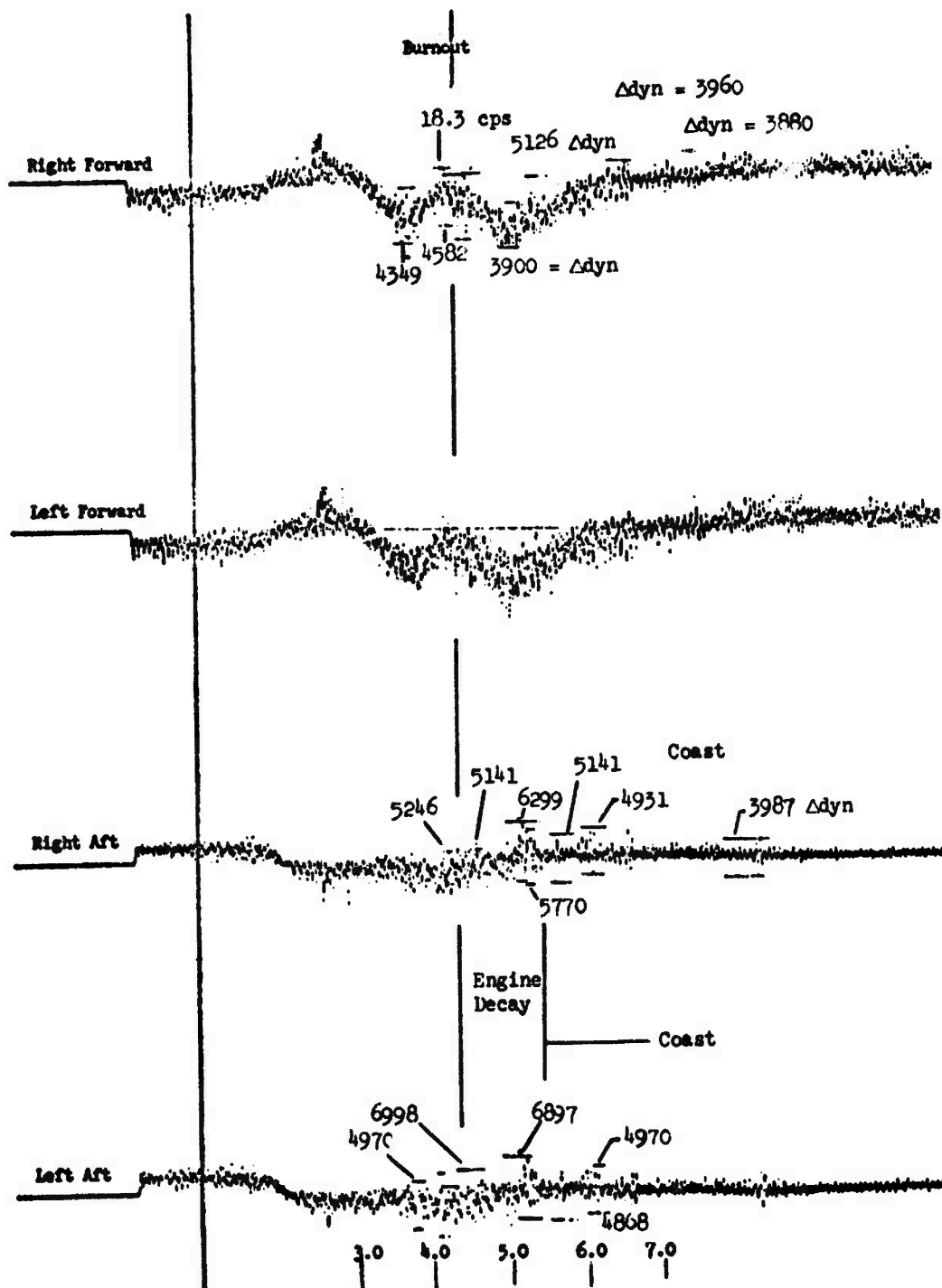


Figure 2.7. Gnu (6208) Slipper Forces

$$SMP = \left[ \frac{KM}{1 + \frac{W}{I}} \right]^{\frac{1}{2}}$$

M = Sled Mass  
I = Sled Pitch Inertia  
K = Slipper Beam Stiffness  
L = Distance From c.g. to Slipper Beam

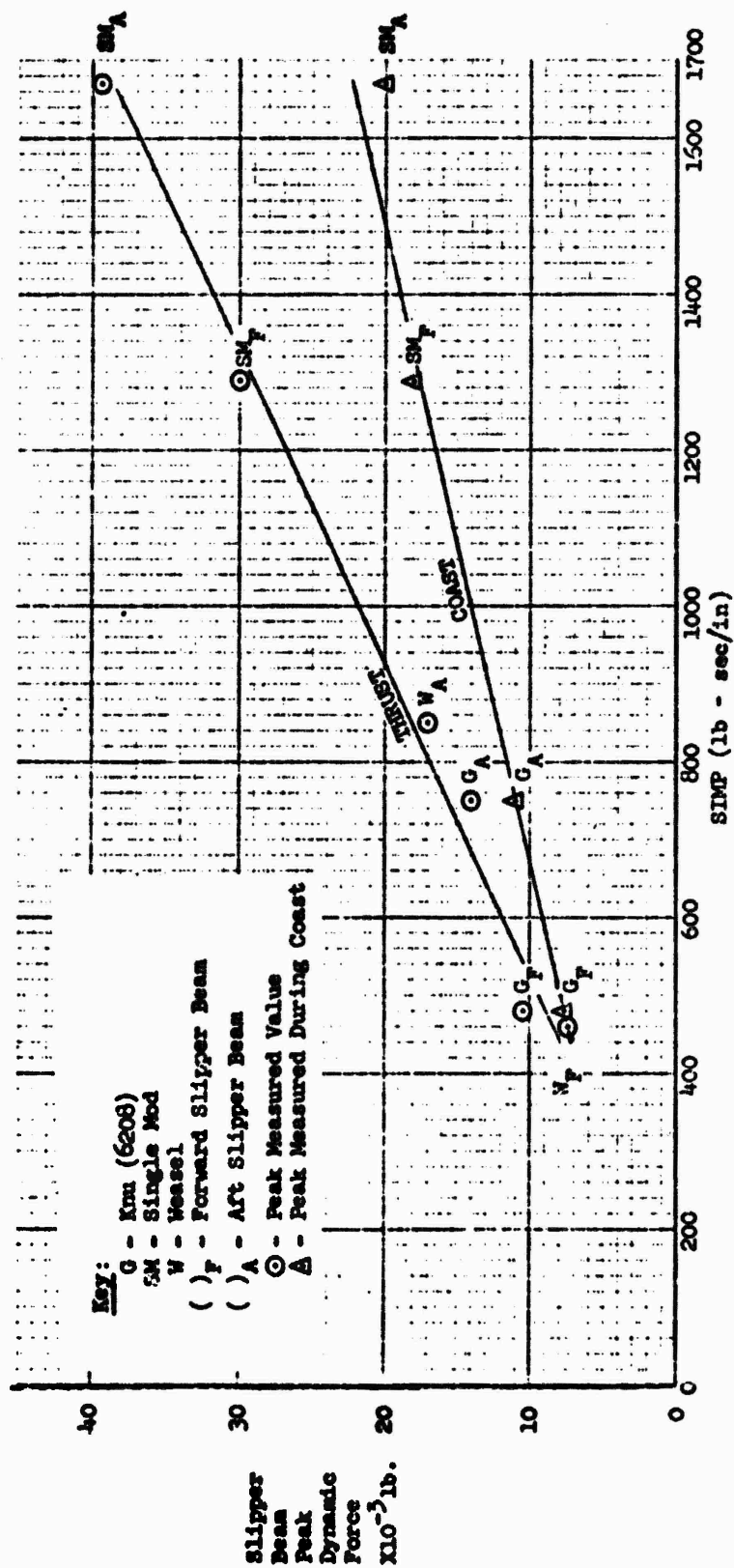


Figure 2.8a. Dual Rail Test Track Data vs SIMP

A pair of points for the Weasel sled has been added to the data discussed previously in this section. No time history data for the Weasel were seen, but these two points were inferred from the Beta factor curve, Figure 29 of Reference (8). It is not certain that the points are from forward and aft slipper beams as assumed.

- Later in the study, a further and more startling observation was made. Measured coast loads, i.e., peak slipper beam dynamic forces measured during coast, and SLEDYNE results were plotted against slipper beam stiffness. Figure 2.8b shows that the data tend toward a straight line. This means that the dynamic response to rail roughness excitation tends to be of constant displacement, the values varying between .070 inch and .130 inch.

## 2.3 Monorail Sleds

By comparison with dual rail sleds, monorail sleds are lighter, faster, traveling at least twice the speed, and perhaps most importantly from the structural dynamics viewpoint, a great deal stiffer. Whereas the slippers of dual rail sleds are in contact with the rails most of the time, monorail sleds spend most of their time flying in the gap. Contacts with the rail are brief and severe impacts. Painted track data indicated that they usually occur at the corners of the rail head. The implication is that while the monorail sled is bouncing it is also rolling from side to side.

Test data for the two monorail sleds described in this section were taken from a specially developed transducer instrumented with strain gages. The strain gages were installed so as to measure two vertical forces, one on each side, lateral force and roll moment. The procedure used is described in Section 2.0 of Reference (2). Installation of the transducer in the monorail sled is illustrated in Figure 2.9.

### 2.3.1 Modular Monorail

The Modular Monorail sled shown in Figure 2.10 weighs 616 pounds and measures 62.2 inches between its slippers. In the 53X-B2 test, the modular monorail reached a velocity of 3500 fps. It was in that test that force data were taken from a transducer, similar to the one illustrated in the Figure of 2.9, mounted above the front slipper. Some of the results of the vertical force measurements are shown in Table I. Each value is a peak dynamic load (the quasi-steady load had been removed) experienced during the indicated tenth second interval. Several observations may be made:

- There is a great deal of scatter in the data. Even though the sled is covering approximately 300 feet in each .1 second interval, the peak forces vary by as much as 100 percent from one interval to the next.
- With the motor on, loads are about 40 percent higher than at the same velocity with motor off (coast).



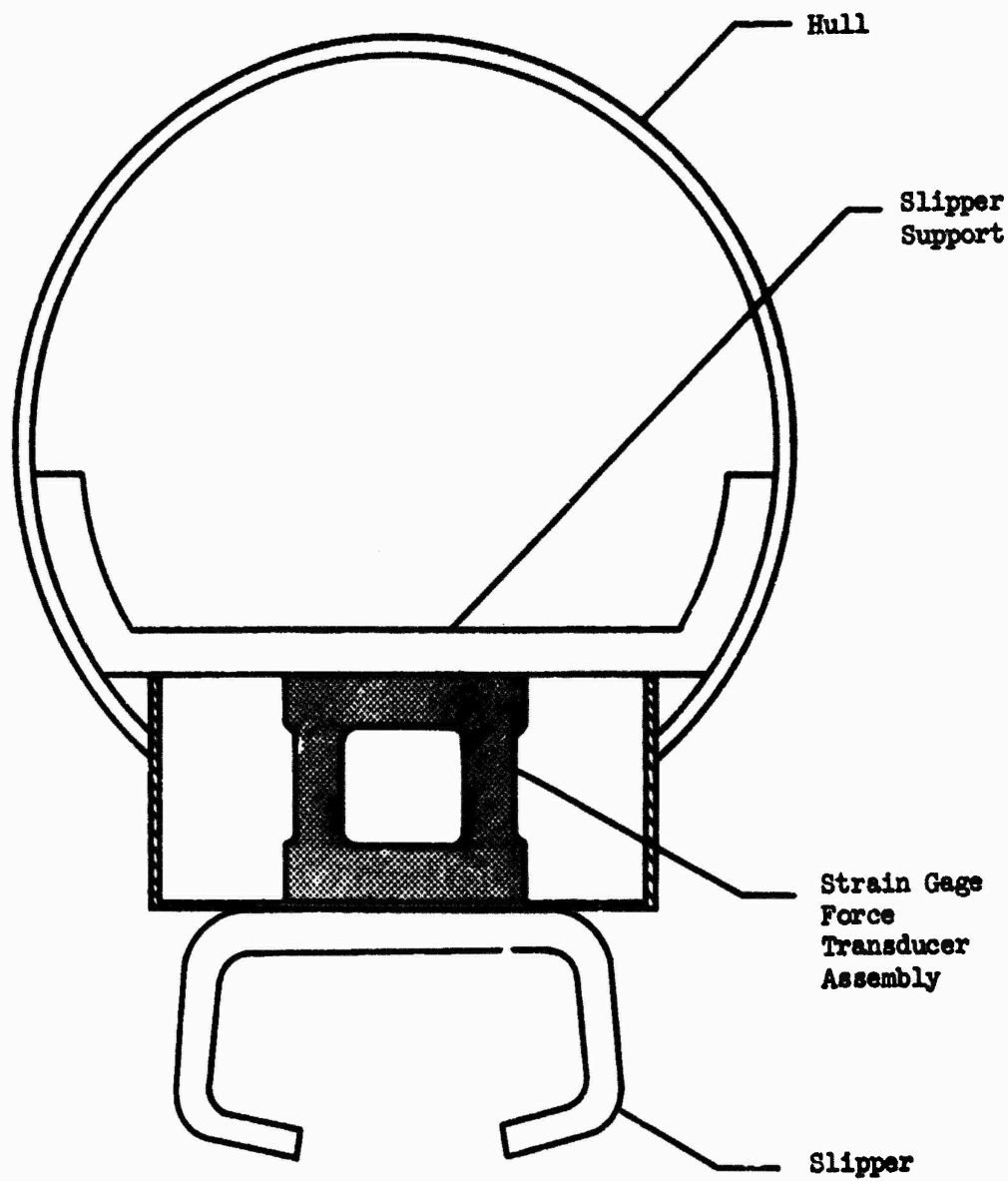


Figure 2.9. Installation of Force Transducer  
in Monorail Sled



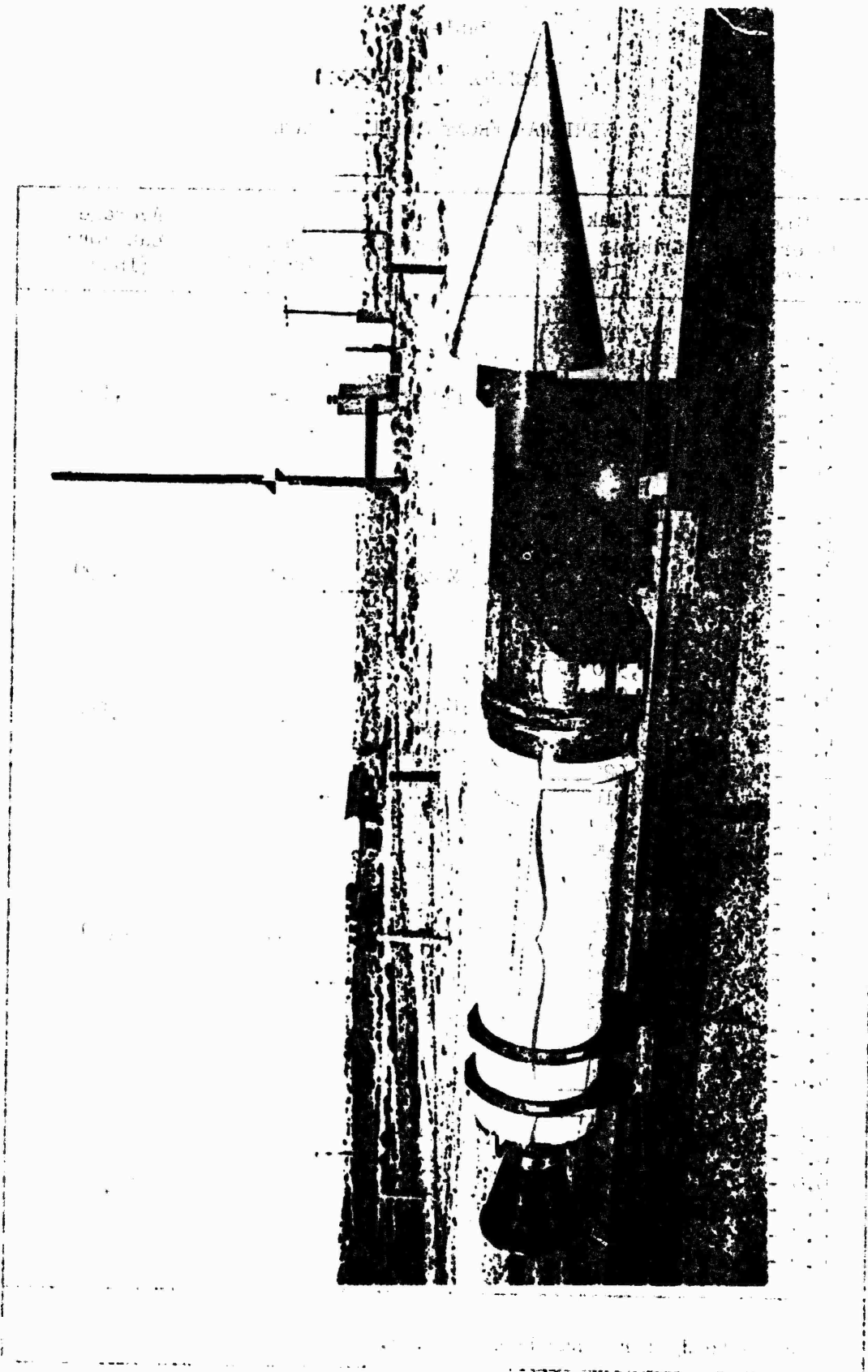


Figure 2.10. Modular Monorail Sled

Table I  
MODULAR MONORAIL  
53X - B2  
VERTICAL FRONT SLIPPER FORCE

Time Interval (sec)	Peak Dynamic Force* (lbs)	Period	V <sub>avg</sub> (ft/sec)	Average Peak Force (lbs)
2.7 - 2.8	18,740	Motor On	2,300	22,123
2.8 - 2.9	23,890			
2.9 - 3.0	20,410			
3.0 - 3.1	22,390			
3.1 - 3.2	21,110			
3.2 - 3.3	26,200			
3.4 - 3.5	15,160	Motor On	3,150	28,590
3.5 - 3.6	30,850			
3.6 - 3.7	33,800			
3.7 - 3.8	31,180			
3.8 - 3.9	25,810			
3.9 - 4.0	34,730			
4.0 - 4.1	24,540	Motor Burnout	3,450	30,800
4.1 - 4.2	26,000			
4.2 - 4.3	23,870			
4.3 - 4.4	42,570			
4.4 - 4.5	37,020			
4.5 - 4.6	16,910			
4.6 - 4.7	27,740	Coast	3,150	20,290
4.7 - 4.8	12,090			
4.8 - 4.9	21,940			
4.9 - 5.0	20,370			
5.0 - 5.1	22,265			
5.1 - 5.2	17,680			
5.2 - 5.3	19,750			
5.3 - 5.4	31,260			
5.4 - 5.5	16,710			
5.5 - 5.6	12,690			
5.6 - 5.7	24,060			
6.4 - 6.5	22,560	Coast	2,300	16,360
6.5 - 6.6	17,300			
6.6 - 6.7	17,410			
6.7 - 6.8	11,890			
6.8 - 6.9	19,930			
6.9 - 7.0	9,110			

\*Quasi-steady force has been removed.

- Loads are sensitive to velocity or at least to the variation in lift which is associated with velocity. The steady-state force on the front slipper at 2,300 fps was about 1,000 pounds upward, while at 3,150 fps it was about 2,200 pounds.
- Whatever happens when the motor burns out (the Modular Monorail used a Genie motor), it gives the sled a rough ride. The peak dynamic load of 42,570 pounds was experienced at burnout.

Figure 2.11 gives a rough idea of the sensitivity of loads to velocity and the relative magnitude of the peak load which occurred at burnout. Figure 2.12, showing a section of the Modular Monorail test data during the burnout phase, illustrates the nature of the phenomenon.

### 2.3.2 Instrumented Monorail

The Instrumented Monorail is a forebody, i.e., it has no on-board propulsion. It weighs 140 pounds and is 46 inches between slippers. Figure 2.13 shows it in its spike test configuration with its pusher.

Force transducers of the type shown in Figure 2.9 were mounted above the fore and aft slippers of the Instrumented Monorail.

Considerable data were taken from numerous Instrumented Monorail tests. These data are presented in Reference (2) as graphs of peak load versus Mach number. Front and aft vertical and lateral force data are reproduced from Reference (2) in Figure 2.14. It is explained in the reference that two peaks were taken from each quarter Mach number range of the test data. It was assumed that these data were extracted from both the boosted and coast phases of the tests. A few sets of time history data were available from the 44X-E2 test. They indicated that loads were no higher during boost phase than during coast.

### 2.3.3 Summary of Conclusions from Monorail Test Data

Despite the limited amount of data available, it seems safe to conclude that the principal source of monorail sled excitation is rail roughness. The stiff, high speed monorail sleds collide with the vertical and lateral "hills" of the test track and are subjected to forces equaling more than 150 times their weight. There is a strong correlation between steady-state lift and the amplitude of the impacts. An on-board thruster seems to increase dynamic load factors, especially at engine burnout.

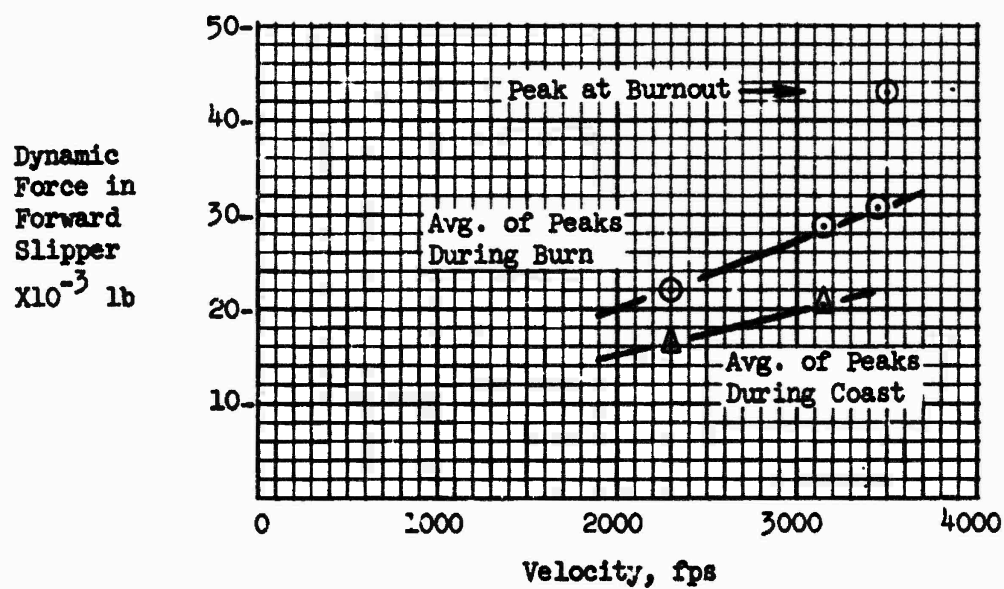


Figure 2.11. Modular Monorail, 53X-B2, Measured Forward Slipper Dynamic Forces

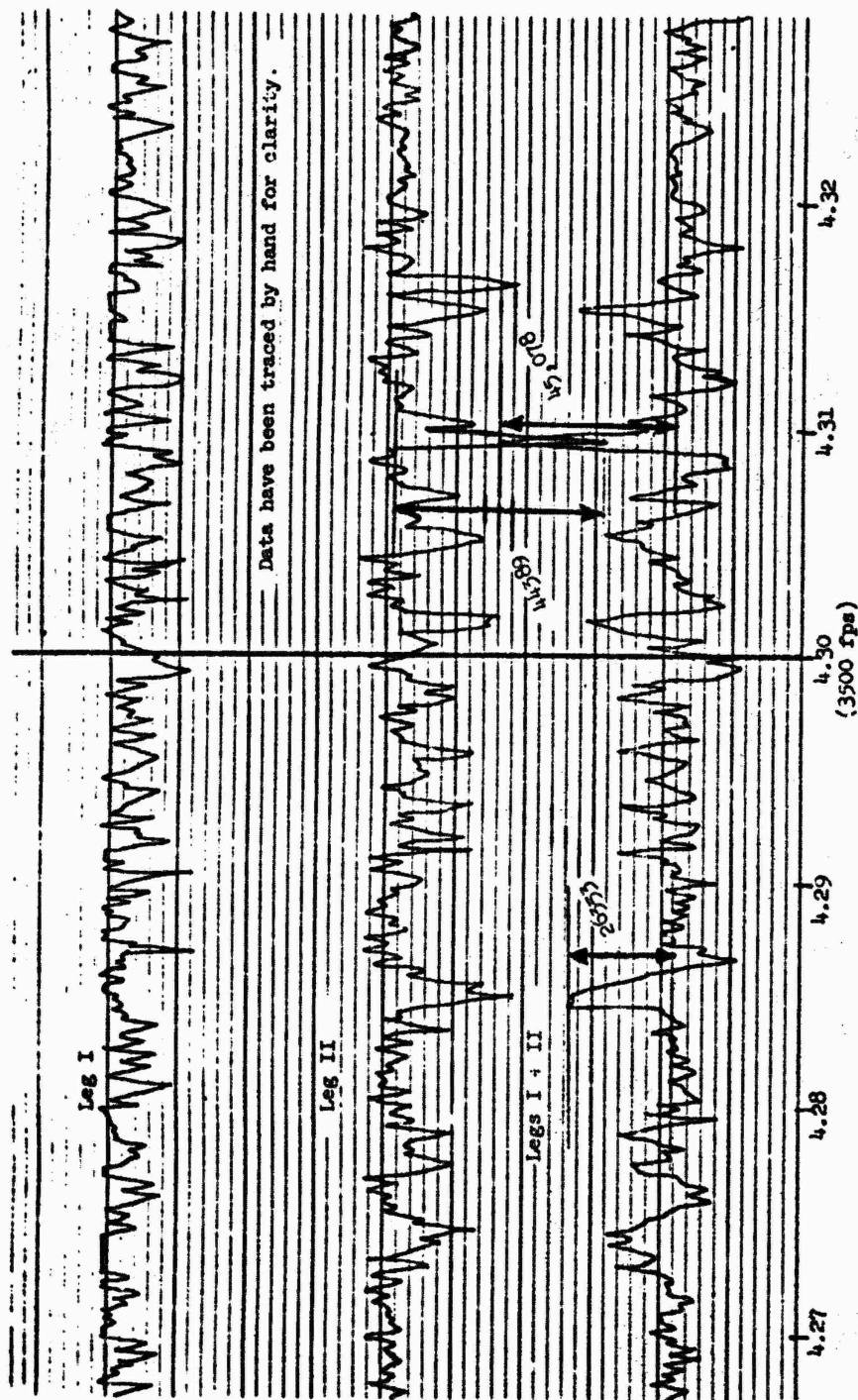
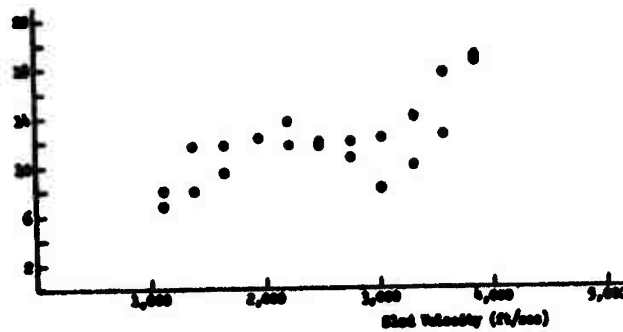


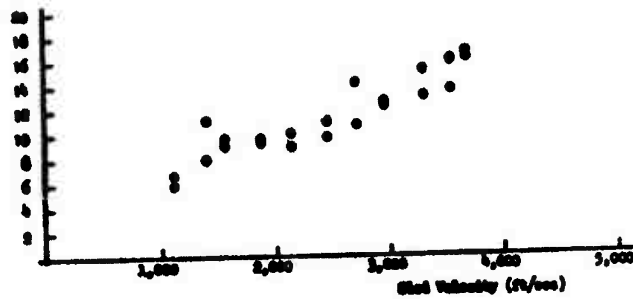
Figure 2.12. Modular Monorail, 53X-B2, Front Slipper  
Force Measurements at Burnout



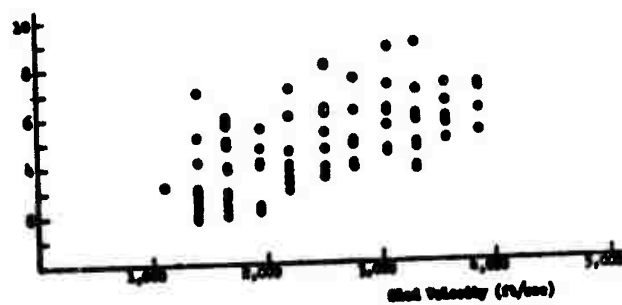
Figure 2.13. Instrumented Monorail with Pusher



Forward  
Slipper  
Vertical  
Kips



Aft  
Slipper  
Vertical  
Kips



Forward  
Slipper  
Lateral  
Kips

Figure 2.14. Instrumented Monorail Slipper Force Measurements,  
44X - E2, E8, Source: Reference (2)



## SECTION III

### FORMULATION OF MATHEMATICAL MODELS

#### 3.1 Nonlinear Dynamic Simulation of Dual and Monorail Sleds

Structural design analysis of sleds for the Holloman track has already become dependent upon the use of powerful finite-element computer programs. Statistical methods and quasi-steady multiple  $g$  loadings ( $\lambda$  factors (1, 2)) have been used to simulate the dynamic loading conditions experienced by test sleds. The desideratum in the current study was a computerized method for directly determining the inertial load distribution associated with test sled dynamic response. Most up-to-date finite-element programs include dynamic response capability, often by the modal method wherein the dynamic response of even very large, complex structures can be analyzed by the solution of decoupled single-degree-of-freedom equations. These methods, however, are all linear and preclude the inclusion of characteristics such as the slipper gap.

##### 3.1.1 Nonlinear Structural Response Theory

The bouncing high speed sled is not the only instance of a complex structural system subjected to rapidly changing boundary conditions. Recontact during staging of large launch vehicles has been studied extensively over the years in the aerospace industry. In that case, the modal method is used, but three sets of structural modes are employed: one for the joined stages, and one each for the separated stages. Each time contact or separation occurs, the equations are switched, one set of modes to another, and reinitialization must be carried out. If this method were used in the dynamic response analysis of sleds, at least four sets of modes would be used: one set associates with each combination of forward and aft slipper contact condition, i.e., fixed-fixed, free-fixed, fixed-free, and free-free. This is obviously not a practical approach.

A method has been developed which permits the continuous integration of one set of modal functions. The disadvantage is that the equations are no longer decoupled as in the classical modal approach, and hence, they must be integrated in time. This is not a great expense, however, because it has been found that a relatively limited number of modes suffices to give good distribution of inertial loads.

The method has been programmed for solution on the Control Data Corporation (CDC) 6600. The program, called SLEDYNE, is described in Section 3.1.2 and Appendix II. The user's manual is Appendix I.

##### Assumptions

The detailed development of the equations of motion is presented in Appendix II. The following discussion explains the important assumptions inherent in the equations. It is intended to give the user of SLEDYNE the insight he needs for intelligent use of the program.



The simulation is of pitch and bounce motion only. The equations do not include roll, yaw, lateral translation, or downtrack translation. Degrees of freedom beyond rigid body pitch and bounce modes account for dynamic structural response of the sled structure via its vibration modes.

One assumption characterizes the method and must be understood for appropriate use of SLEDYNE. The theory is based on the premise that it is possible to isolate two portions of the sled structure and call those the slipper stiffnesses. The stiffnesses transmit vertical forces only from the track to the remainder of the sled structure (when the slippers are in contact with the rail). Motion of the remainder of the sled, called the sled body, is defined in terms of a set of normal modes of vibration. These modes are computed for the sled body where the points of attachment of the slipper stiffnesses are restrained against displacement. This method, if properly employed, does not eliminate any essential behavior of the structure. Whatever stiffness is isolated out of the sled body by the restraints is included in the slipper stiffness, and vice versa.

#### Calculation of Slipper Stiffness

The practical problem of isolating the slipper stiffness from the structure of the sled body is illustrated in Figure 3.1. The approach is more straightforward for the dual rail sled because generally the sled body separates itself naturally from the slipper beam. In the case of the Single Mod sled, shown in Figure 3.1a, the slipper stiffness is the force which, when applied at the tie point between the sled body and slipper beam, causes the sled center-line to deflect one inch. Based on this definition, of slipper stiffness, the model used for calculating the sled body modes will be constrained with pin restraints at the corners of the bulkhead.

Figure 3.1b shows the instrumented monorail as an example of monorail sleds. In this case, the sled body was restrained at the points shown, and the stiffness of the structure from those points to the point of contact with the rail is calculated as the slipper stiffness. Since that may depend on whether the sled is riding on the slipper lips or the slipper base, the user must consider the quasi-steady lift forces. The large lift forces produced at the high velocities of monorail sleds almost always cause them to ride on the slipper lips.

#### Modal Representation in Simulation

In the simulation, the motion of sled is defined at any instant as the rigid body motion plus the response of the vibration modes (see Figure 3.2). Since the modes are defined with no deflection at the slippers, the slipper springs, the slipper gaps, and the rail roughness affect only the rigid body behavior. The vibration modes are excited by the rigid body response through the mass coupling terms. The important fact is that whether or not the slipper springs are in contact with the rail, the proper modes of vibration are being used. This is demonstrated in Table II in a comparison based on the Single Mod sled. The frequencies taken from SLEDYNE were calculated using the mass matrix (which does not change) and the stiffness matrix as it is, (a) when both slippers are in contact with the rail,

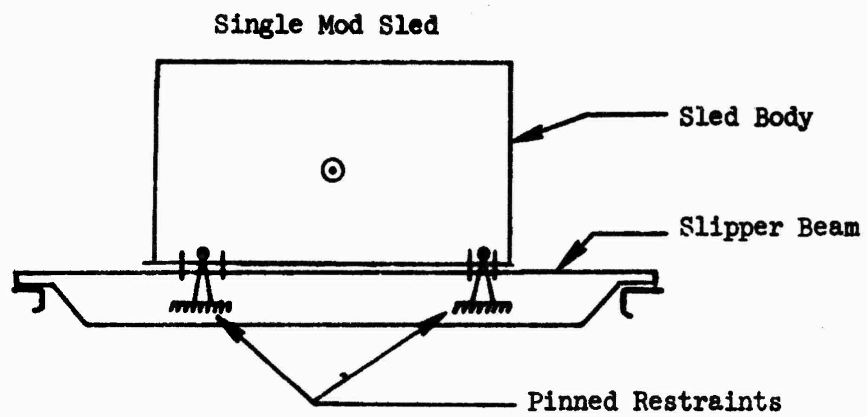


Figure 3.1a. Restraints Applied to Dual Rail Sled  
for Calculation of SLEDYNE Modes

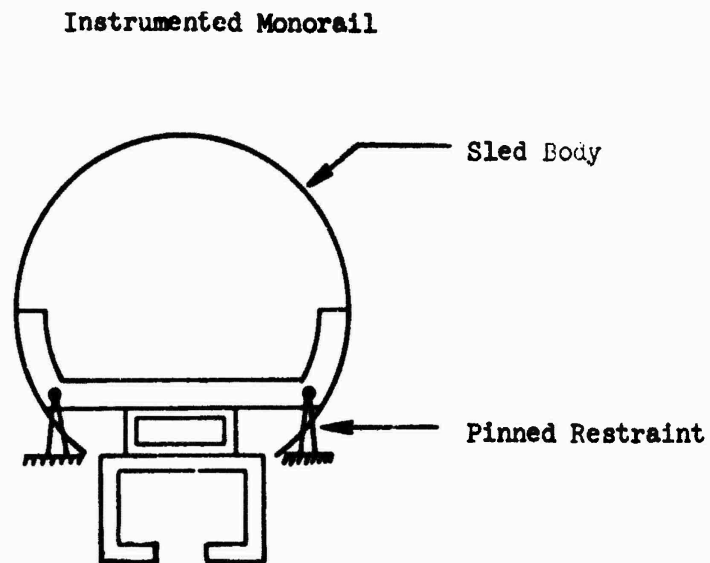
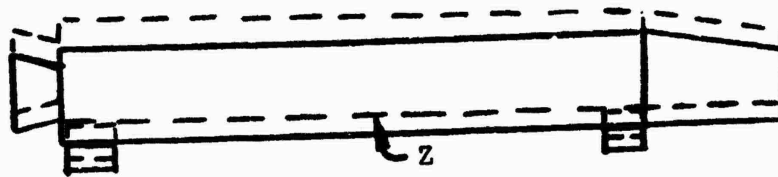
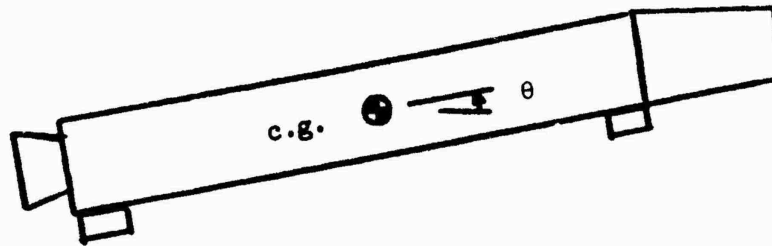


Figure 3.1b. Restraints Applied to Monorail Sled  
for Calculation of SLEDYNE Modes

Rigid  
Translation



Rigid  
Rotation  
About c.g.



Vibration  
Modes of  
Pinned-Pinned  
Sled Structure

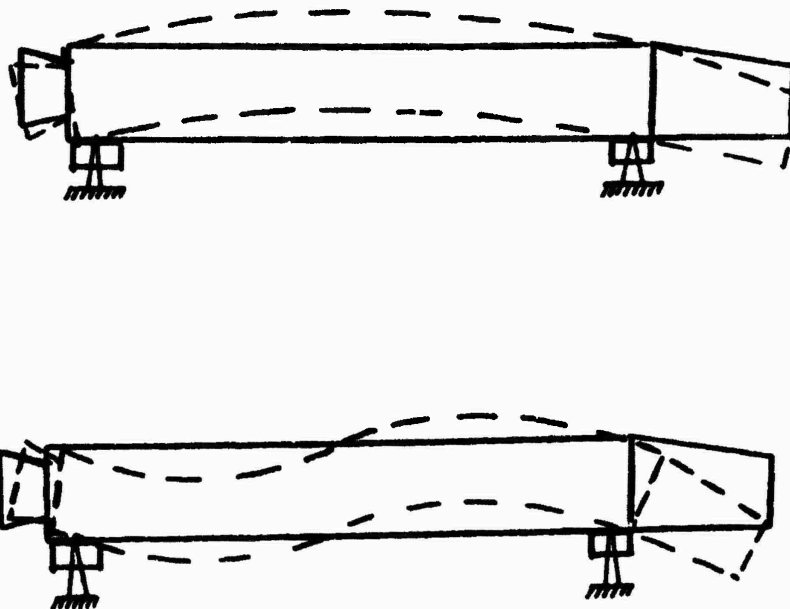


Figure 3.2. Displacement Functions Used In  
Nonlinear Dynamic Response  
Simulation

Table II  
COMPARISON OF SLEDYNE MODAL REPRESENTATION  
WITH "EXACT" STARDYNE MODES

	STARDYNE Modal Calculation	SLEDYNE* Equations
Fixed-Fixed	20.2	20.6
(Slippers in Contact with Rail)	27.6	27.9
	56.2	55.4
	125.1	124.6
	195.3	192.0
Free-Free	0.	0.
(Slippers in Gap)	0.	0.
	51.1	51.2
	121.7	122.9
	186.2	189.4
Single Mod Natural Frequencies - cps		

\*Based on two rigid plus five pinned-pinned vibration modes.

and (b) when both slippers are in the gap. For this comparison, the same 300 dof STARDYNE model which had been used to calculate the SLEDYNE modes were first restrained at the slippers, and then left free. Five modes (plus the two rigid body ones) were used in the SLEDYNE solution.

The method is seen to achieve a reasonable level of accuracy in representing various constraint conditions while using only one set of vibration modes. When considered that it is usually the lower modes of vibration that contribute most to structural response, the sufficiency of the method becomes even more convincing.

The importance of the structural vibration modes, especially for monorail sleds, was illustrated by a series of SLEDYNE runs using the Instrumented Monorail. Figure 3.3 shows how slipper loads are overpredicted when the sled body is rigid, i.e., when there are no modes. Addition of the structural modes permits some of the impact energy to go into deformation of the sled body hence relieving the slipper loads. This is, of course, what is happening on the track. Three percent damping is apparently a good estimate based on the underprediction of a five percent case.

### 3.1.2 Description of SLEDYNE

In essence, SLEDYNE is a nonlinear dynamic response analysis program which treats a very specialized problem -- a test sled bouncing along a rough rail while subjected to lift, drag and thrust forces. In practical application, it is a design tool providing a means for estimating the inertial loads to which a dual rail or monorail sled will be subjected by rail roughness excitation. The load vectors which are computed are due to dynamic response alone and must be superimposed on quasi-steady forces for analysis of design conditions. Moreover, since those dynamic loads are due to rail roughness only, factors are input so that the dynamic effects of motor transients and oscillating aerodynamics may be included. SLEDYNE's use in the Design/analysis process is described in Section 6.0. The user's manual is Appendix I.

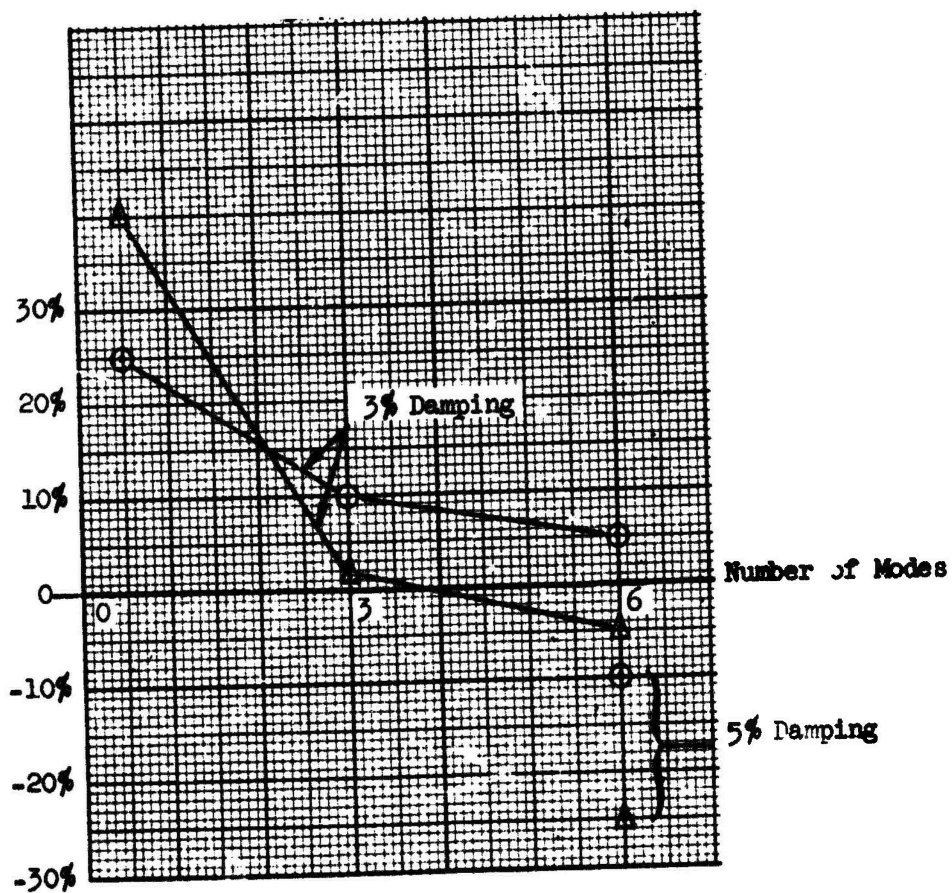
The rail roughness model used in SLEDYNE is based on a set of 440 measurements made of rail height on a 400 foot section of the Holloman test track. Mean height and slope were removed from these data (see Figure 3.4), and they were divided into ten segments such that the first and last value of each segment is zero. In SLEDYNE, these segments are placed randomly one after the other in order to generate a random rail of any required length. On the CDC 6600, the random number generates the same sequence of random numbers every time. This means that from the beginning of an execution, the same rail will always be generated.

One somewhat ambiguous factor deserves special mention here. The user specifies values of  $\zeta_z$  and  $\zeta_\theta$  which are the damping coefficients (percent damping) in the bounce and pitch equations. It is not meaningful to specify damping as a proportion of critical damping for these two modes because they are coupled. SLEDYNE adds the bounce and pitch damping effects, and then distributes them to the slippers in proportion to the slipper stiffness. The damping force acts only when the slipper is in contact the rail. The equations are presented and explained in Appendix II.

Error

○ Foreward Slipper

△ Aft Slipper



Flight Values Fore - 16,000 lbs  
Aft - 17,000 lbs

Figure 3.3. Percent Error In Calculated Results Compared With Test Data - Instrumented Monorail  
4000 fps ( $M = 3.6$ )

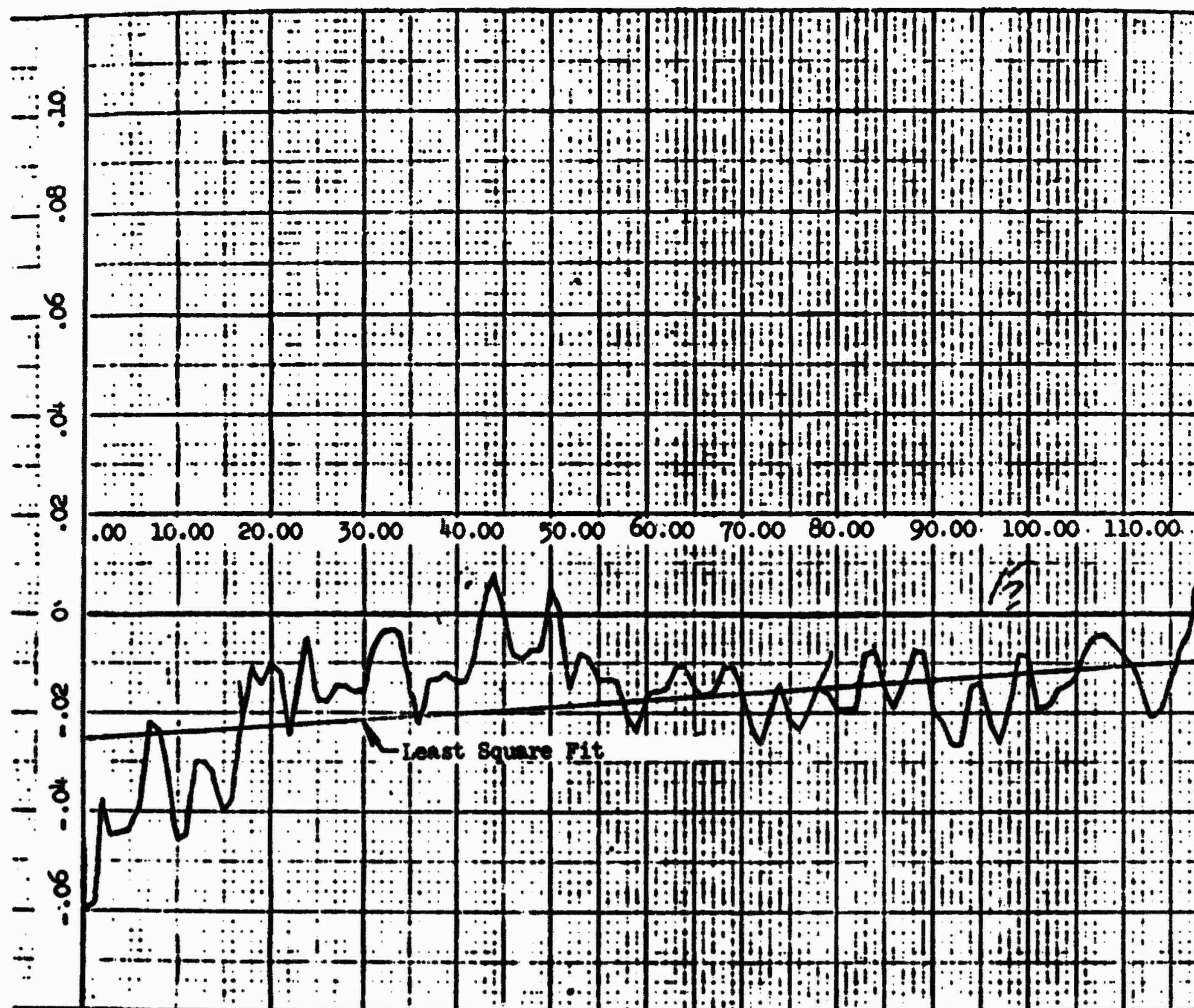


Figure 3.4. Section of Sample Rail Height Measurements (Both Scales Inches)

### 3.1.3 Comparison of Analytical and Test Results

#### Dual Rail Sleds

Since the SLEDYNE simulation contains the rail roughness as the sole source of excitation, it would be expected that correlation between its results and flight test data would hold only for coast. As explained in Section 2.1, engine transients and oscillating aerodynamics cause amplified dynamic response levels. Time history data were available only for the Gnu (6208) sled, and the Single Mod. Peak response levels for those two sleds versus SIMP are shown in Figure 3.5. The measured slipper forces have been doubled and are called slipper beam forces in the figure. Also plotted in the figure are peak responses observed in the two-second runs made with the SLEDYNE simulation. For both sleds, SLEDYNE underpredicts the response in the forward slipper beam and overpredicts that in the aft slipper beam. This discrepancy cannot currently be explained.

During the development of SLEDYNE several studies were made which led to the following conclusions:

- Dual rail sled response to rail roughness is not sensitive to velocity. Runs were made at velocities ranging from between 1,000 and 2,000 fps, and there was no significant variation in peak forces so long as the length of rail covered was held constant.
- Peak force is independent of the quasi-steady loads so long as they are great enough to hold the slippers in contact with the rail most of the time.
- Four thousand feet of track seems to be enough to give a nearly invariant peak. Runs made over longer sections of track occasionally gave higher loads but not significantly.

#### Monorail Sleds

Monorail sleds are quite different in their dynamic behavior from dual rail sleds. They go at higher velocity and are much stiffer, exhibiting higher frequency behavior. Slipper forces are a series of high amplitude impact spikes. Their wide dispersion in amplitude precludes the possibility of predicting absolute peak values through simulation. A method was adopted which was based on Nixon's (2) scheme for reducing data from the Instrumented Monorail tests. He extracted the peak slipper force from each quarter Mach number velocity range. During the acceleration phase, that corresponded to about .1 second intervals. This was done for several runs giving a number of peak amplitudes for each value of Mach number. These were averaged and plotted as average peak versus Mach number. The analogous method used with the computer simulation is to make a run of constant velocity and look at the peak amplitude in each .1 second interval. A run of 1.0 second, for example, yields ten values which are then averaged.

Table III compares data taken from the forward slipper of the Modular Monorail and the forward and aft slippers of the Instrumented



$$SDP = \left[ \frac{KM}{1 + \frac{M^2}{I}} \right]^{1/2}$$

M = Sled Mass  
 I = Sled Pitch Inertia  
 K = Slipper Beam Stiffness  
 L = Distance from C.G. to Slipper Beam

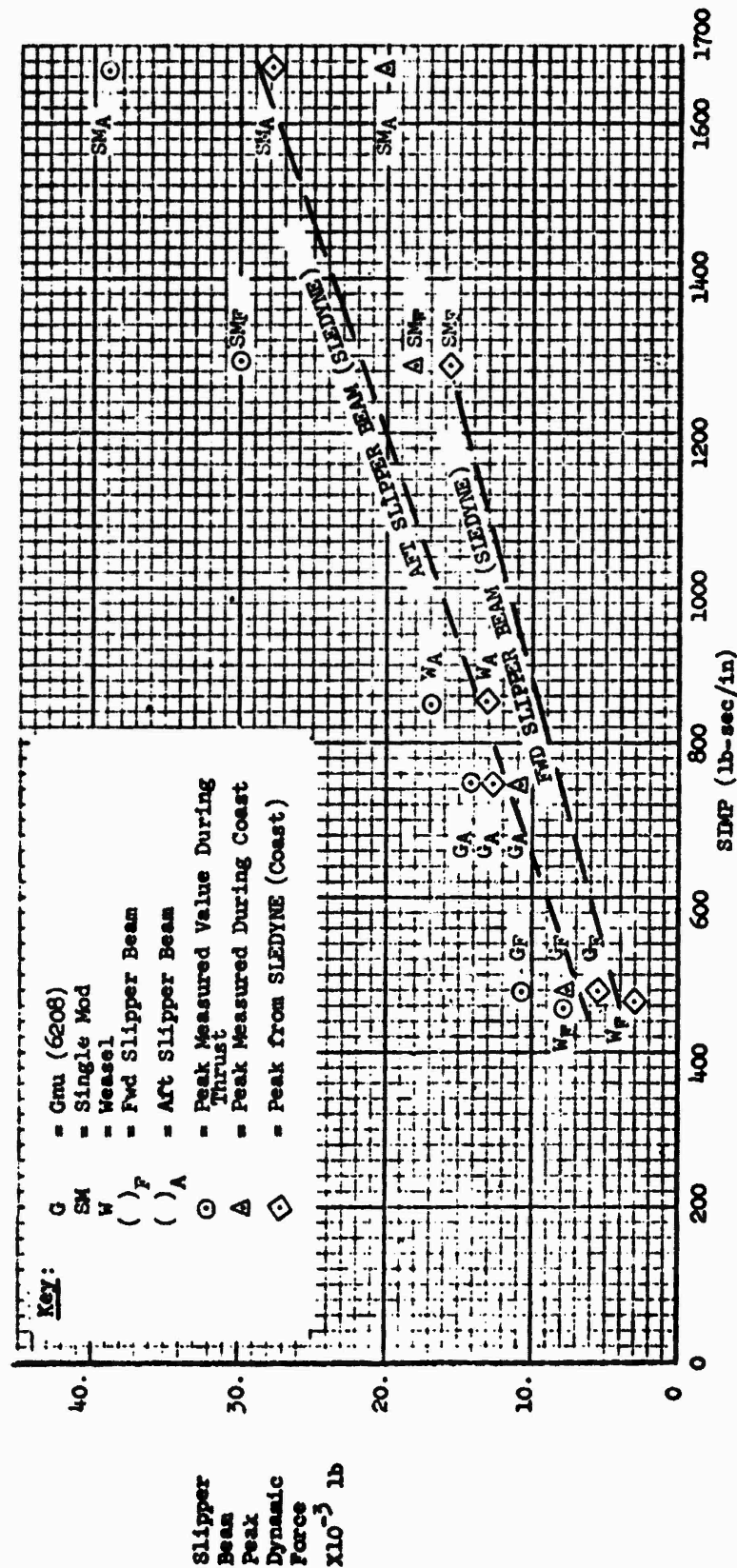


Figure 3.5. Comparison of SLEDYNE Results with Test Track Data Dual Rail Sleds

Table III

COMPARISON OF SLEDYNE RESULTS WITH TEST TRACK DATA  
MONORAIL SLEDS - VERTICAL FORCE DURING COAST (lbs)

Vehicle	Velocity (fps)	Average of Peaks*		Peak	
		SLEDYNE**	Test	SLEDYNE**	Test
Modular Monorail (fwd)	3400	21,800	22,280	34,900	30,240
Modular Monorail (fwd)	2300	18,430	17,700	29,000	23,720
Instrumented Monorail (fwd)	4000	16,610	16,000	20,680	16,000
Instrumented Monorail (fwd)	2900	13,270	12,500	19,860	14,000
Instrumented Monorail (aft)	4000	16,520	17,000	23,280	19,000
Instrumented Monorail (aft)	2900	13,400	13,600	17,820	12,000
*Average of peaks measured in .1 second intervals					
**Three percent damping, six vibration modes					

Monorail with SLEDYNE results. The SLEDYNE calculations included six modes of vibration and three percent damping. Comparison by the averaging method is good, whereas absolute peak values do not agree well. Note that the peaks shown for the Modular Monorail came from the coast phase and that peaks from engine burnout were 50 percent higher.

A typical monorail slipper force time history is shown in Figure 3.6. It was calculated by SLEDYNE for the Modular Monorail at 3,500 fps using five modes of vibration. In comparing Figures 3.6 and 2.12, one notices that the calculated impacts are of considerably longer duration than the measured. Mixon's data (2) shows the same discrepancy for which no explanation has yet been found. Whatever the cause of the discrepancy, however, the peak forces show good agreement between test and analysis.

### 3.2 Simplified Impact Model for Monorail Sleds

As explained in Section 2.2, monorail sleds experience large, discrete impacts with the rail. Typically, each monorail slipper impacts the rail independently. Furthermore, the force in one slipper is usually maximum while the other slipper is in the gap. These phenomena suggested that monorail sleds could be analyzed using a simplified model of the sled where one slipper at a time impacts the rail. Based upon this conjecture, a method was developed for analyzing monorail sleds using an impact model.

In this technique, a structural model of the sled is impacted vertically on one slipper against a rigid surface. The impact velocity is the principal factor that determines the resulting structural loads.

The important parameters in choosing the impact velocity seem to be sled velocity, lift-to-weight ratio, and the impact duration. The objective is to correlate test data with these parameters and in so doing, develop a technique for predicting the required impact velocity.

This model to be used for vertical loads is illustrated in Figure 3.7, which shows the pertinent response parameters. The same procedure is used for lateral loads.

Application of this method of analysis requires two major computations: (a) determination of the effective impact frequency; and (b) determination of the sled loads resulting from the prescribed impact. Two methods for performing these computations are described in the following sections.

#### 3.2.1 Procedure A

This procedure is easiest to use but is not as accurate as Procedure B. The sled is idealized as a rigid body supported on springs. Effective impact frequency,  $f$ , can be expressed in terms of the impacting spring stiffness,  $K$ , and an effective mass,  $M_{eff}$ , i.e.,

$$f = \frac{1}{2\pi} \sqrt{\frac{K}{M_{eff}}} \quad (3.1)$$

Modular Monorail Sled  
 V = 3400 fps  
 No. Modes = 5

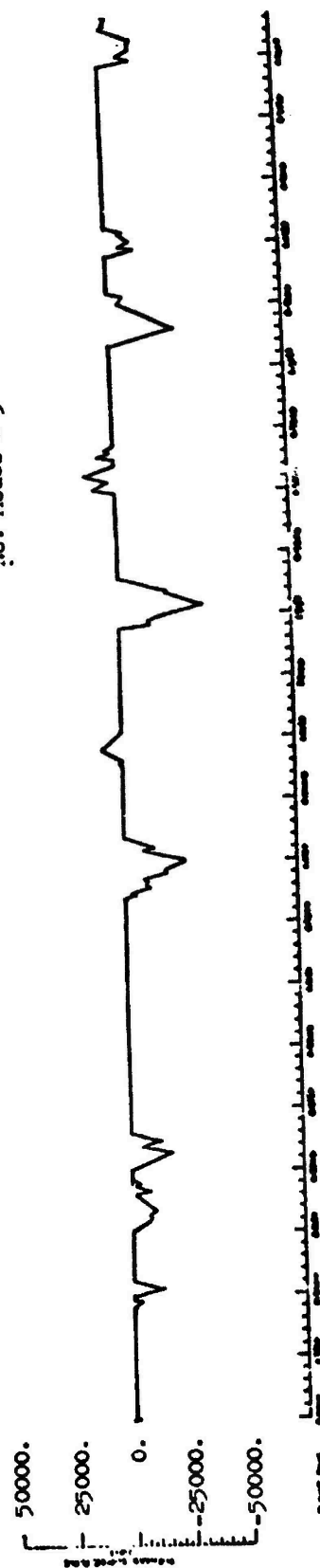
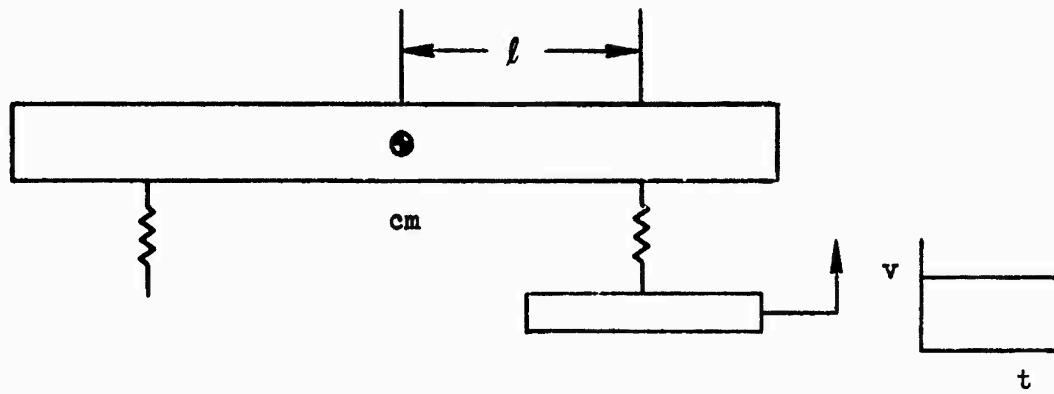
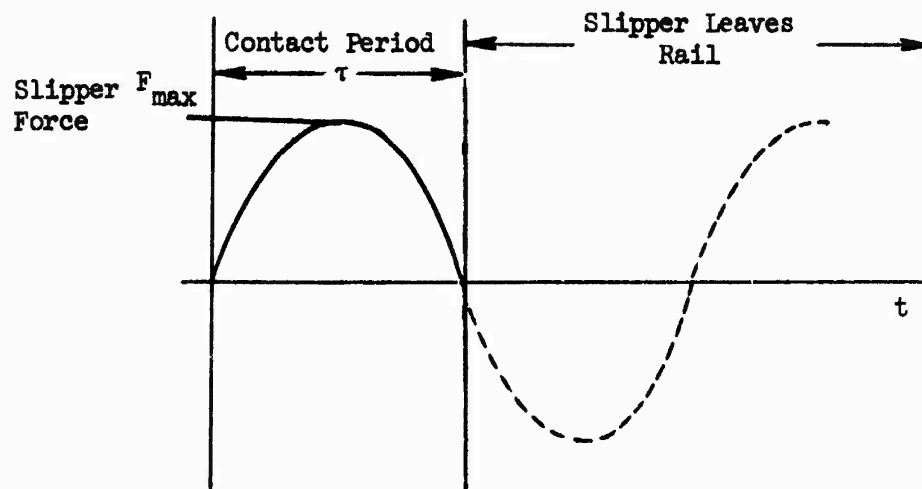


Figure 3.6. Time History of Vertical Force from SLIDING Modular Monorail -- Forward Slipper, 3400 fps



Impact equivalent to step velocity  $v$  imparted to contacting slipper



$F_{\max}$  = maximum slipper force

$f = \frac{1}{2\tau}$  = effective impact frequency

Figure 3.7. Impact Model for Monorail Sleds

where (see Figure 3.7):

$$M_{\text{eff}} = \frac{M}{1 + \frac{Ml^2}{I}} = \text{effective mass} \quad (3.2)$$

$K$  = impacting slipper and support structure stiffness

$M$  = sled mass

$I$  = sled moment of inertia

$l$  = distance between center of mass and impacting slipper

Slipper and associated support structure stiffness can be determined as shown in Figure 3.8. In Figure 3.8a the slipper is pinned to the rail; in Figure 3.8b the slipper is constrained against translations and roll moment. Stiffness is defined as the force in pounds which causes a one-inch displacement between the rail and the sled "main body."

Careful judgement should be exercised in determining the force which causes unit deflection of the sled center-line. Unlike dual rail sleds, the flexibility of typical monorail sled bodies is on the order of the flexibility of the slippers. Significant flexibilities in slipper support structure which contribute to deflection between the sled "main body" and the track should be included in the calculations. By ignoring flexibility of the sled body, the effective impact frequency will be overestimated and a conservative estimate of dynamic loads will result.

The impact velocity  $v$  can be determined as a function of  $f$ ,  $L/W$  computed for the impacting slipper (see Figure 3.9), and sled velocity  $V$ , as explained in Section 3.2.3.

The peak slipper force is given by

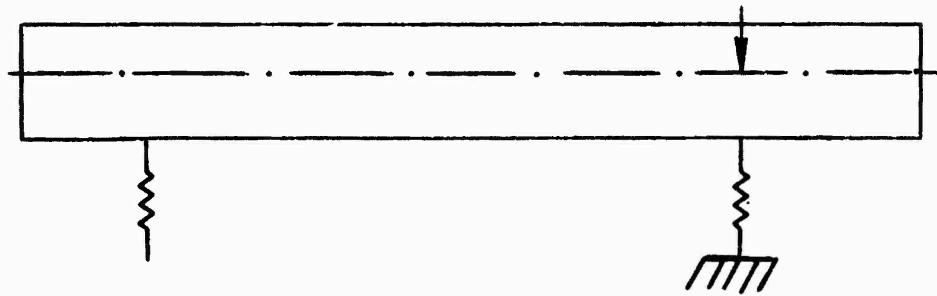
$$F_{\text{max}} = 2\pi f v M_{\text{eff}} \quad (3.3)$$

The resulting acceleration responses are given by

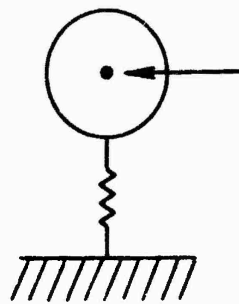
$$\begin{aligned} \ddot{z} &= F_{\text{max}}/M \\ \ddot{\theta} &= F_{\text{max}}l/I \end{aligned} \quad (3.4)$$

where  $\ddot{z}$  and  $\ddot{\theta}$  are the translational and rotational accelerations, respectively, of the center of mass.

Distribution of these loads over the sled for the vertical case is illustrated in Figure 3.10.

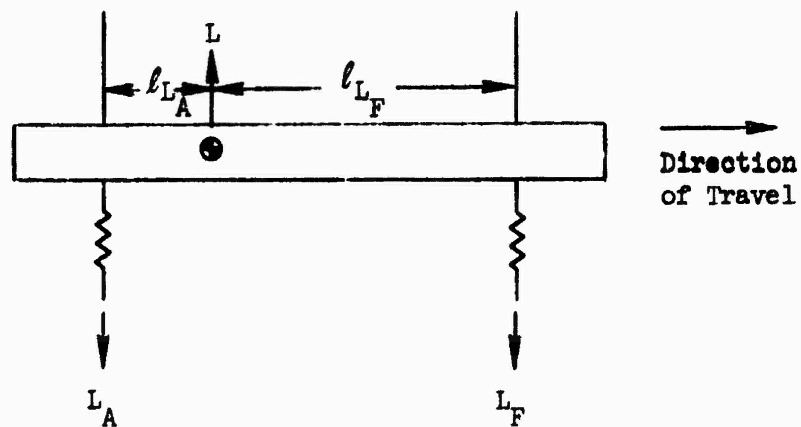
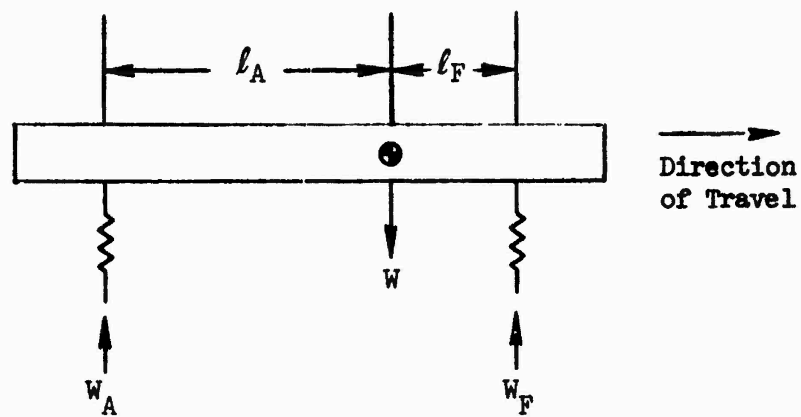


(a) Vertical



(b) Lateral

Figure 3.8 Models for Computing Slipper and Support Structure Stiffness



$$\frac{L_A}{W_A} = \frac{l_{L_F}}{l_F} \frac{L}{W}$$

$$\frac{L_F}{W_F} = \frac{l_{L_A}}{l_A} \frac{L}{W}$$

Figure 3.9. Distributions of Sled Weight and Lift Force



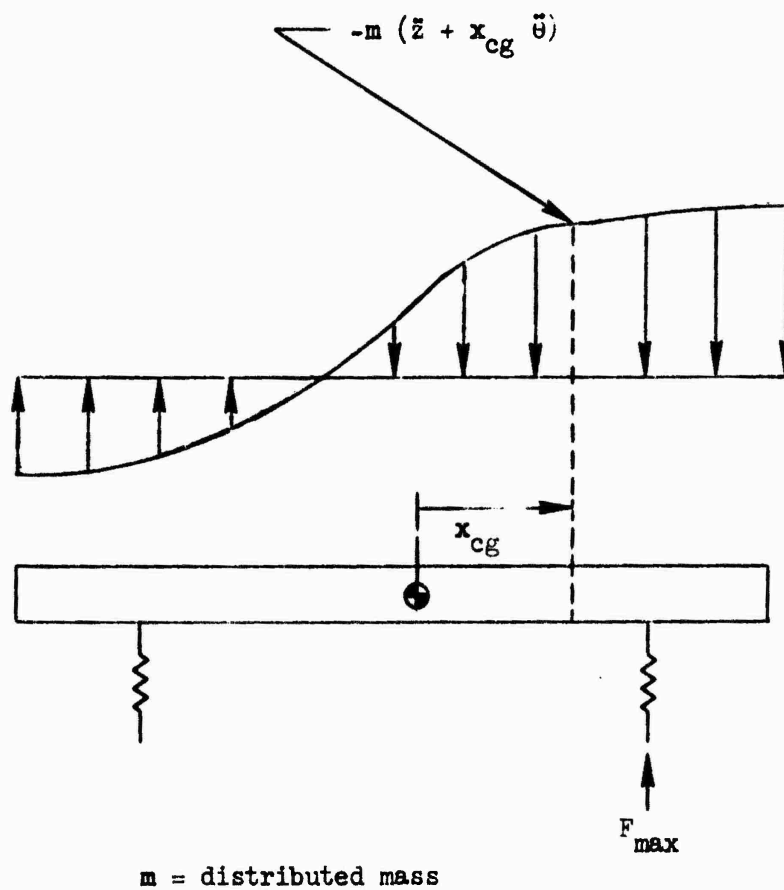


Figure 3.10. Distribution of Impact Acceleration

For predicting maximum dynamic loads, the foregoing procedures should be applied to both the forward and aft slippers in both vertical and lateral directions.

### 3.2.2 Procedure B

This procedure should provide more accuracy in predicting preliminary dynamic loads.

A preliminary simplified finite-element model of the sled with one slipper constrained and the other slipper free is used with a program, such as STARDYNE, to determine natural modes and frequencies.

Next, using a dynamic response program, such as DYNREL, a unit step velocity is applied to the constrained slipper and the following items are computed:

- a. The force-time history of the contacting slipper.
- b. The contact period and the associated effective impact frequency, as shown in Figure 3.7. If the time of the peak force  $\tau_{\text{peak}}$  is different from  $\tau/2$ , compute an effective impact frequency based on the average; i.e.,

$$f = \frac{1}{2} \left( \frac{1}{2\tau} + \frac{1}{4\tau_{\text{peak}}} \right) \quad (3.5)$$

See Figure 3.11.

- c. The load distribution at the time of maximum slipper force.

The impact velocity  $v$  is then determined, as in Procedure A, and the loads obtained for the unit impact velocity are multiplied by  $v$  to obtain the peak dynamic loads.

### 3.2.3 Determination of Sled-Rail Impact Velocity

It was postulated that the impact behavior of a monorail sled and hence, the impact velocity required for peak loads, could be approximated by flight simulations using a nonlinear single-degree-of-freedom model for the sled-rail system. The model (Figure 3.12) consists of a mass, a spring, a linear dashpot, a slipper with a gap, and a simulated rail. The frequency of the model corresponds to the effective impact frequency of the sled impacting on one slipper as described in the previous two sections. The dashpot does not represent actual structural damping but, rather, accounts for the dissipation of energy into the various vibration modes of the sled. The operational parameters include the sled velocity,  $V$ , and the lift-to-weight ratio  $L/W$ . The same model is used for lateral impacts by setting the ratio  $L/W = 1$ . Simulation of a flight was accomplished by the identical procedure as that used in SLEDYNE (Section 3.1.2) except for the simplified sled model.

The foregoing procedure was used to generate the impact velocity curves of Figure 3.13. A critical damping ratio of 0.10 was selected, based on comparisons of predictions and flight data for the Instrumented Monorail

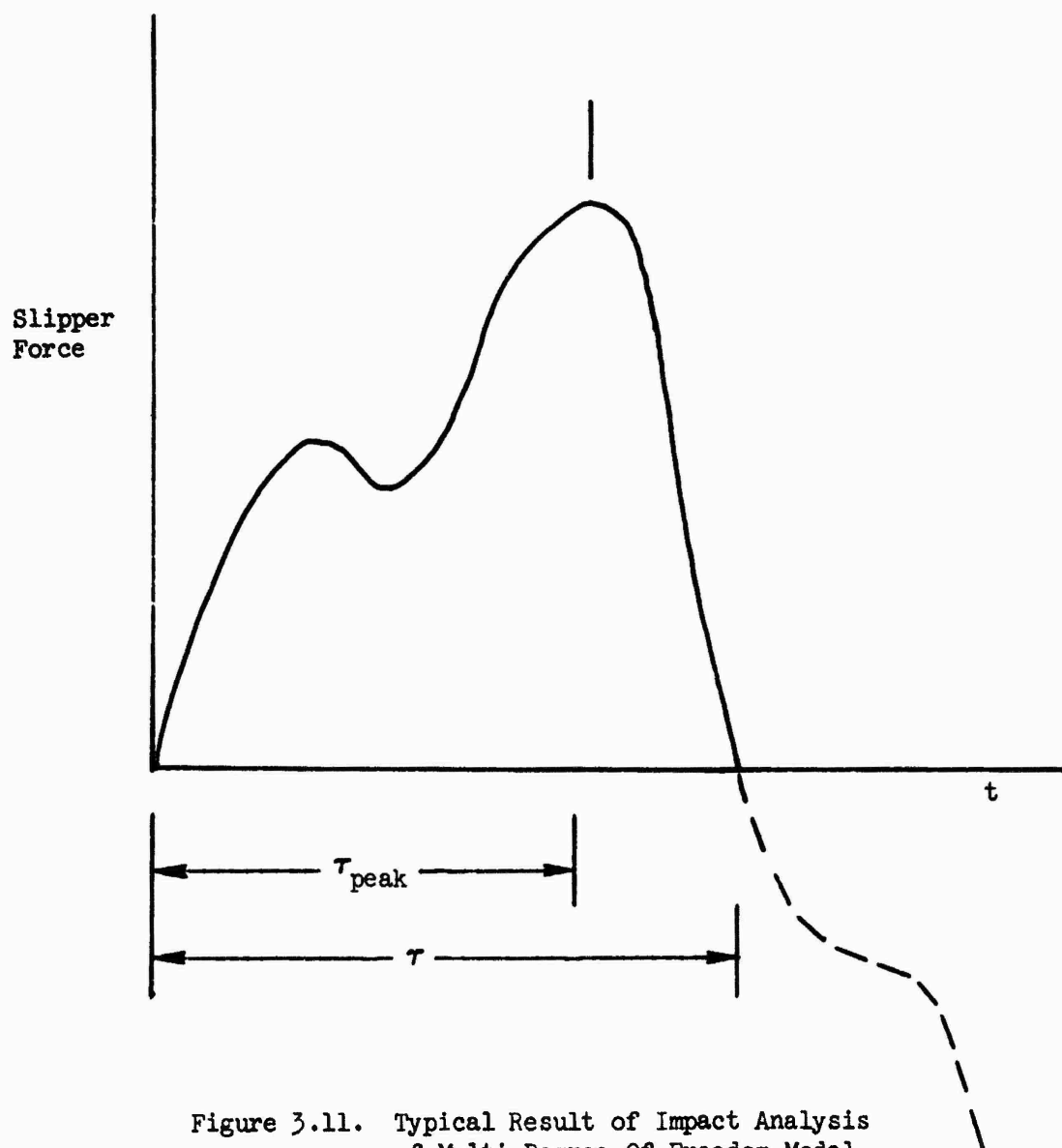


Figure 3.11. Typical Result of Impact Analysis of Multi-Degree-Of-Freedom Model

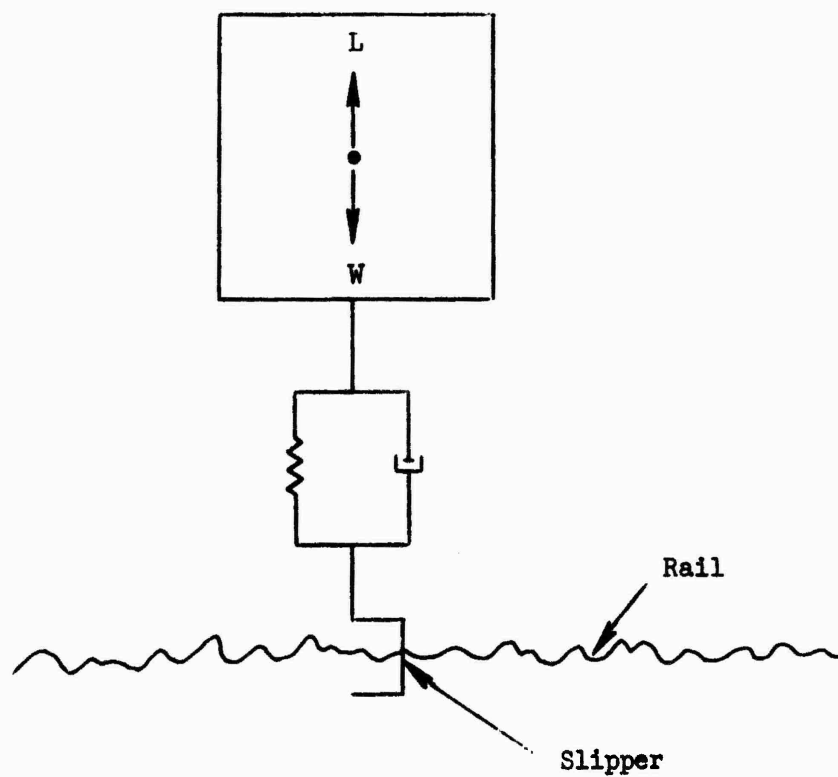


Figure 3.12. Single-Degree-of-Freedom Model  
Used for Design Curves

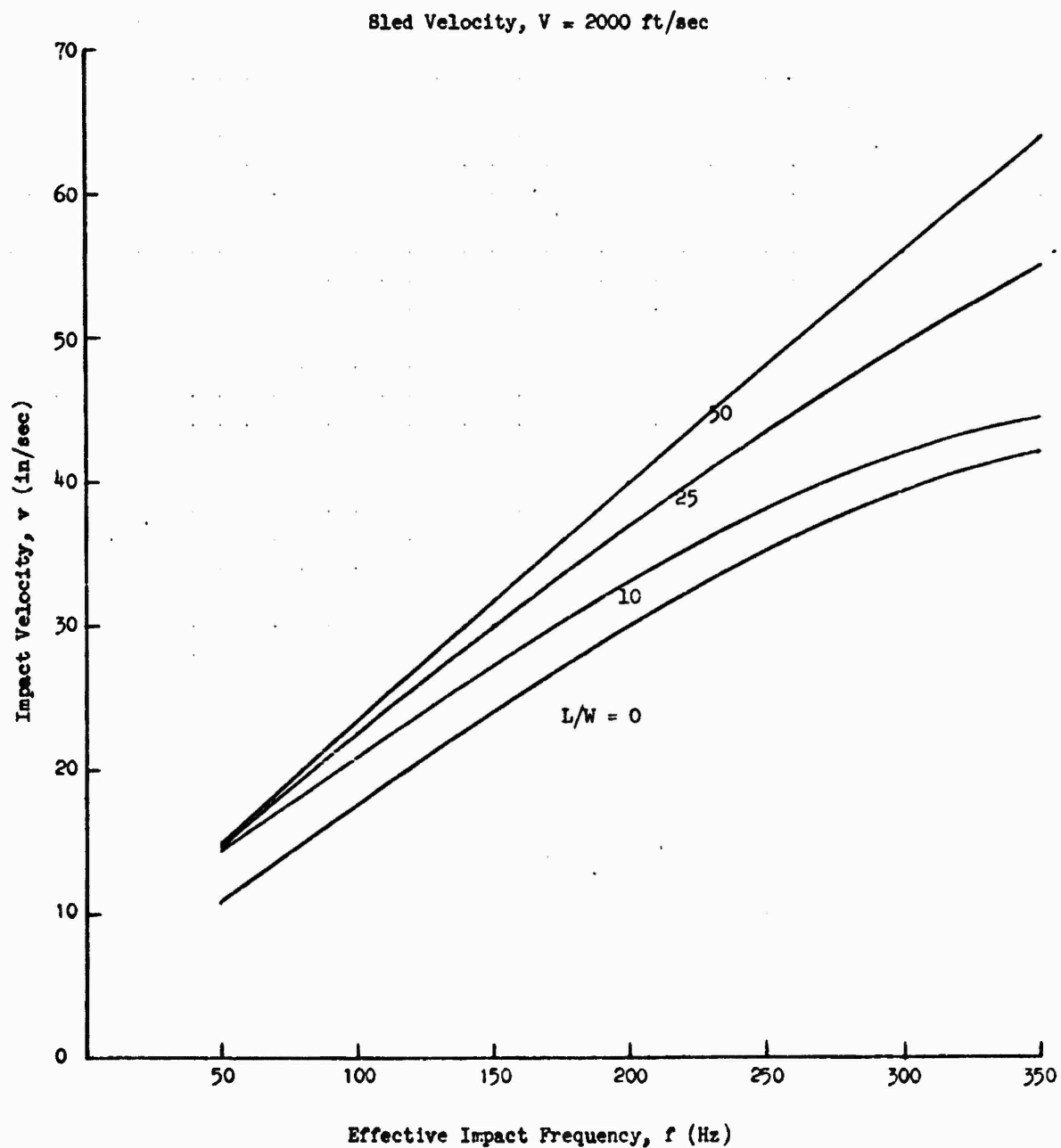


Figure 3.13. Impact Velocity For Monorail Sleds

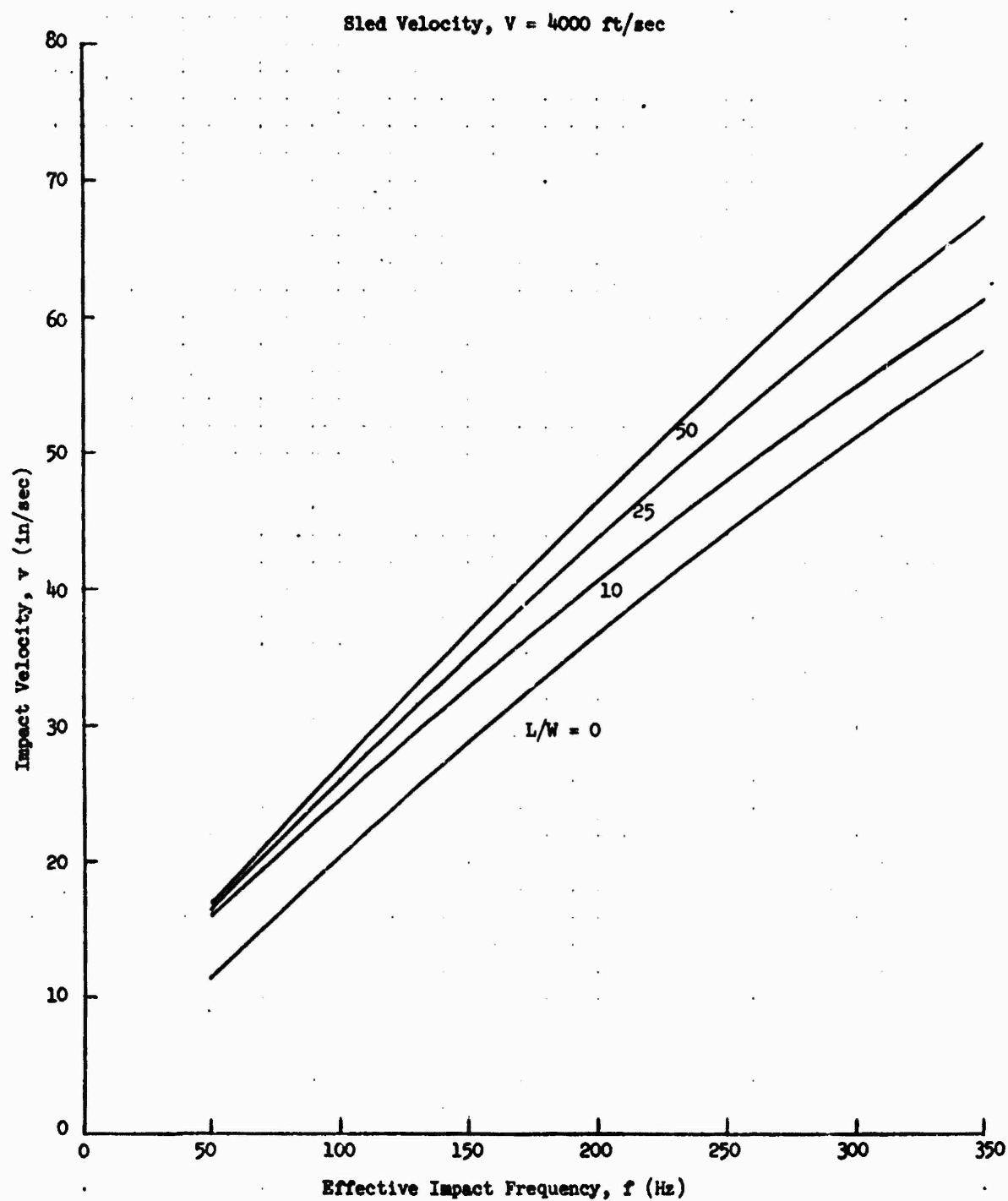


Figure 3.13. Impact Velocity For Monorail Sleds (Continued)

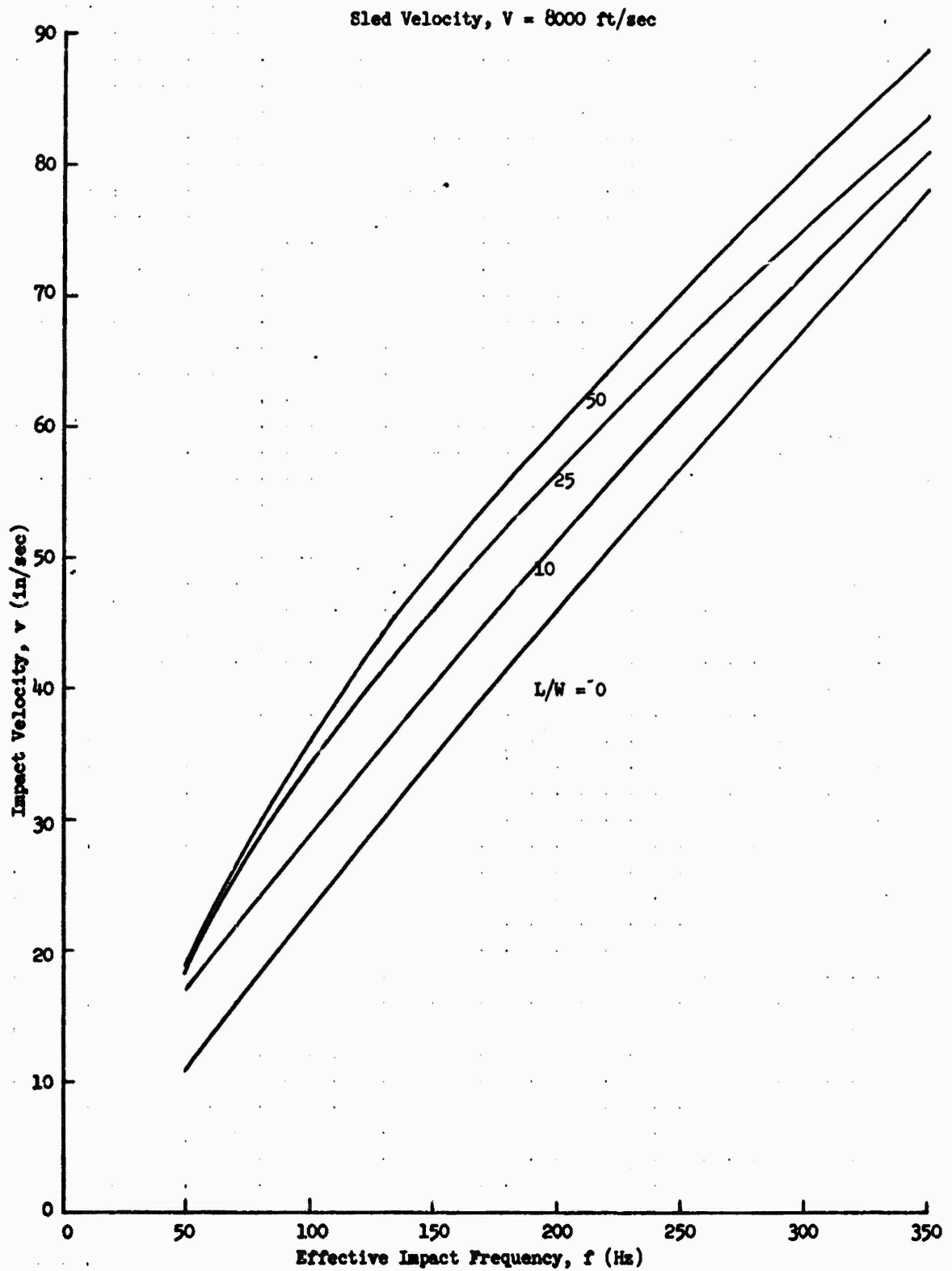


Figure 3.13. Impact Velocity For Monorail Sleds (Continued)

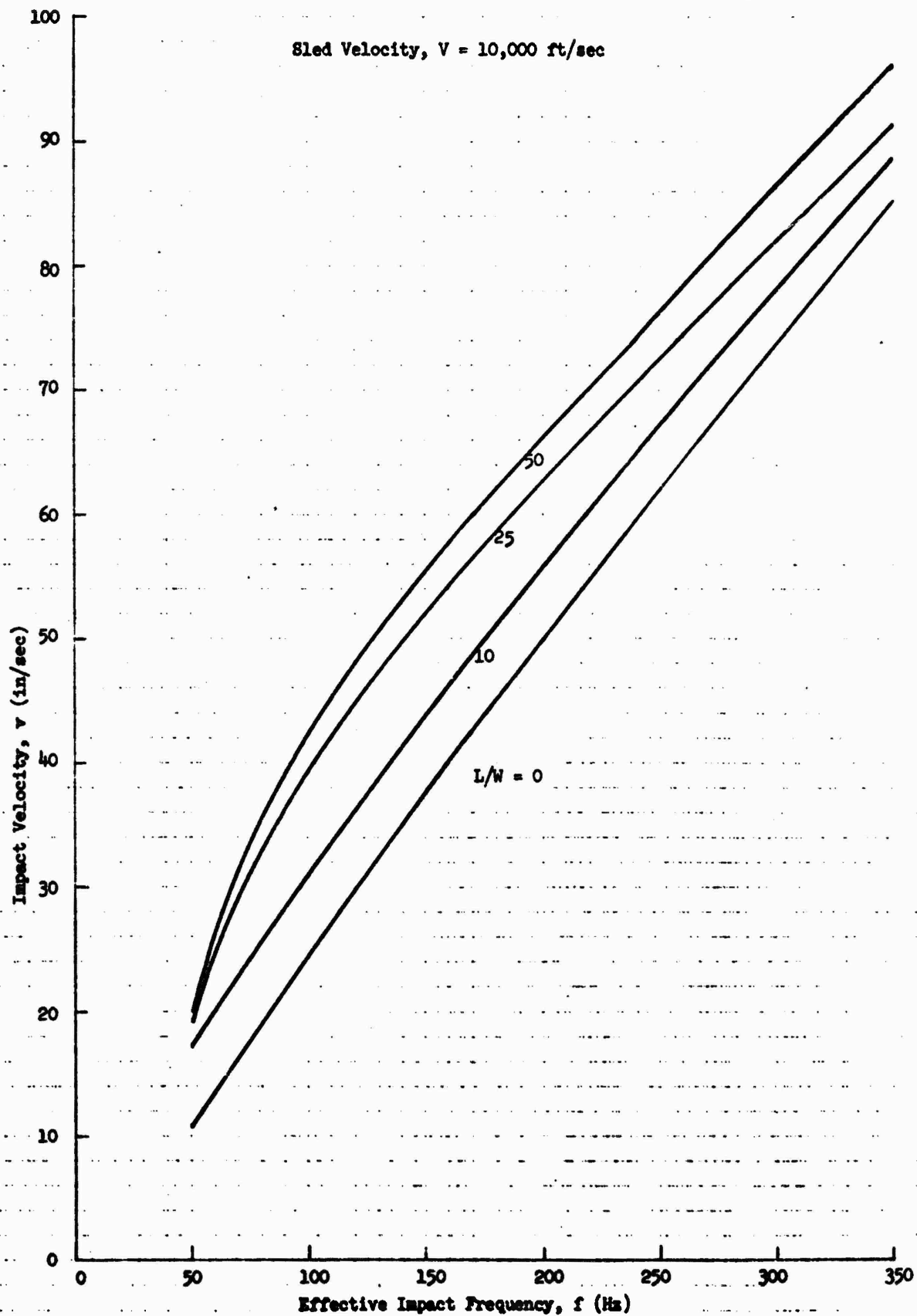


Figure 3.13. Impact Velocity For Monorail Sleds (Continued)



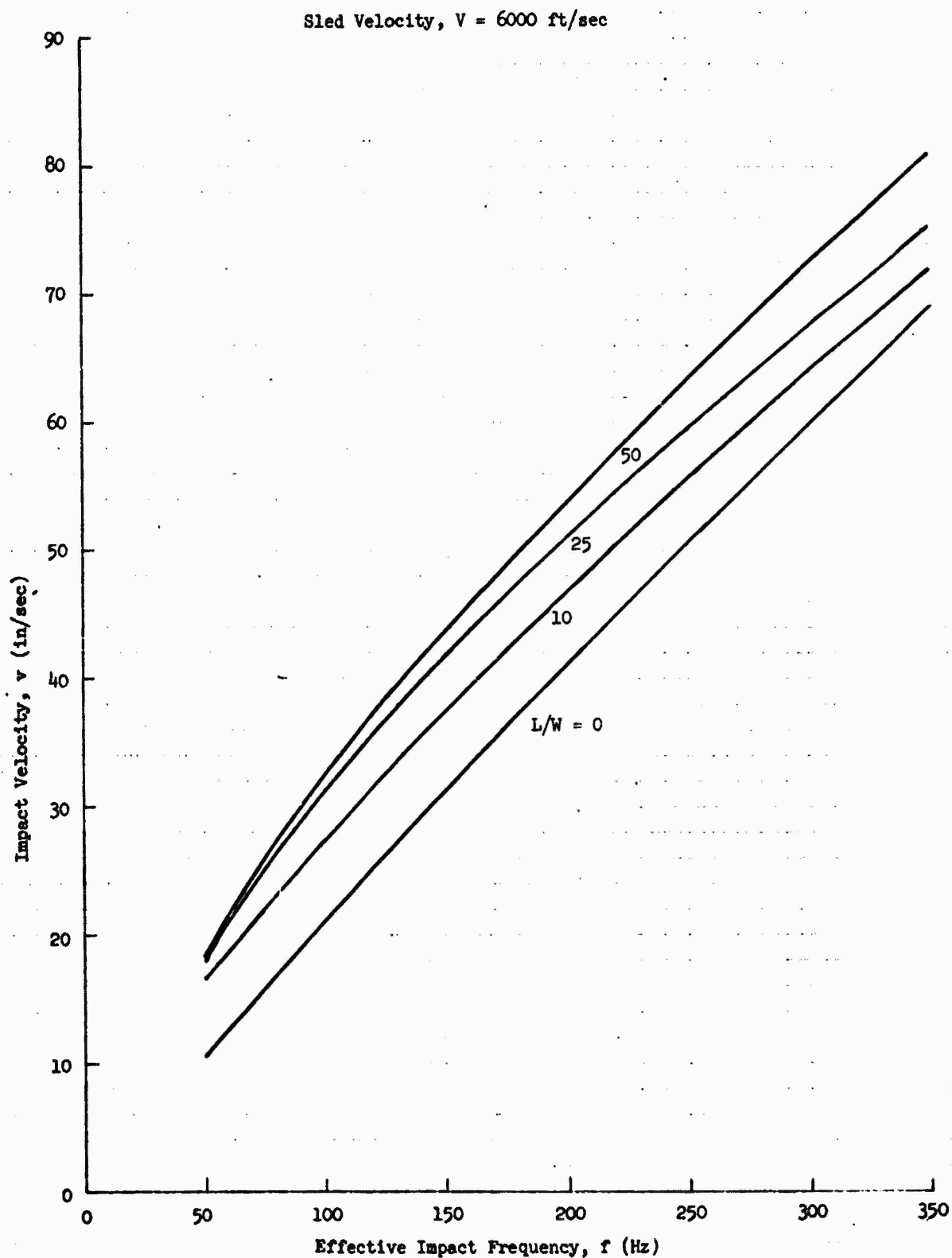


Figure 3.13. Impact Velocity For Monorail Sleds (Continued)

and the Modular Monorail sleds using Procedure B of Section 3.2.2. These predictions and comparisons are summarized in Section 3.2.4. For each combination of parameters, four 4,000 foot simulated flights were made and the average of peak loads in each 0.1 second interval was determined. Significant statistical variations were apparent in the resulting peak loads even with 4,000 foot flight distances. The data were cross-plotted and smoothed to produce the curves of Figure 3.13. Thus, the quantity  $v$  represents an impact velocity which can be used to predict average peak loads in a flight, but it does not predict the value of the highest peak.

#### 3.2.4 Examples and Comparison with Flight Data

The foregoing procedures are illustrated, in part, for the Instrumented Monorail and Modular Monorail Sleds. Results are compared with flight data.

##### Instrumented Monorail

Coast phase dynamic loads resulting from impacts on the forward slipper were predicted using Procedure B (Section 3.2.2).

##### Vertical Loads

The finite element model for the vertical loads is illustrated in Figure 3.14. This is the same as Model 1 of Reference (2), except for the boundary conditions. In the present case, the forward slipper is pinned to the rail and the aft slipper is free. Modes and frequencies were computed by STARDYNE.

Response to a step velocity of one inch per second was determined using DYNREL with nine flexural modes. For this example, only the load history in the forward slipper was determined. Pertinent parameters are shown in Figure 3.15. For design purposes all the loads of interest would, of course, be determined. The peak vertical force is 339 pounds and the contact period is .0016 second, corresponding to an effective contact frequency,  $f = 312$  Hz.

Lift-to-weight ratios were determined for various velocities from Reference (2), page 225, as follows:

Total weight,  $W = 132.9$  pounds

"Forward slipper weight",  $W_F = 71.8$  pounds

Sled Forward Velocity, $V$ (fps)	Lift on Forward Slipper, $L_F$ (lb)	$L_F/W_F$
1000	-200	-2.9
2000	300	4.3
3000	550	7.9
4000	1650	24.

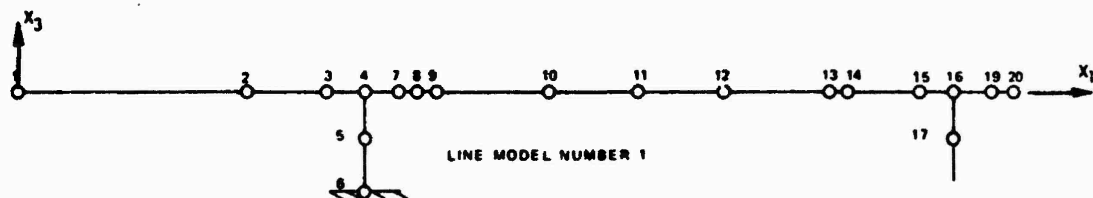


Figure 3.14. Finite Element Model - Forward Slipper Impact

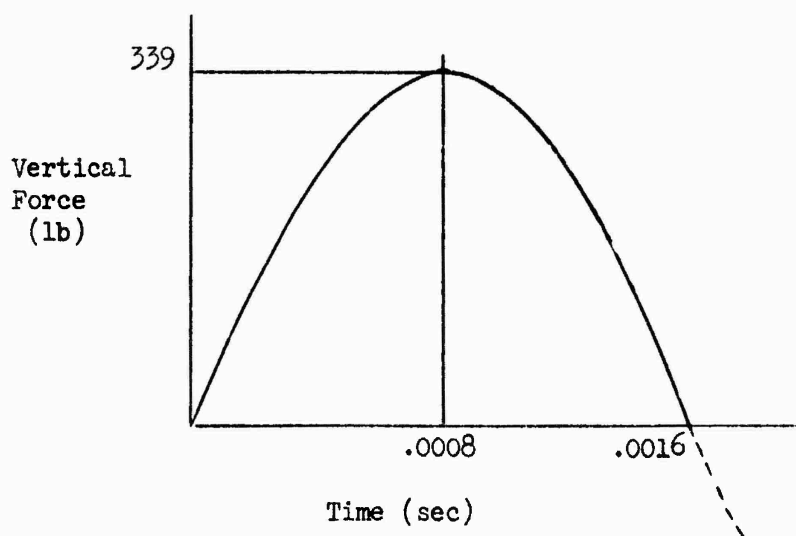


Figure 3.15. Forward Slipper Vertical Force Time History for Unit Step Velocity

Impact velocity as a function of sled velocity was determined from Figure 3.13 using  $f = 312$  Hz, with values of  $V$  and  $L_T/W_T$  from the preceding table<sup>2</sup>. The peak loads corresponding to a unit impact velocity were multiplied by these values of impact velocity. The predicted forward slipper vertical force as a function of sled velocity is shown in the following table.

Sled Forward Velocity, $V$ (fps)	Design Impact Velocity, $v$ (ips)	Predicted Forward Slipper Average Peak Vertical Force (lb)
1000	28	9,490
2000	41	13,900
3000	48.5	16,440
4000	61	20,680

These values represent average peak dynamic forces, as explained in Section 3.2, and are shown in Figure 3.16 along with flight data for total vertical forward slipper force (2).

#### Modular Monorail -- Vertical Loads

Coast phase dynamic loads resulting from impacts on the forward slipper were predicted using Procedure B (Section 3.2.2), with STARDYNE and DYNREL finite-element computer programs. The finite-element model is illustrated in Figure 3.17.

Response to a unit vertical step velocity was determined. Pertinent parameters for the vertical force time history is shown in Figure 3.18. The effective contact frequency, determined from an average of the time at peak load and the contact period, is 128 Hz. Peak force is 665 pounds.

Weight and lift distributions are summarized in Figure 3.19 for sled velocities of 2,300 and 3,400 fps. Impact velocities from Figure 3.13 and predicted forward slipper forces are summarized in the following table, along with flight data.

<sup>2</sup>The curves must be interpolated and extrapolated for different velocities. Also, for negative values of  $L/W$  use  $|L/W| + 1$ .

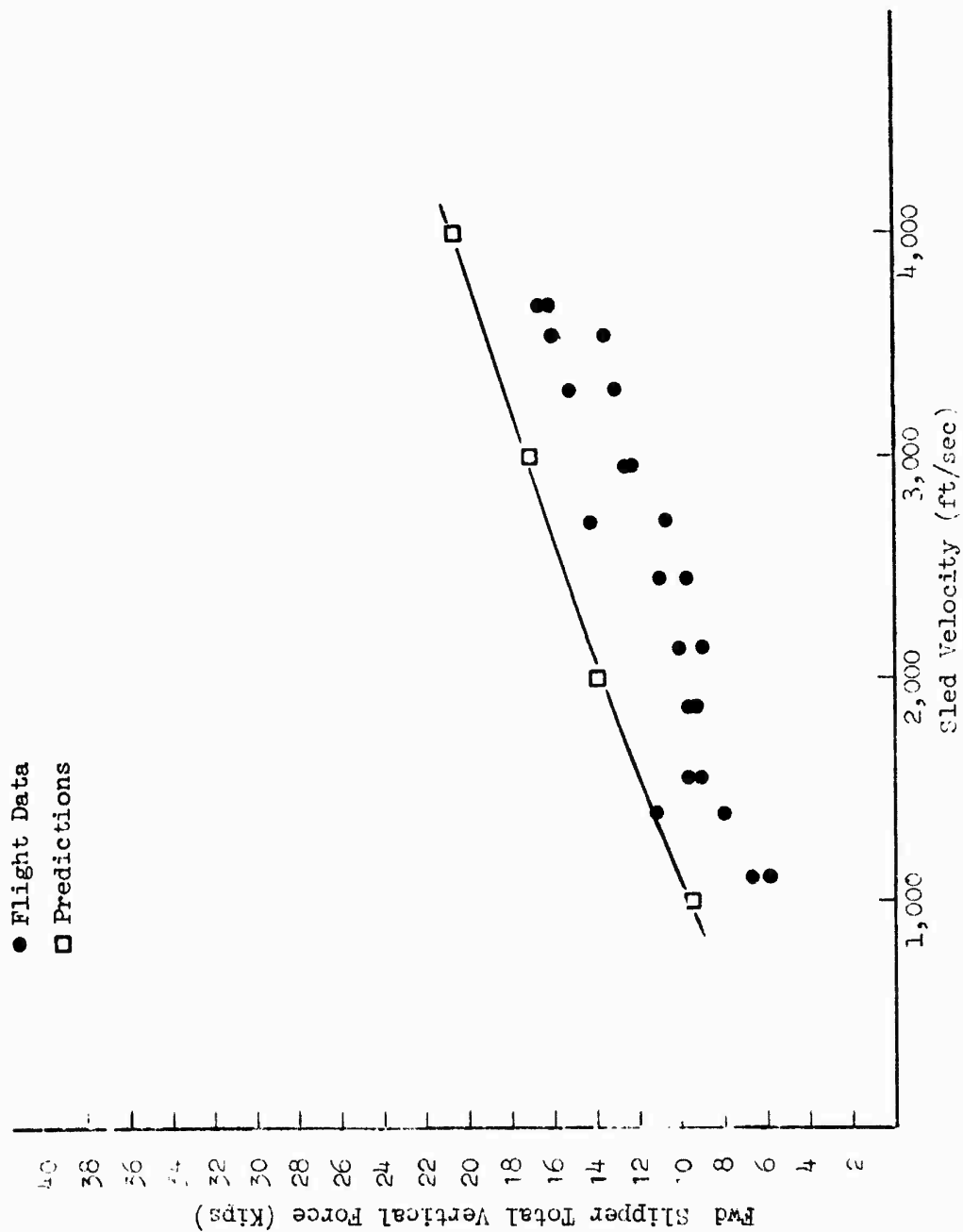


Figure 3.16. Instrumented Monorail Forward Slipper Vertical Force

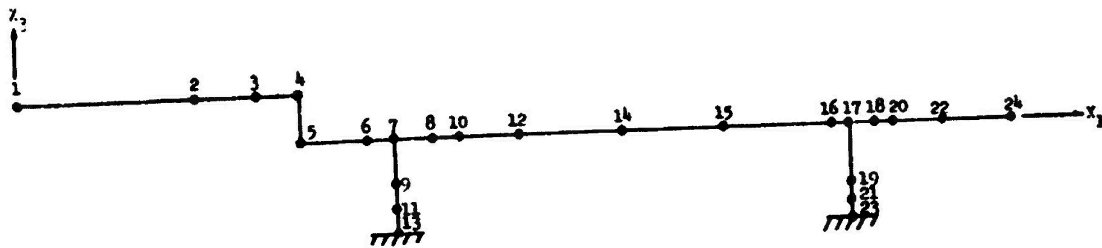


Figure 3.17. Modular Monorail Finite Element Model

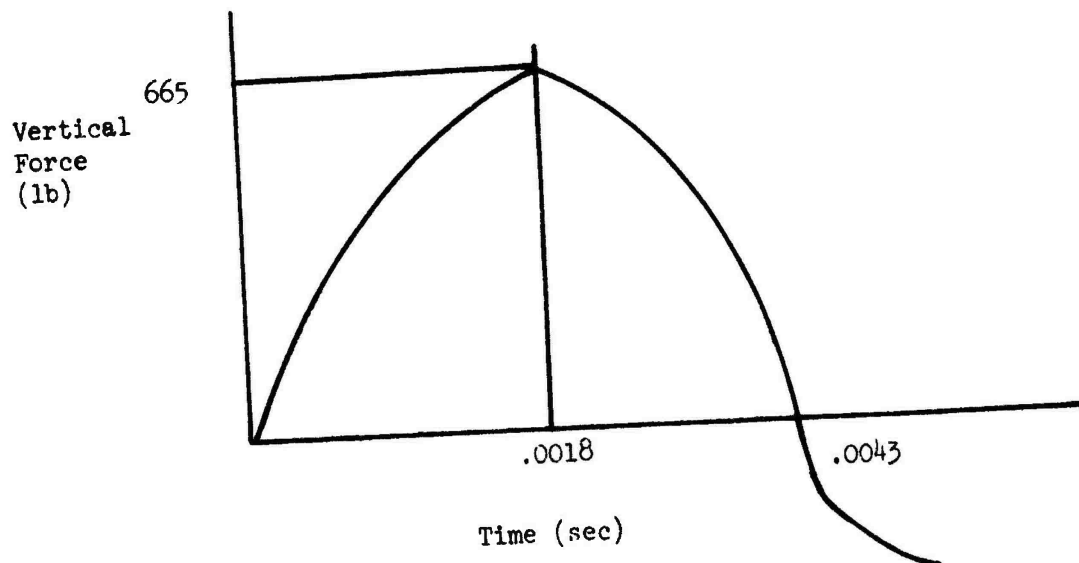
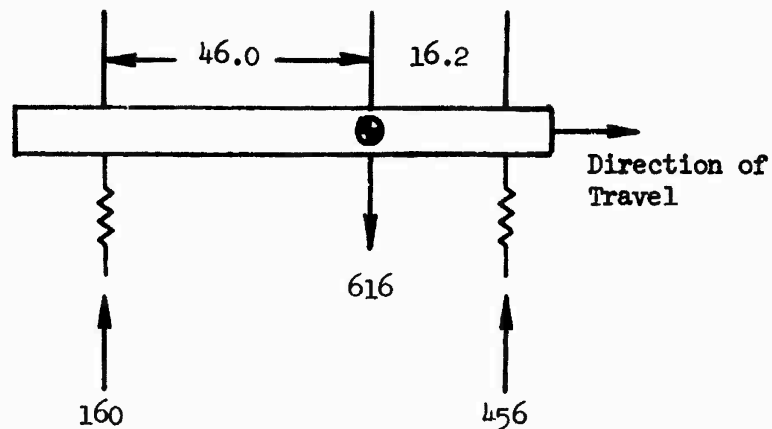
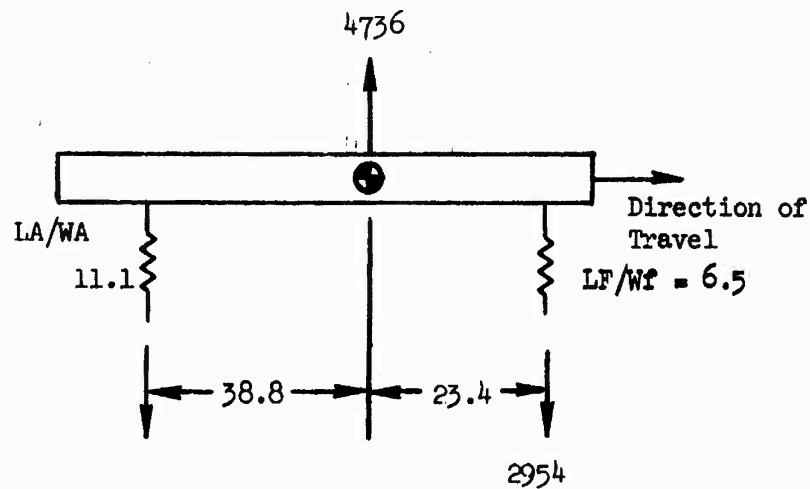


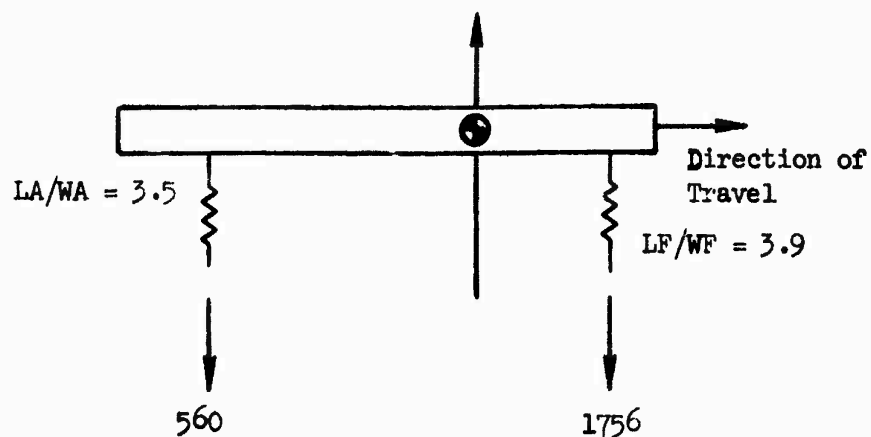
Figure 3.18. Forward Slipper Vertical Force Time History for Unit Velocity Impact



Weight Distribution



Lift Distribution -  $V = 3400$  fps



Lift Distribution -  $V = 2300$  fps

Figure 3.19. Modular Monorail Sled - Weight and Lift Distributions

# SUMMARY OF MODULAR MONORAIL FORWARD SLIPPER VERTICAL FORCES

Flight Condition	Average Sled Velocity (fps)	Impact Velocity (ips)	Average Peak Vertical Force (lb) (0.1 sec intervals)	
			<u>Flight</u>	<u>Predictions</u>
Motor On	3150		30,630	
Motor Off	3150		22,040	
(coast)				
Motor Off	3400	27	22,276	18,000
(coast)				
Motor B.O.	3450		42,300	
Motor Off	2300	24	17,686	16,000

## Discussion of Results

Inspection of Figure 3.16 and the preceding table indicates that the impact velocity method gives reasonable estimates of coast phase dynamic loads in monorail sleds. In selecting the damping used to generate the de-curves, emphasis was placed on vertical loads since rail roughness measurements used for the simulated rail were obtained in the vertical direction.

The method overestimates the Instrumented Monorail vertical slipper force (Figure 3.16) and underestimates the Modular Monorail slipper force (preceding table). The value of 10 percent critical damping gave best correlation, considering both cases.

## Evaluation of Procedure A

The foregoing comparisons of predictions and flight data were made with Procedure B since it represents the more rigorous approach. Procedure A, although easier to use, is an approximation of Procedure B. It is therefore of interest to compare Procedure A with Procedure B.

For comparison, Procedure A was used to predict forward slipper vertical and lateral loads for the Instrumented Monorail sled. The following data were assumed (2):

Sled weight,  $w = 140$  lb

Pitch and yaw moment of inertia,  $I = 131 \text{ lb-sec}^2\text{-in}$

Distance between cm and forward slipper,  $l = 23.0$  in

Slipper and support structure stiffnesses were computed for the two-beam elements connecting Node 4 (main body) and Node 6 (rail) in the finite-element model of Figure 3.14. The results are:

Vertical Stiffness,  $K_v = 5.53 \times 10^5 \text{ lb/in}$

A comparison of predicted loads and other pertinent parameters is shown in Table I of Appendix IV.



It may be seen that Procedure A also gives reasonable estimates of monorail sled coast phase dynamic loads for preliminary design purposes.

An attempt to predict lateral loads using Procedures A and B was also made. However, the analytical results underpredicted test results considerably. The conclusion reached was that rail roughness in the lateral direction could indeed be larger than in the vertical direction. No lateral rail roughness measurements have ever been performed to verify this opinion.

## SECTION IV

### INVESTIGATION OF OTHER EXCITATION SOURCES

A major part of the early period of performance of this study was pervaded by frustration. The principal objective of the study was to develop a new design procedure for dual rail sleds. Analysis of the response of the Single Mod sled to rail roughness did not give results which correlated with test track data. Numerous variations in velocity, lift, damping coefficients, and rail roughness were tried without success. Ultimately, it was learned that the test data were in error by about one-third. With that information, correlation was finally achieved. The studies did show that dynamic loads in the dual rail sled are not sensitive to variations in quasi-steady lift or in velocities below 2,000 fps.

In addition to these parametric studies, two other brief analytical efforts were motivated by the lack of correlation. They merit description in this report although there are currently no experimental data to verify or refute their existence.

#### 4.1 Dynamic Interaction of Pusher and Forebody

The search for sources of higher dynamic amplification led to the idea that the Single Mod sled might be interacting with its forebody. In the 24X-C1 test the Single Mod sled pushed a FDN5810-T6 forward vehicle. That forebody weighs 3,140 pounds, measures 108 inches between slipper beams and has a cg 17.2 inches above the rail head. A simple model was made of the two sleds joined by the standard Coleman coupling device. Natural frequencies were obtained and the first three were 18.0 cps, 20.4 cps and 22.5 cps. The model was then run over the rough rail in the simulation program. The results showed a variation of about 20 percent from the model used without the forebody. Loads in the forward slippers went down and those in the aft slippers went up. The variations, however, were not much more than were being seen from run to run due to the randomness of rail roughness. (It was subsequently learned that the runs being made at that time were too short for consistency in results.) Since this change was not nearly the magnitude needed to give correlation with what were then believed to be test levels, the effort was abandoned because later correction of the test data showed that the sled model without forebody was giving agreement. This investigation was never revived.

In retrospect it might be observed that the configuration of these two sleds would not be expected to give dynamic coupling. Each has a low center cg comparable to the height of the coupler. Such a phenomenon might be more expectable in a sled combination where high cg's would induce pitch interaction with axial forces being transmitted through a low coupler.

#### 4.2 Dynamic Interaction of Sled and Test Track

Another dynamic phenomenon offered itself enticingly as an explanation for the unresolved disparity in data. The possibility that the test track behaving as a beam on an elastic foundation (where the soil is

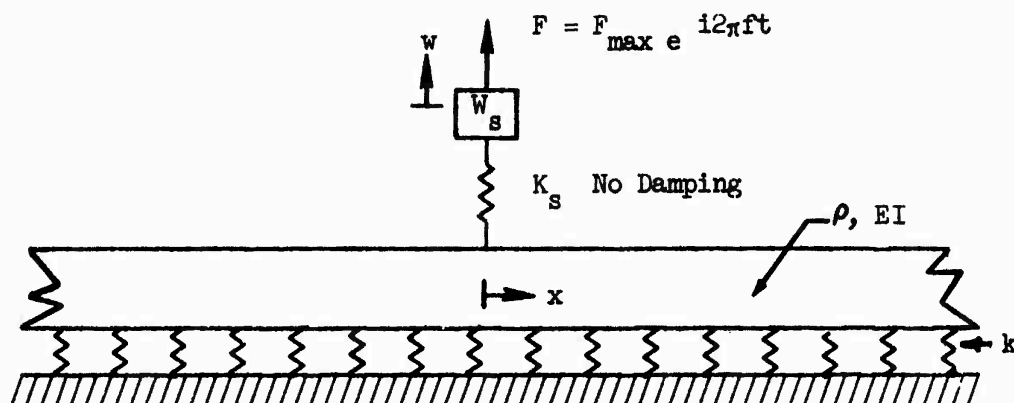
the elastic foundation) could be interacting with the sled was investigated by some renowned men 14 years ago (9). The theoretical and limited test results were not very conclusive although they indicated that this possibility does exist.

The problem is that a bouncing sled is traveling over a beam on an elastic foundation at close to its wave propagation velocity. Theoretically, the problem is tractable if the force is constant or if the force is oscillating but its point of action is stationary. The well-known solution for the point force traveling at the propagation velocity shows infinite bending moments developing just under the force. Of course, it does not indicate what happens to the vehicle producing that force.

Motivated by the hope of uncovering additional information about the behavior of the Single Mod sled, an analytical study was made of a bouncing single-degree-of-freedom model on a beam on an elastic foundation. The model and its relevant parameters are shown in Figure 4.1. The single-degree-of-freedom system idealizing the Single Mod sled has a natural frequency of 20.8 cps. A harmonic force is applied to the single-degree-of-freedom model with the intention of studying its frequency response. The estimate of the stiffness of the elastic foundation was made based on results presented in Chapter 7, Reference (9). The track parameters, bending stiffness and distributed mass which includes an estimate of the added mass effect of the soil were taken from Chapter 5, Reference (9).

The rather laborious analytical effort in the solution of the partial differential equations led to results which are presented graphically in Figure 4.2. The three graphs correspond to three weights of the single-degree-of-freedom model. One is equal to the weight of the Single Mod sled at burnout, and the other two correspond to half and double that number. It is observed that as the weight of the sled increases the major response moves from the resonance of the sled to that of the track, which is nominally at 15.7 cps. Although not shown here, the results also indicate that for heavier sleds the amplitude of response of the track is greater.

One of the reasons for doing this analytical study was that the results could be compared with a fairly easily conducted test on the track itself. Several sleds could be tied to the track and excited with reaction-type vibrators over a frequency range sufficient to reproduce these curves. Two purposes would be served with the results. A more refined estimate of the track's dynamic properties could be made. In addition, it could be verified that the dynamic behavior of the sled could, indeed, be affected by interaction with the test track. With this information, an assessment could be made of the value of proceeding with an analytical study of a moving dynamic model.



$$\rho = 165 \text{ slugs/ft}$$

$$k = 1.6 \times 10^6 \text{ lb/ft}^2$$

$$EI = 9 \times 10^9 \text{ lb-ft}^2$$

$$\sqrt{\frac{k_s g}{W_s}} / 2\pi = 20.8 \text{ cps}$$

Figure 4.1. Single dof on Beam-On-Elastic Foundation  
Model of Sled on Test Track Bed

$$\frac{W_{\max}}{F_{\max}/k_s}$$

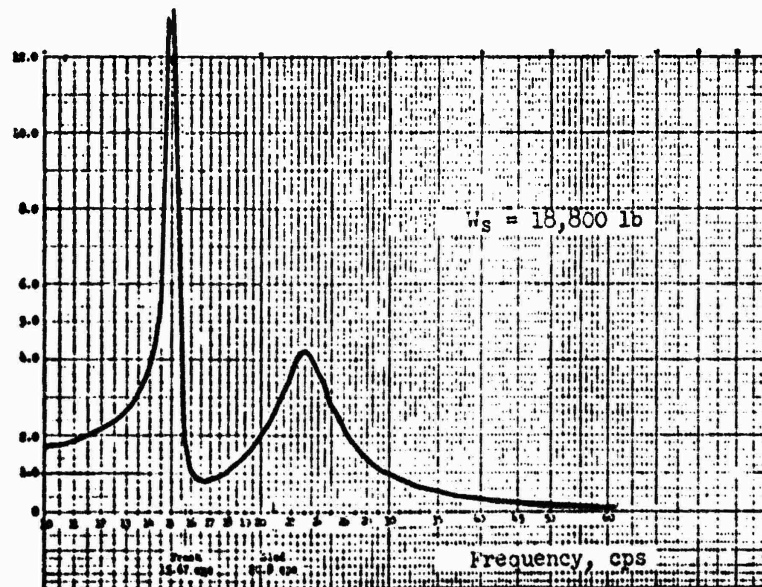
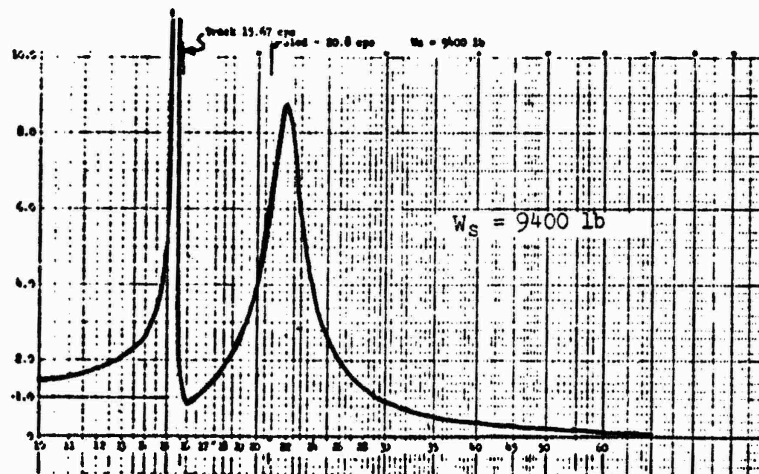
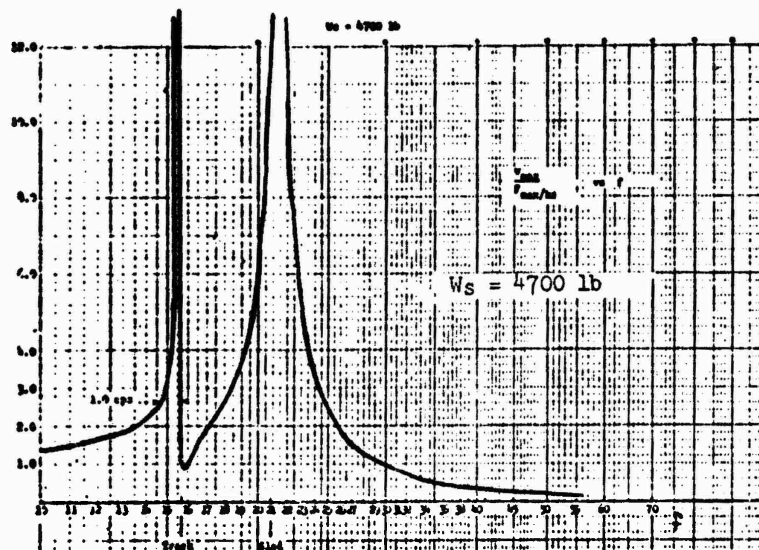


Figure 4.2. Dynamic Amplification of Single dof on Beam on an Elastic Foundation

## SECTION V

### DEVELOPMENT OF DESIGN AND ANALYSIS PROCEDURES

#### 5.1 Introduction

This section of the report describes the basis for the design analysis procedures which were finally selected for dual and monorail sleds, and are presented in Section 6.0 of this report. In some respects, especially with regard to estimation of dynamic loads, the design analysis procedures presented in Section 6.0 depart significantly from current design procedures. The estimates, assumptions and judgements upon which this guide was formulated are discussed in this section.

It has been emphasized earlier in this report, and is restated here, that the design criteria incorporated in this new design analysis procedure are based on minimal test data and what insight could be gleaned from analysis. They must be dynamic, changing and improving as more test data become available. Hopefully, some of the new approaches, especially the more refined dynamic analysis, will provide a rational base which can be easily expanded to new sled configurations and velocity ranges. Of critical importance is the establishment of a consistent and systematic program of test data acquisition.

Clarity of the following discussion depends on an understanding of two points. "Dynamic loads" are herein defined to be inertial loads in the vertical and lateral directions which arise from bouncing of the sled on the rails. This bouncing is induced by engine transients, rail roughness and oscillating aerodynamics. Forces due to aerodynamic lift, thrust, thrust offset moments, drag and all inertial loads in the downtrack direction, even oscillatory ones, are herein called "quasi-steady loads."

#### 5.2 Factors Used With Quasi-Steady Loads for Dual and Monorail Sleds

The "dynamic" loads calculated in the preliminary and final design phases (described below) give inertial loads in the vertical and horizontal directions only. Downtrack dynamic amplification due to thrust ignition, thrust transients and onset of braking must be included in the quasi-steady loads by use of appropriate factors.

At ignition thrust is multiplied by 2.0 to account for axial and pitch response to a step function. The factor of 1.3 used with it at other times in the trajectory accounts for downtrack vibrations which may result from thrust perturbations and "hot" engine burning. Design conditions must include any possibilities for asymmetric firing due to malfunctioning engines.

Although there are some wind tunnel and test track measurements of lift forces, they are sparse and difficult to generalize into prediction techniques. For this reason and because lift forces may be the greatest source of loads, a factor of 1.6 is used to account for uncertainty.

As at thrust ignition, the onset of braking force is considered to be a step function having an amplification of 2.0. An additional .2 (giving 2.2) is added because of the uncertainty in analytical methods for predicting braking loads.

### 5.3 Dynamic Load Prediction for Design of Dual Rail Sleds

During the course of this study it came to light that the available dual rail dynamic load data tended toward a straight line correlation with a parameter, subsequently named SIMP (Sled IMPact Parameter). The correlation was best between loads measured during coast and those calculated in the computer simulation program. Even maximum values measured in tests showed some correlation although it can be seen in Figure 5.1 that the Single Mod maximum values are more extreme than those from the Weasel and Gnu tests. This is not really surprising because Figure 2.1, showing test data from burnout of one of the Single Mod tests, is rather extreme.

A single slipper beam load versus SIMP curve is attractive from the designer's viewpoint. Furthermore, there are almost no data available on the interaction of specific motors with test sleds. Therefore, a single SIMP curve has been chosen on the basis of the design criteria. More specifically, it is the basis of prediction of the vertical and lateral dynamic loads. Quasi-steady loads, which for dual rail sleds are usually roughly the same magnitudes as the dynamic loads, must be estimated by the designer. SIMP, however, will help him estimate the dynamic loads which must be superimposed.

Peak dynamic loads are evidently induced not only by engine burnout conditions, but by oscillating aerodynamics. This was observed in the only test data for which there were detailed time histories, the Single Mod, where the forward slipper beam felt highest loads during passage through the transonic range (with engine on). For this reason, full vertical dynamic loads, i.e., those associated with the top SIMP line, must be superimposed on all quasi-steady conditions during engine burning. Since braking occurs during coast and, as can be seen from Figure 5.1, coasting loads are less than 70 percent of the full vertical, 0.7 is the factor used during braking.

The same thrust amplification factors are specified for pushed as for self-propelled sleds. A few points in a beta factor curve (8) are the only data available for forward vehicle behavior. They showed loads as high as comparable sleds with on-board motors and, hence, this decision. (More data might change it.)

There are no measurements of lateral loads for dual rail sleds. In the tried and proven lambda factor method (1), the same dynamic loads are applied laterally as vertically. Despite an intuitive judgement that lateral dynamic loads ought to be lower than vertical, the dictate of maintaining conservative design practice demands that lateral loads continue to be set equal to vertical dynamic loads (until experimental data is obtained).

$$SIMP = \left[ \frac{KM}{1 + \frac{MZ}{I}} \right]^{\frac{1}{2}}$$

M = Sled Mass  
I = Sled Pitch Inertia  
K = Slipper Beam Stiffness  
l = Distance from c.g. to Slipper Beam

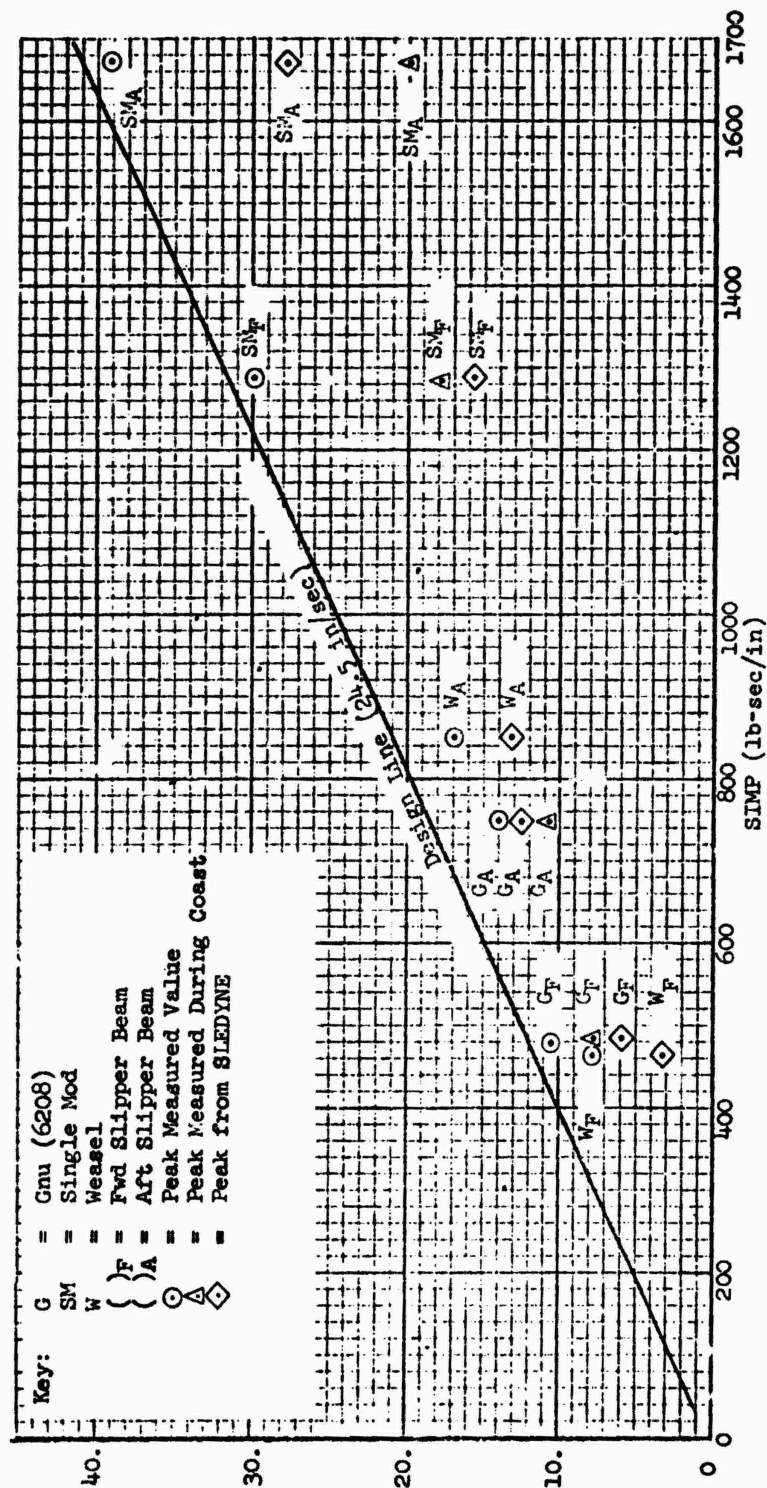


Figure 5.1. SIMP Line for Design of Dual Rail Sleds



### Preliminary Dynamic Loads

For estimation of dynamic loads, the design procedure is divided into two phases, preliminary and final. Since the final design requires formulation of a detailed finite-element model of the sled, followed by use of the SLEDYNE simulation, the designer needs some help in making his preliminary estimates. He starts off by making a simple estimate of the sled body mass distribution and the stiffness of the fore and aft slipper beams. This gives him peak forward and aft slipper beam forces from the SIMP curve. He uses two cases for distributing the inertial loads -- one a hard impact on the forward slipper beam and the other a hard impact on the aft.

### Final Dynamic Loads

When he has a fairly detailed structural configuration, the designer proceeds to the final design phase. He runs his structural model over the rough rail using SLEDYNE, which gives him four inertial load vectors. These vectors are the vertical inertial forces on the structure at the times when the four slippers felt their maximum dynamic force. SLEDYNE calculates dynamic response to rail roughness alone which corresponds to coast phase dynamic loads. In order to bring the dynamic loads up to "full vertical," design factors (DFACF and DFACA) are read in by the user and used for scaling by SLEDYNE. These design factors are also based on the information in the SIMP graph. They are the ratios of the peak to the coast dynamic loads. SLEDYNE seems to be underpredicting forward slipper beam loads and overpredicting aft. Until this discrepancy is resolved, it will be necessary to use two design factors. These factors are based on the curves in Figure 3.5.

Two factors are also specified for scaling the vectors before they are applied in the lateral direction. They also correspond to vectors associated with peak forward and peak aft slipper forces.

## 5.4 Dynamic Load Prediction for Design of Monorail Sleds

Unlike dual rail sleds which have soft suspensions, monorail sleds are stiff and have high natural frequencies. This results in dynamic loads which are much greater than quasi-steady loads. Furthermore, the hard suspension produces greater dependencies of the dynamic loads on quasi-steady loads and forward velocity. A significant reduction in monorail sled dynamic loads could be achieved by reducing the stiffness of the slipper and/or support structure. A possible design approach is the use of elastic metallic devices such as Bellville springs or other compact springs between the slipper inserts and slipper structure. A significant and rather surprising consequence of properly designed soft metal slippers is that they would produce little, if any, increase in rail roughness induced dynamic deflections of the sled, although deflections due to quasi-steady loads, oscillating aerodynamic and thrust loads would increase. This is further discussed in Section 7.4 of this report.

Monorail peak dynamic loads also appear to be amplified by engine thrust and burnout. Figure 2.11 gives some idea of the extent of this effect for the Modular Monorail sled. It may be seen that the average peak loads during engine burn are approximately 50 percent higher than during

coast at the same velocity. Furthermore, the Modular Monorail sled test showed that around engine burnout the peak loads are almost 2.5 times the average coast loads. The Modular Monorail used a Ginie motor. Whether the phenomenon holds for other engines is a matter of conjecture, since no other data are available. The Instrumented Monorail did not have an on-board motor and did not exhibit higher loads during boost than during coast. Thus, it appears that a pushed monorail sled need not be designed to these higher dynamic loads. However, more data are needed to confirm this conjecture.

A factor of 2.5 also provides a conservative estimate for peak to average variations in lateral coast loads and analysis uncertainty, based on limited data for the Instrumented Monorail.

Oscillating aerodynamic loads do not appear to be an important excitation source for monorail sleds. Typically, monorail sleds go to speeds over Mach 3.0 and experience peak dynamic loads at maximum velocity. If softer slippers are adopted which bring major reductions in impact loads on future monorail sleds, oscillating aerodynamic loads at transonic speeds could become more significant.

#### Preliminary Dynamic Loads

For preliminary estimation of monorail dynamic loads, an impact model of the sled is employed (see Section 3.2). The purpose of this model is to estimate the impact frequency of the sled from which the impact velocity and the resulting dynamic loads can be computed. Two procedures for constructing this model are described in Section 6.2.2.1. Typically, the impact frequency of hard suspension monorail sleds will be between 130 Hz and 250 Hz. After the impact frequency of the sled is estimated, Figure 6.13 can be used to calculate the sled impact velocity for various forward velocities and lift-to-weight ratios ( $L/W$ ). These impact velocities are then scaled by a factor of 2.5 to account for engine burnout loads and peak to average load variations. Peak forward and aft slipper loads can then be calculated and equilibrated with sled inertial loads for calculating internal stresses.

#### Final Design Loads

When the sled design has progressed to the point of detailed structural definition, the final design procedure is employed. This requires that a finite-element model of the sled be constructed and its mode shapes and frequencies calculated. These data are read into SLEDYNE, which give four vertical inertial dynamic load vectors. SLEDYNE calculates the average dynamic response to rail roughness alone. In order to bring the dynamic loads up to "full vertical" and account for engine burnout, a design factor of 2.5 is read in by the user and is used by SLEDYNE to scale the results. The factor of 2.5 was chosen to yield conservative results. During braking a scale factor of 1.6 is used to account for the ratio between peak and average dynamic load.

The final dynamic lateral loads for monorail sleds are calculated assuming that these loads are a percentage of the vertical loads. The

exact percentage is a function of the cg height above the rail as shown in Figure 5.2.

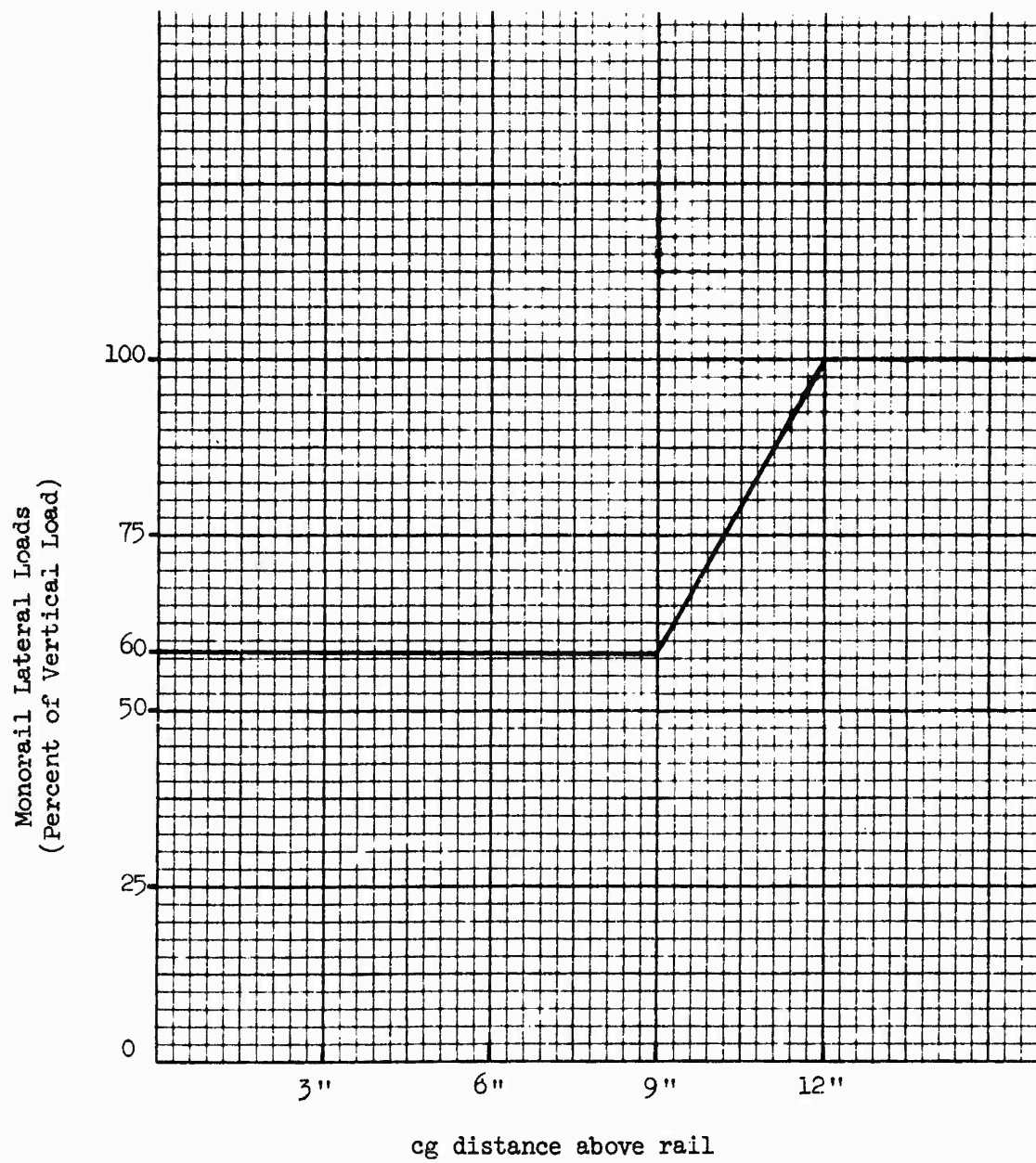


Figure 5.2. Magnitude of Lateral Loads for Monorail Sleds

## SECTION VI

### SLED STRUCTURAL DESIGN ANALYSIS PROCEDURES

The following criteria for structural design of dual rail and monorail sleds are based on limited test track data and estimates of partially understood phenomena. They are intended to be conservative. However, they cannot substitute for the good judgement of the design-analyst who applies them and is responsible for the adequacy of the resulting design. This is especially so with sleds of unusual configurations or trajectories with severe loading where these criteria may not be conservative. It may be more apt to view these criteria as guidelines which the design-analyst uses as a starting point in establishing the appropriate design loading conditions for his particular configuration/trajectory requirements.

The sources of loading are categorized here as quasi-steady and dynamic. "Dynamic" designates those inertial loads which are caused by bouncing and pitching of the sled in the vertical and horizontal planes. All other loads, including downtrack inertial loads, are referred to as "quasi-steady". For each critical trajectory point, quasi-steady loads are estimated, and the dynamic loads, which are oscillatory, are superimposed in the direction that gives the worst internal loads.

#### 6.1 Dual Rail Sled Structural Design Procedure

Determination of quasi-steady loads for dual rail sleds is discussed in Section 6.1.1. Section 6.1.2 explains the method for definition of dynamic loads, first at the preliminary design level where the sled configuration is known only in a gross sense (Section 6.1.2.1). When structural details and sizing are sufficiently defined so that a finite-element representation can be made, a more refined dynamic loads analysis is performed as specified in Section 6.1.2.2.

Table IV summarizes the overall design procedure for dual rail sleds.

##### 6.1.1 Dual Rail Sled -- Quasi-Steady Loads

The following procedure pertains for both preliminary and final design analyses.

##### Motor Pusher Loads (Figure 6.1)

###### a. Ignition

At ignition of on-board motors and pushers, maximum thrust (or maximum transmitted force where sled is being pushed) should be multiplied by 2.0 and downtrack acceleration applied to get inertial loads which equilibrate thrust. Include drag force and its moment if sled is in motion.

TABLE IV

## SUMMARY OF DUAL RAIL SLED DESIGN CONDITIONS

Event	Quasi-Steady Loads	Dynamic Loads <sup>2</sup>
Thrust Ignition	$T \times 2.0$ $\left( \begin{matrix} L \times 1.6^1 \\ D \end{matrix} \right)^3$ A Required for Equilibrium	$0.$ $\left( \begin{matrix} FV \\ Lat \end{matrix} \right)^3$
Max Lift	$T \times 1.9$ $L \times 1.6^1$ D A Required for Equilibrium	FV Lat
Max Velocity (Burnout)	$T \times 1.9$ $L \times 1.6^1$ D A Required for Equilibrium	FV Lat
Braking	$B \times 2.2$ $L \times 1.6^1$ D A Required for Equilibrium with $B \times 2.2$	$FV \times .7^4$ $Lat \times .7^4$
<p>Stress induced by these loads should be compared with allowable stresses. Allowable stress for normalized 4130 steel should be the yield stress, with a safety factor of 1.2. Allowables for other materials will be defined at a later date.</p> <p><b>Key:</b></p> <ul style="list-style-type: none"> <li>T - All on-board and transmitted thrust forces</li> <li>L - Lift forces due to choking and induced effects; should be distributed, if possible, for preliminary design and must be for final</li> <li>D - Drag</li> <li>A - Down-track inertial force; should be distributed for preliminary design and must be for distributed for final design.</li> <li>B - Braking forces; there will generally be both horizontal and vertical components</li> <li>FV - Full vertical dynamic loads; this is defined for preliminary and final design in Section 6.1.2 and includes the effects of rail roughness, thrust transients and aerodynamic oscillating loads</li> <li>Lat - Lateral dynamic loads as defined for preliminary and final design in Section 6.1.2</li> </ul> <p><b>Notes:</b></p> <ol style="list-style-type: none"> <li>1. This factor accounts for uncertainty in prediction and should be considered a minimum</li> <li>2. The procedure for calculating dynamic loads for preliminary and final design is described in Section 6.1.2</li> <li>3. These forces are applied at ignition of other than the first stage</li> <li>4. This factor brings full vertical forces down to coast levels</li> </ol>		

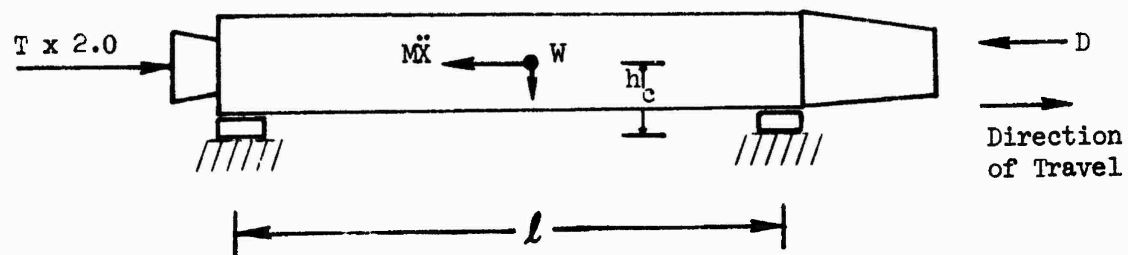


Figure 6.1. Equilibrium of Thrust Induced Loads

Quasi-steady load cases must be considered for every contingency of asymmetric firing for multiple engine sleds.

b. Maximum Lift

If maximum lift is not at maximum velocity, a separate loading condition should be specified with thrust factored by 1.9.

c. Thrust Termination

During burn and just before thrust termination, multiply maximum thrust by 1.9; react with predicted drag and axial acceleration loads required for equilibrium. Add slipper reactions necessary for moment equilibrium.

Aerodynamic Lift

Distributed aerodynamic lift forces are estimated for critical points in the trajectory. These should include quasi-steady choking effects but not oscillating loads. A factor to consider uncertainty should be used, depending on the estimated reliability of the predictions, but in no case less than 1.6. Slipper reaction forces should be added.

Braking Forces

The maximum applied braking forces, horizontal and vertical, should be multiplied by 2.2 to account for dynamic amplification and uncertainty in their prediction (see Figure 6.2).

6.1.2 Dual Rail Sled -- Dynamic Loads

Dynamic loads are defined as those slipper reactions and distributed inertial forces which derive from the oscillatory response of the sled to rail roughness, motor transients, and aerodynamic oscillating loads. They are almost exclusively in the lateral and vertical directions. (A tall sled may have some downtrack inertial loads due to pitch rotation.)

The dynamic loads must be added to the quasi-steady loads in the "worst direction", i.e., in the positive or negative direction depending on which gives the worst internal loads. The dynamic loads described below are independent of velocity over the range of 750 fps to 2,000 fps.

Two methods are used for obtaining the dynamic loads, one for preliminary design and the other, used after a detailed structural model has been prepared, for final design. Both require that the sled be idealized as a central body and two springs which support that body on the track. For the preliminary design, the central body is assumed to be rigid. In the final design analysis, the modes of vibration of the central body are used in the dynamic response analysis (in SLEDYNE).

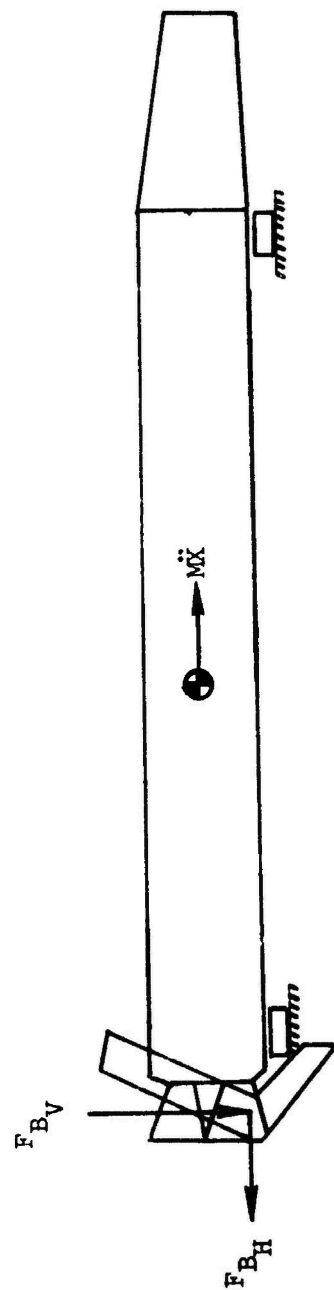


Figure 6.2. Application of Quasi-Steady Braking Forces



The analyst starts the design/analysis cycle by making estimates of the following sled parameters:

- Weight or Mass (M)
- cg Station
- Pitch Mass Moment of Inertia About cg (I)
- Slipper Beam Stiffness ( $K_F$  and  $K_A$ )

The slipper beam stiffness should be thought of as the vertical force which when applied to the slipper beam through the sled body supports, causes a one-inch deflection of the sled center-line. This is schematically illustrated in Figure 6.3.

The next step is calculation of the Sled Impact Parameter (SIMP) for the forward and aft slipper beams:

$$\text{SIMP-F} = \left[ \frac{K_F M}{1 + \frac{M l_F^2}{I}} \right]^{1/2} \quad \text{Forward Slipper Beam}$$

$$\text{SIMP-A} = \left[ \frac{K_A M}{1 + \frac{M l_A^2}{I}} \right]^{1/2} \quad \text{Aft Slipper beam}$$

where M and I are in mass units, and all dimensions are in inches.

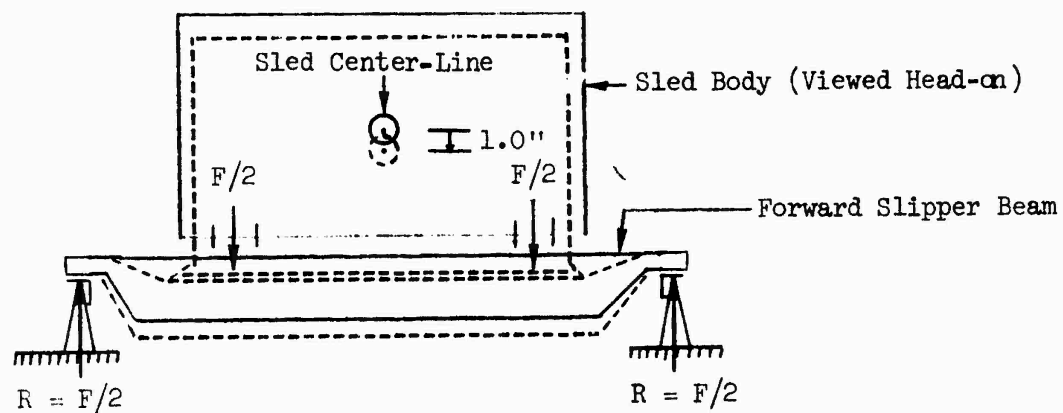
Figure 6.4 illustrates these parameters. The associated design slipper beam forces,  $F_F$  and  $F_A$ , are found from Figure 6.5.  $F_F$  is the slipper beam force associated with SIMP-F and  $F_A$  with SIMP-A.

$F_F$  and  $F_A$  are combined to define two inertial loading conditions:

Case 1

$$\ddot{z}_1 = \frac{F_F + F_A/2}{M} \quad (\text{in/sec}^2)$$

$$\ddot{\theta}_1 = \frac{F_F l_F - \frac{F_A l_A}{2}}{I} \quad (\text{rad/sec}^2)$$



$F$  causes sled center-line to deflect one inch (in the plane of the forward slipper beam).

$$K_F = F/1.0 = F$$

Figure 6.3

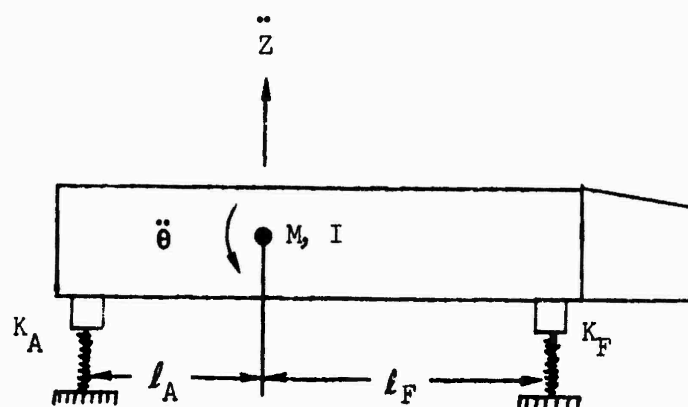


Figure 6.4

$$SIMP = \left[ \frac{\frac{KM}{1 + \frac{M}{I}}}{\frac{M}{I}} \right]^{\frac{1}{2}}$$

M = Sled Mass  
 I = Sled Pitch Inertia  
 K = Slipper Beam Stiffness  
 l = Distance from c.g. to Slipper Beam

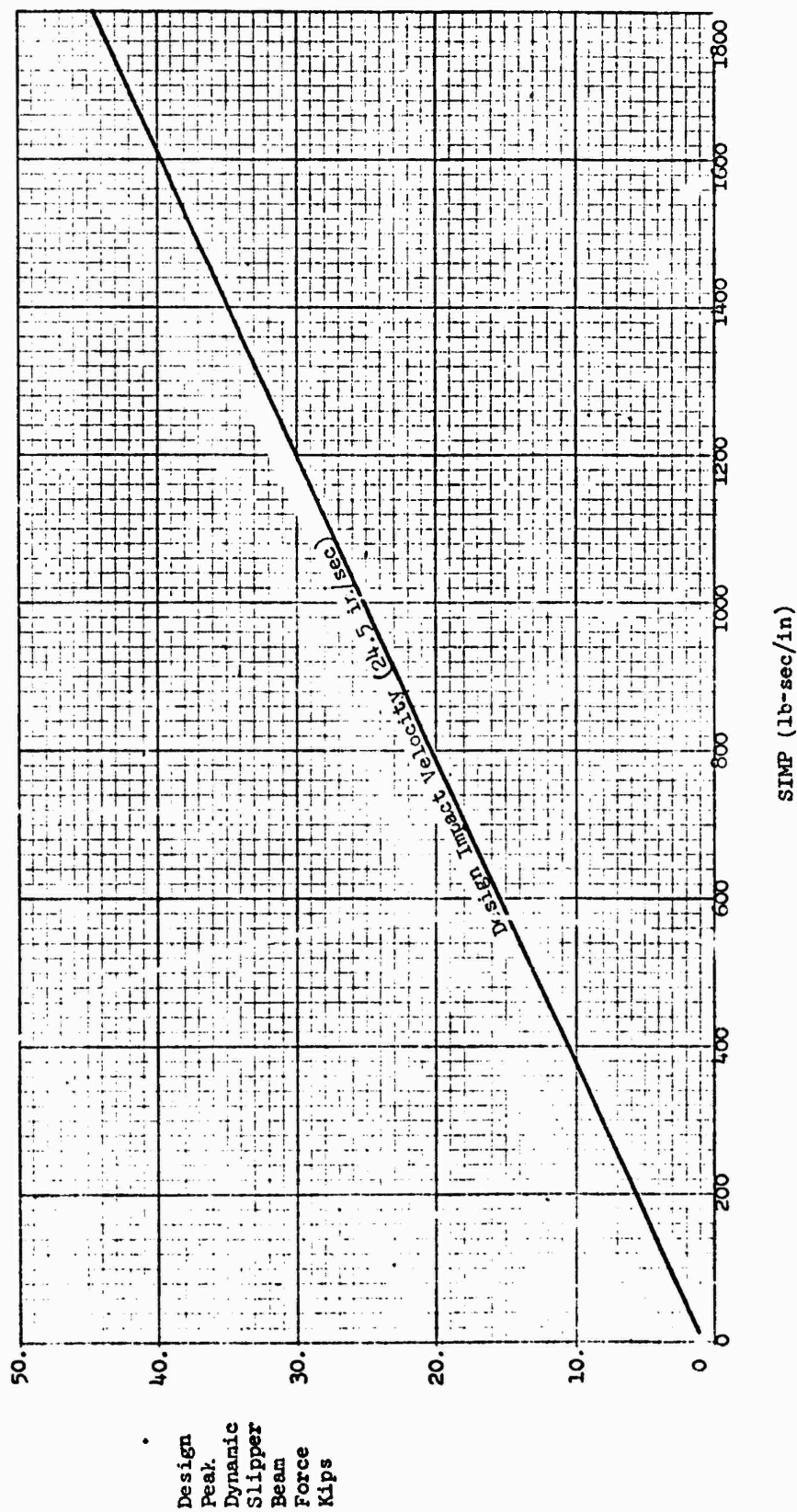


Figure 6.5. Dynamic Slipper Beam Force vs SIMP, Dual Rail Sleds

### Case 2

$$\ddot{z}_2 = \frac{F_{F/2} + F_A}{M} \quad (\text{in/sec}^2)$$

$$\ddot{\theta}_2 = \frac{\frac{F_F \ell_F}{2} - F_A \ell_A}{I} \quad (\text{rad/sec}^2)$$

Distribution of these preliminary dynamic loads over the sled structure is illustrated in Figure 6.6. These inertial loads are "full vertical" as referred to in Table VI.

Preliminary design loading conditions may now be synthesized by proper combination of the quasi-steady and dynamic loads. For each critical quasi-steady loading condition (except thrust ignition at zero velocity where dynamic loads are ignored), at least two loadings must be examined -- the quasi-steady loads plus each dynamic loading. The dynamic loadings must be added to the quasi-steady loads in the "worst" direction, i.e., so as to give worst internal loads.  $\ddot{z}_i$  and  $\ddot{\theta}_i$  should be both positive or both negative, depending on which gives more severe loading, but should not be of opposite sign. If it is not obvious which direction gives worst internal loads, four loadings should be examined for each quasi-steady condition.

### Preliminary Lateral Loads

Lateral dynamic loads must be combined with vertical loads at every design point, except thrust ignition at rest. For preliminary design, the same two inertial calculated force distributions for vertical loads, Case 1 and Case 2, should be applied laterally in the horizontal plane of the cg.

### Dynamic Braking Loads

For preliminary design, dynamic braking loads should be taken as .7 of the full vertical, i.e., .7 of the Case 1 and Case 2 conditions defined above.

#### 6.1.2.2 Final Dynamic Loads

When the design has progressed to a detailed configuration with structural members sized according to the preliminary design loads, a more refined dynamic analysis is necessary. This procedure is based on a dynamic analysis performed by SLEDYNE. The analyst proceeds as follows:

1. Make a detailed finite-element model of the sled structure including distribution of the weight. This model must be related to the X1, X2, and X3 triad so that:
  - a. X3 is vertical and positive upward;

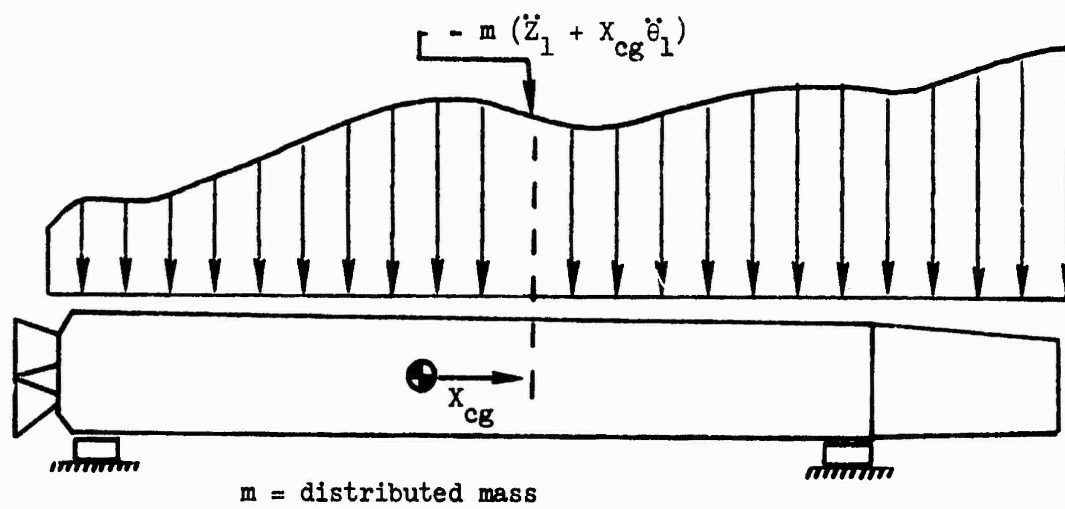


Figure 6.6. Distribution of Preliminary Dynamic Loads Case 1

- b. X1 and X3 lie in the sled's vertical plane of symmetry;  
(the sled cg may be anywhere in the X1 - X3 plane)
  - c. A positive rotation about X2 is nose up, i.e., X1 is positive aft.
2. Restrain the model at the points where the sled body is tied to the slipper beams. The flexibility which is isolated out of the structure by these restraints is precisely that contributed by the slipper beam springs. The restraints should be "displacement-only" and should not restrain rotation, especially not about the X2 axis.
  3. Extract the eigenvalues of eigenvectors for the model and store them, and the geometry, on tape or punched cards.
  4. Run the model at its maximum velocity over 4,000 feet of the rail in SLEDYNE, i.e., set  $TIMEF = 4000/V_{design}$ . Use six modes of structural vibration and .03 proportion of critical damping for each mode.

Since SLEDYNE calculates sled responses to rail roughness alone, the results must be scaled to include the excitation of motor transients, transonic buffeting, etc. DFACF and DFACA are design factors which scale up the load vectors calculated by SLEDYNE for the forward and aft slipper beams, respectively. Values of DFACF and DFACA are given in Figure 6.7. The analyst should request lateral loads from SLEDYNE, in which case the same loads will be added to the load vectors in the X2 direction. DFACFL and DFACAL are the forward and aft scale factors by which the lateral force vectors are multiplied.

5. Transfer the scaled load vectors from SLEDYNE to the structural analysis program and combine them with the quasi-steady loads for the design stress analysis<sup>3</sup>. There will be four load vectors from SLEDYNE associated with the peak loads at the four slippers. Before running the stress analysis the analyst must examine each SLEDYNE load vector and combine with it the quasi-steady loads in the direction which will give maximum internal loads. In ambiguous cases it is best to run two solutions for each SLEDYNE vector.

---

<sup>3</sup>The structural model used for step 5 is restrained only at the slippers and does not have the restraints which were imposed for the step 3 modal extraction. If lumped masses were placed along the slipper beams, their effect will be included in the load vectors from SLEDYNE.

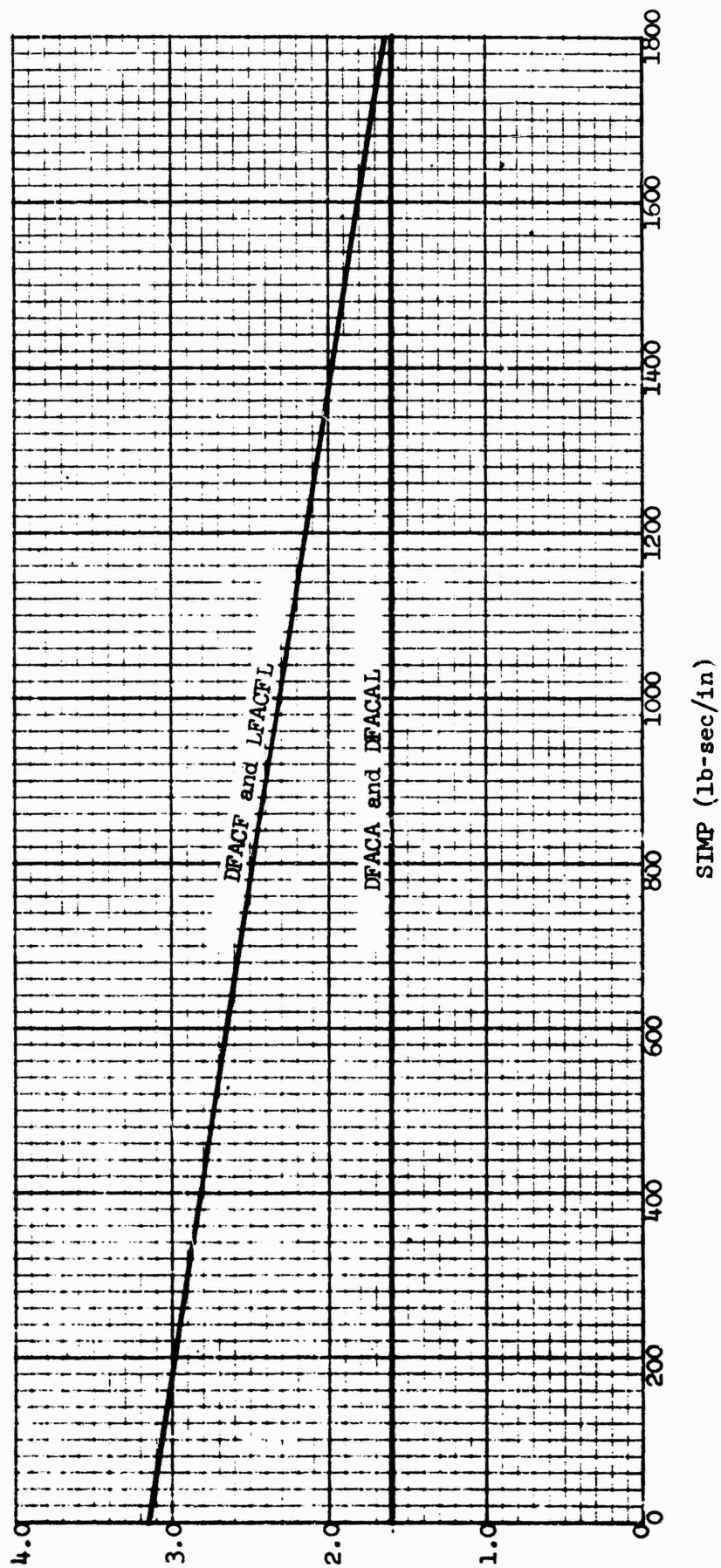


Figure 6.7. Design Factors vs SIMP

6. Calculate the dynamic braking loads in SLEDYNE. Input the nominal quasi-steady braking forces (they become negative thrust and negative lift) and drag. Set DFACF, DFACA, DFACFL, and DFACAL to 1.0. The resulting dynamic force vectors are superimposed on the nominal quasi-steady braking forces multiplied by 2.2.

## 6.2 Monorail Sled Structural Design Procedure

Determination of quasi-steady loads for monorail sleds is discussed in Section 6.2.1. Section 6.2.2 explains the method for definition of dynamic loads, first at the preliminary design level where the sled configuration is known only in a gross sense (Section 6.2.2.1). When structural details and sizing are sufficiently defined so that a finite-element representation can be made, a more refined dynamic loads analysis is performed as specified in Section 6.2.2.2.

Table V summarizes the overall design procedure for monorail sleds.

### 6.2.1 Monorail Sled -- Quasi-Steady Loads

The following procedure pertains for both preliminary and final design analyses.

#### Motor and Pusher Loads (Figure 6.8)

##### a. Ignition

At ignition of on-board motors and pushers, maximum thrust (or maximum transmitted force where sled is being pushed) should be multiplied by 2.0 and down-track acceleration applied to get inertial loads which equilibrate thrust. Include drag force and its moment if sled is in motion.

Quasi-steady load cases must be considered for every contingency of asymmetric firing for multiple engine sleds.

##### b. Maximum Lift

If maximum lift is not at maximum velocity, a separate loading condition should be specified with thrust factored by 1.9

##### c. Thrust Termination

During burn and just before thrust termination, multiply maximum thrust by 1.9; react with predicted drag and axial acceleration loads required for equilibrium. Add slipper reactions necessary for moment equilibrium.



TABLE V

## SUMMARY OF MONORAIL SLED DESIGN CONDITIONS

Event	Quasi-Steady Loads	Dynamic Loads <sup>2</sup>
Thrust Ignition	$T \times 2.0$ $(L \times 1.6^1)^3$ D A Required for Equilibrium	0. (Vert) <sup>3</sup> (Lat)
Max Lift	$T \times 1.9$ $L \times 1.6^1$ D A Required for Equilibrium	Vert Lat
Max Velocity (Burnout)	$T \times 1.9$ $L \times 1.6^1$ D A Required for Equilibrium	Vert
Braking	$B \times 2.2$ $L \times 1.6^1$ D A Required for Equilibrium with $B \times 2.2$	Vert $\times .7^4$ Lat
<p>Stress induced by these loads should be compared with allowable stresses. Allowable stress for normalized 4130 steel should be the yield stress, with a safety factor of 1.2. Allowables for other materials will be defined at a later date.</p> <p><b>Key:</b></p> <ul style="list-style-type: none"> <li>T - All on-board and transmitted thrust forces</li> <li>L - Lift forces due to choking and induced effects; should be distributed, if possible, for preliminary design and must be for final</li> <li>D - Drag</li> <li>A - Down-track inertial force; should be distributed for preliminary design and must be for distributed for final design.</li> <li>B - Braking forces; there will generally be both horizontal and vertical components</li> <li>Vert- Vertical dynamic loads as defined for preliminary and final design in Section 6.2.2; these includes the effects of rail roughness, thrust transients and aerodynamic oscillating loads</li> <li>Lat - Lateral dynamic loads as defined for preliminary and final design in Section 6.2.2</li> </ul> <p><b>Notes:</b></p> <ol style="list-style-type: none"> <li>1. This factor accounts for uncertainty in prediction and should be considered a minimum</li> <li>2. The procedure for calculating dynamic loads for preliminary and final design is described in Section 6.1.2</li> <li>3. These forces are applied at ignition of other than the first stage</li> <li>4. This factor brings the vertical loads down to coast levels</li> </ol>		

## Aerodynamic Lift

Distributed aerodynamic lift forces are estimated for critical points in the trajectory. These should include quasi-steady choking effects but not oscillating loads. A factor to consider uncertainty should be used depending on the estimated reliability of the predictions, but in no case less than 1.6. Slipper reaction forces should be added.

## Braking Forces

The maximum applied braking forces, horizontal and vertical, should be multiplied by 2.2 to account for dynamic amplification and uncertainty in their prediction (see Figure 6.9).

### 6.2.2 Monorail Sled -- Dynamic Loads

Dynamic loads are defined as the slipper reactions and distributed inertial forces which derive from the oscillatory response of the sled to rail roughness and motor transients. They are of importance only in the vertical and lateral directions.

The dynamic loads must be added in the "worst direction" -- i.e., in the positive or negative direction depending on which gives the worst internal loads -- to the quasi-steady loads for obtaining the design loads.

Two methods are used for obtaining the dynamic loads, one for preliminary design and the other, used after a detailed structural model has been prepared, for final design.

#### 6.2.2.1 Preliminary Dynamic Loads

Preliminary dynamic loads are determined from a model in which the sled impacts the rail on one slipper. The impact velocity used for the design is determined from a prescribed set of curves as a function of sled forward velocity, an effective impact frequency, and lift-to-weight-ratio computed for each slipper. The effective impact frequency and the loads resulting from a specified impact velocity are determined from preliminary models of the sled. Two alternate procedures are presented.

#### Procedure A

This procedure is the easiest to use, but also tends to be the most conservative. If the slipper support structure is significantly stiffer than the sled body, this procedure is misleading and should be skipped.

The sled is idealized as a rigid body supported on springs (slippers and support structure). Loads are determined in the vertical and lateral directions so responses to both vertical and lateral impacts must be determined.

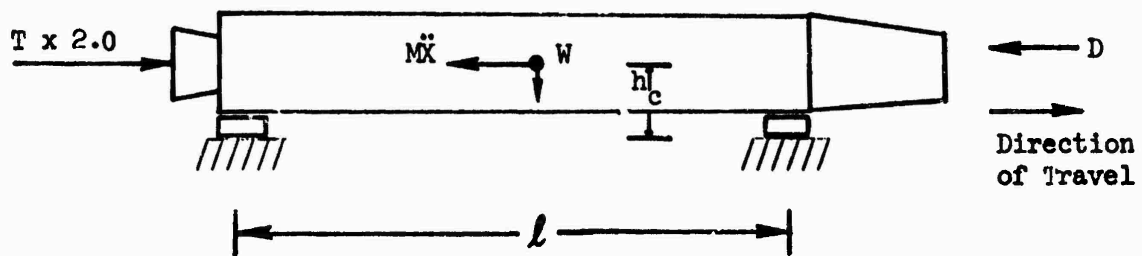


Figure 6.8. Equilibrium of Thrust-Induced Loads

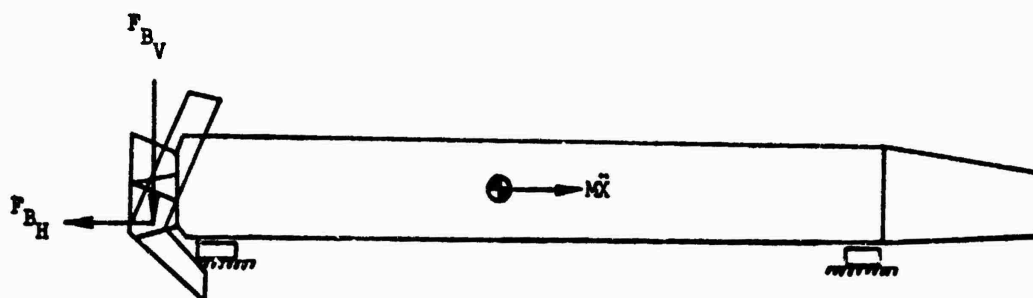


Figure 6.9. Application of Quasi-Steady Braking Forces

• Step 1

Estimate the following parameters:

Sled Mass, M

Distance Between Center of Mass (cm) and Forward and Aft Slippers,  $l_F$ ,  $l_A$

Pitch Moment of Inertia about cm,  $I_P$

Yaw Moment of Inertia about cm,  $I_Y$

Vertical Stiffness of Slippers and Associated Support Structure,  $K_{FV}$ ,  $K_{AV}$

Lateral Stiffness of Slippers and Associated Support Structure,  $K_{FL}$ ,  $K_{AL}$

Slipper and associated support structure stiffness can be determined as shown in Figures 6.10 and 6.11. In Figure 6.10 the slipper is pinned to the rail; in Figure 6.11 the slipper is constrained against translations and roll moment. Stiffness is defined as the force in pounds which causes a one-inch displacement of the sled "main body" relative to the rail.

Careful judgement should be exercised in determining the force which causes unit deflection of the sled center-line. Unlike dual rail sleds, which can be idealized as a rigid central body and springs which support the body on the track, the flexibility of typical monorail sled bodies is on the order of the flexibility of the slippers. Significant flexibilities in slipper support structure which contribute to deflection between the sled "main body" and the track should be included in the calculations. By ignoring flexibility of the sled body, the effective impact frequency will be overestimated and a conservative estimate of dynamic loads will result.

• Step 2

Calculate four values of the sled effective mass corresponding to forward (F) and aft (A) slippers impacting in vertical (V) and lateral (L) directions:

$$M_{eff_{FV}} = \frac{M}{1 + \frac{M l_F^2}{I_P}} \quad (\text{lb-sec}^2/\text{in})$$

$$M_{eff_{AV}} = \frac{M}{1 + \frac{M l_A^2}{I_P}} \quad (\text{lb-sec}^2/\text{in})$$

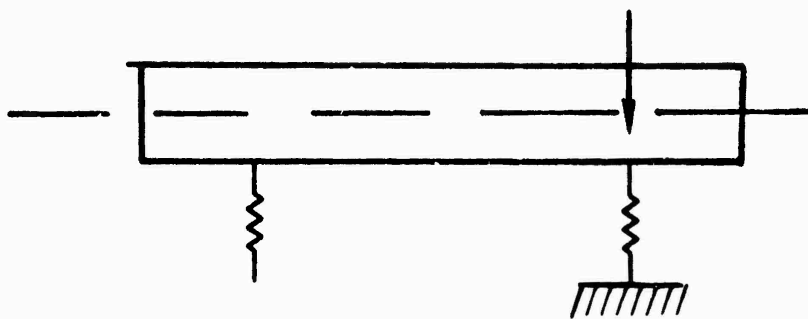


Figure 6.10. Model for Computing Vertical Stiffness of a Slipper and Support Structure

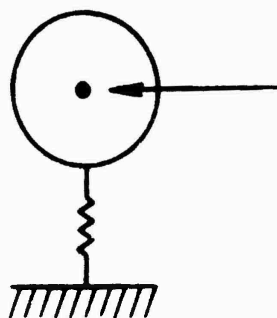


Figure 6.11. Model for Computing Lateral Stiffness of a Slipper and Support Structure

$$M_{\text{eff}_{FL}} = \frac{M}{1 + \frac{M l_F^2}{I_Y}} \quad (\text{lb-sec}^2/\text{in})$$

$$M_{\text{eff}_{AL}} = \frac{M}{1 + \frac{M l_A^2}{I_Y}} \quad (\text{lb-sec}^2/\text{in})$$

where  $M$ ,  $I_P$ , and  $I_Y$  are in mass units and all dimensions are in inches.

• Step 3

Calculate the effective impact frequencies as follows:

$$f_{FV} = \frac{1}{2\pi} \sqrt{\frac{K_{FV}}{M_{\text{eff}_{FV}}}} \quad (\text{Hz})$$

$$f_{AV} = \frac{1}{2\pi} \sqrt{\frac{K_{AV}}{M_{\text{eff}_{AV}}}} \quad (\text{Hz})$$

$$f_{FL} = \frac{1}{2\pi} \sqrt{\frac{K_{FL}}{M_{\text{eff}_{FL}}}} \quad (\text{Hz})$$

$$f_{AL} = \frac{1}{2\pi} \sqrt{\frac{K_{AL}}{M_{\text{eff}_{AL}}}} \quad (\text{Hz})$$

• Step 4

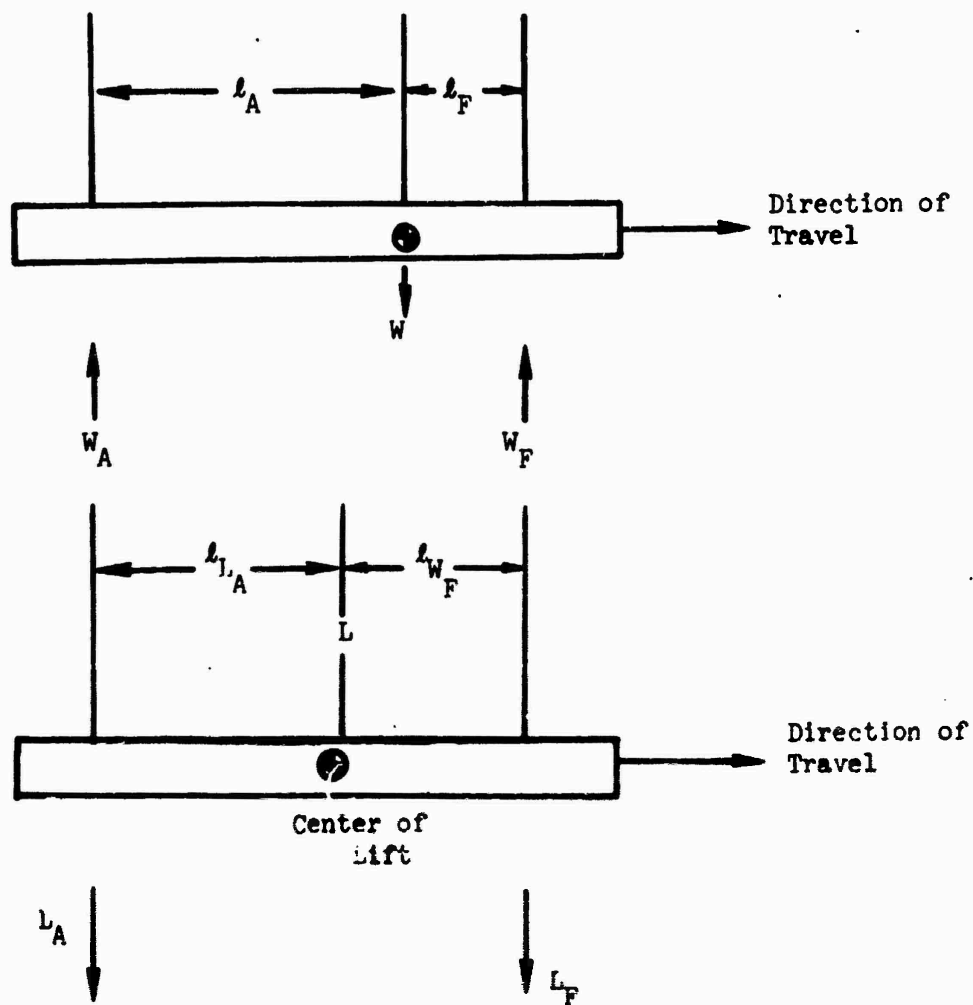
Determine lift-to-weight ratios distributed to each slipper,  $L_F/W_F$  and  $L_A/W_A$ , as shown in Figure 6.12, for expected critical points of the trajectory.

• Step 5

Enter the curves of Figure 6.13 with appropriate values of sled forward velocity,  $V$ , effective impact frequency,  $f$ , and  $L/W$ , to determine the design impact velocities,  $v_{FV}$ ,  $v_{AV}$ ,  $v_{FL}$ , and  $v_{AL}$ . For negative values of  $L/W$  use the value,

$$|L/W| - 1$$

For lateral impacts use  $L/W = 1$ .



$$\frac{L_A}{W_A} = \frac{l_{l,F}}{l_F} \quad \frac{L}{W}$$

$$\frac{L_F}{W_F} = \frac{l_{l,A}}{l_A} \quad \frac{L}{W}$$

Figure 6.12. Distribution of Sled Weight and Lift Force

Sled Velocity,  $V = 2000$  ft/sec

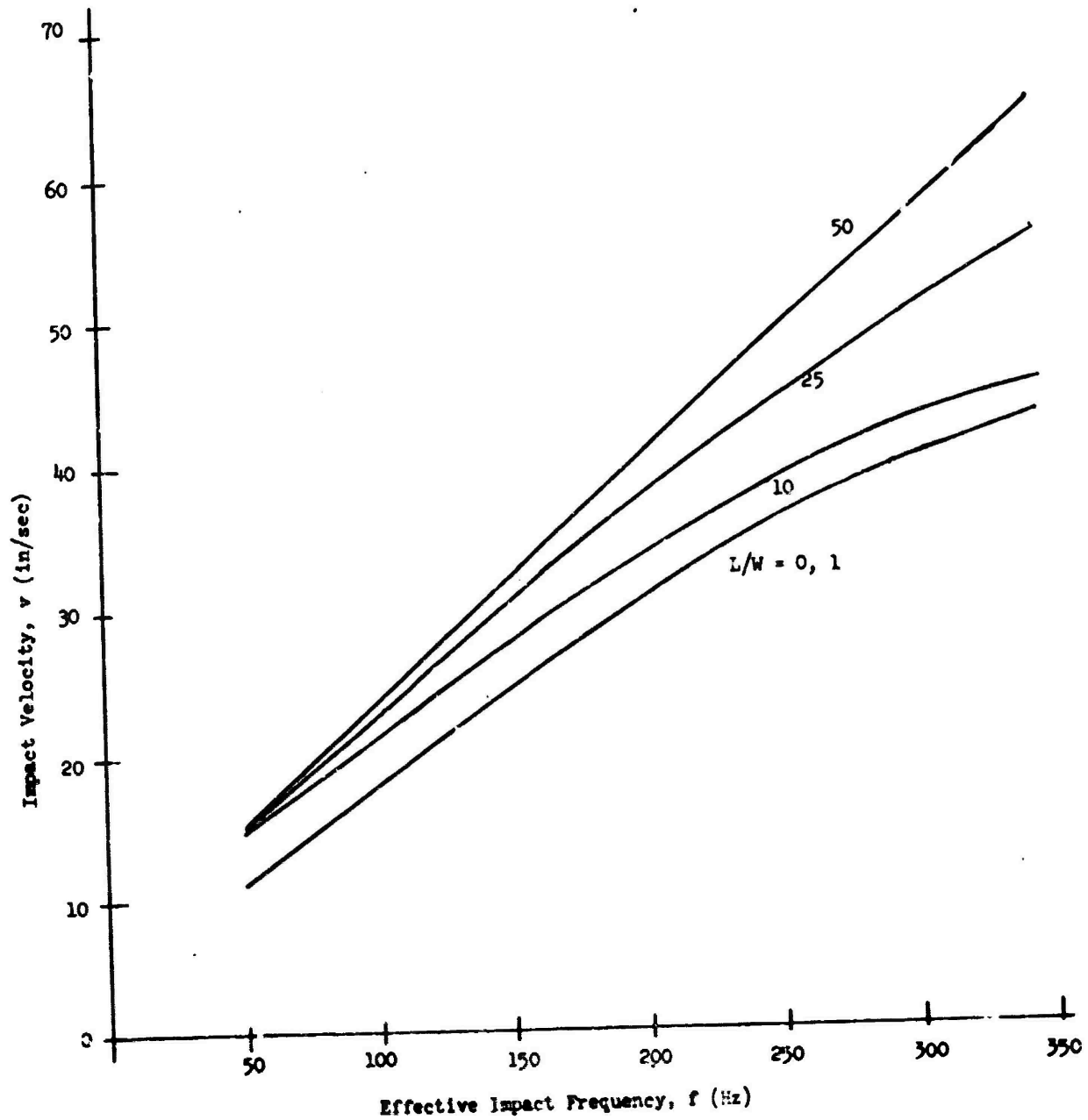


Figure 6.13. Impact Velocity for Monorail Sleds



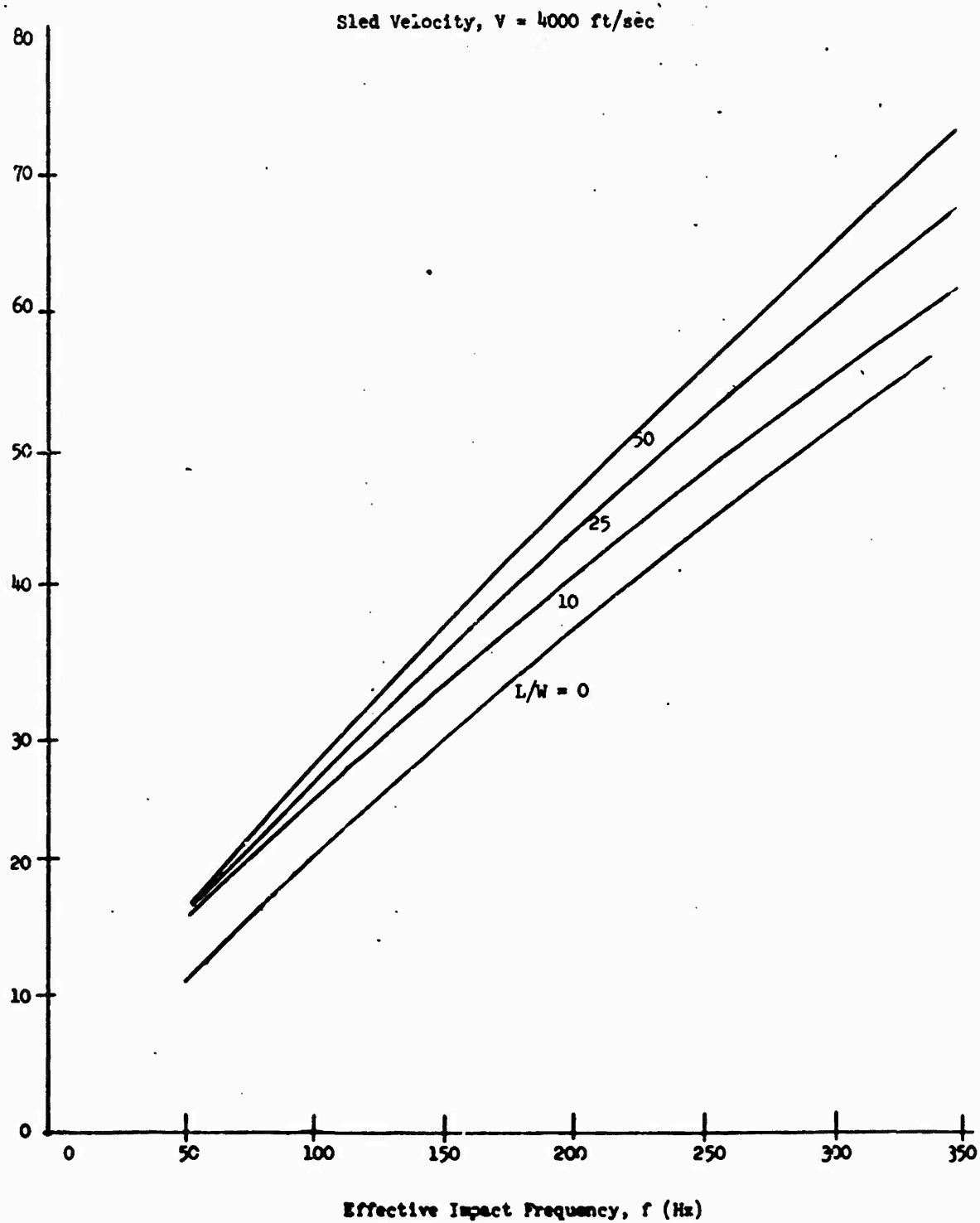


Figure 6.13. Impact Velocity for Monorail Sleds (Continued)

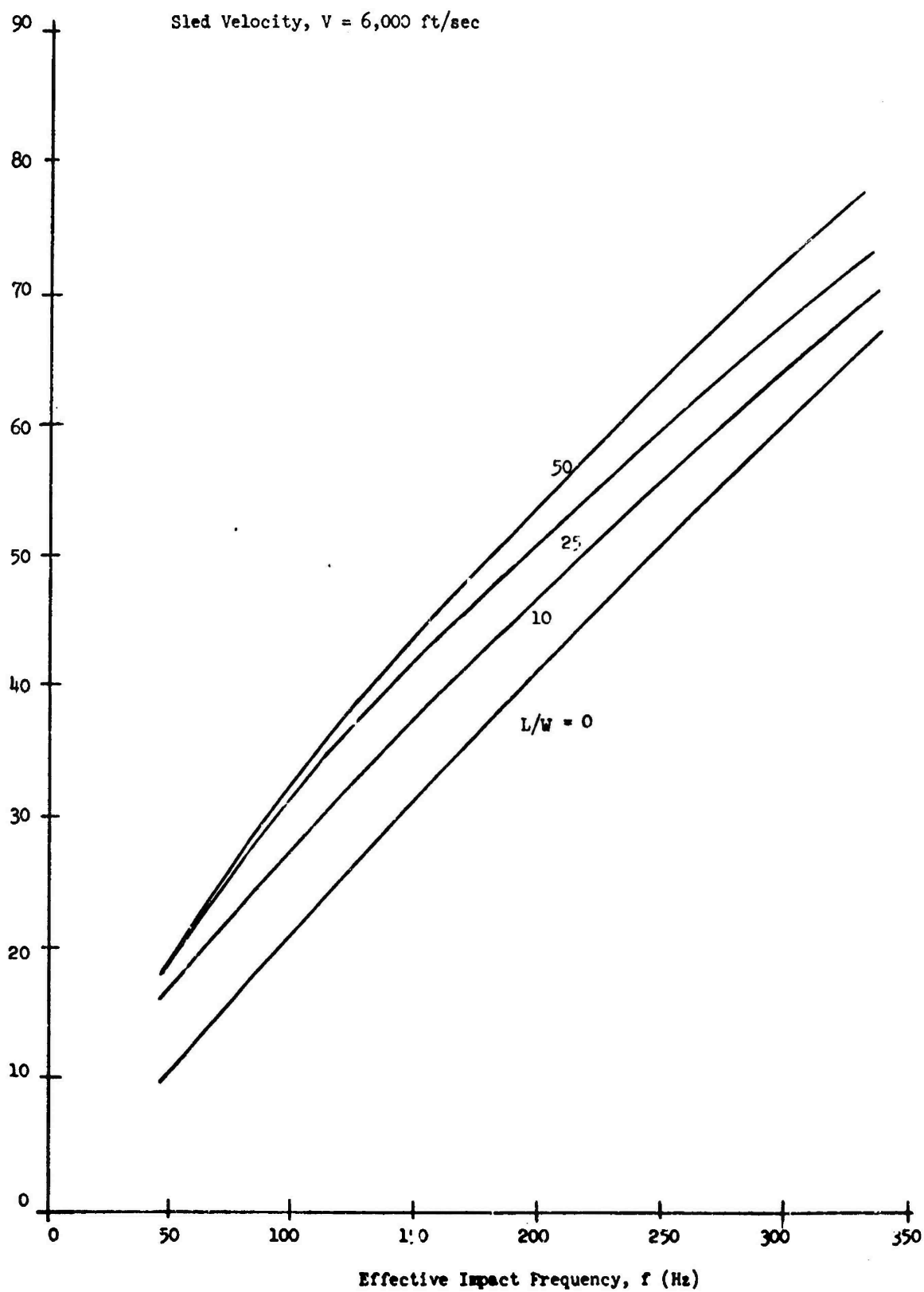


Figure 6.13. Impact Velocity for Monorail Sleds (Continued)

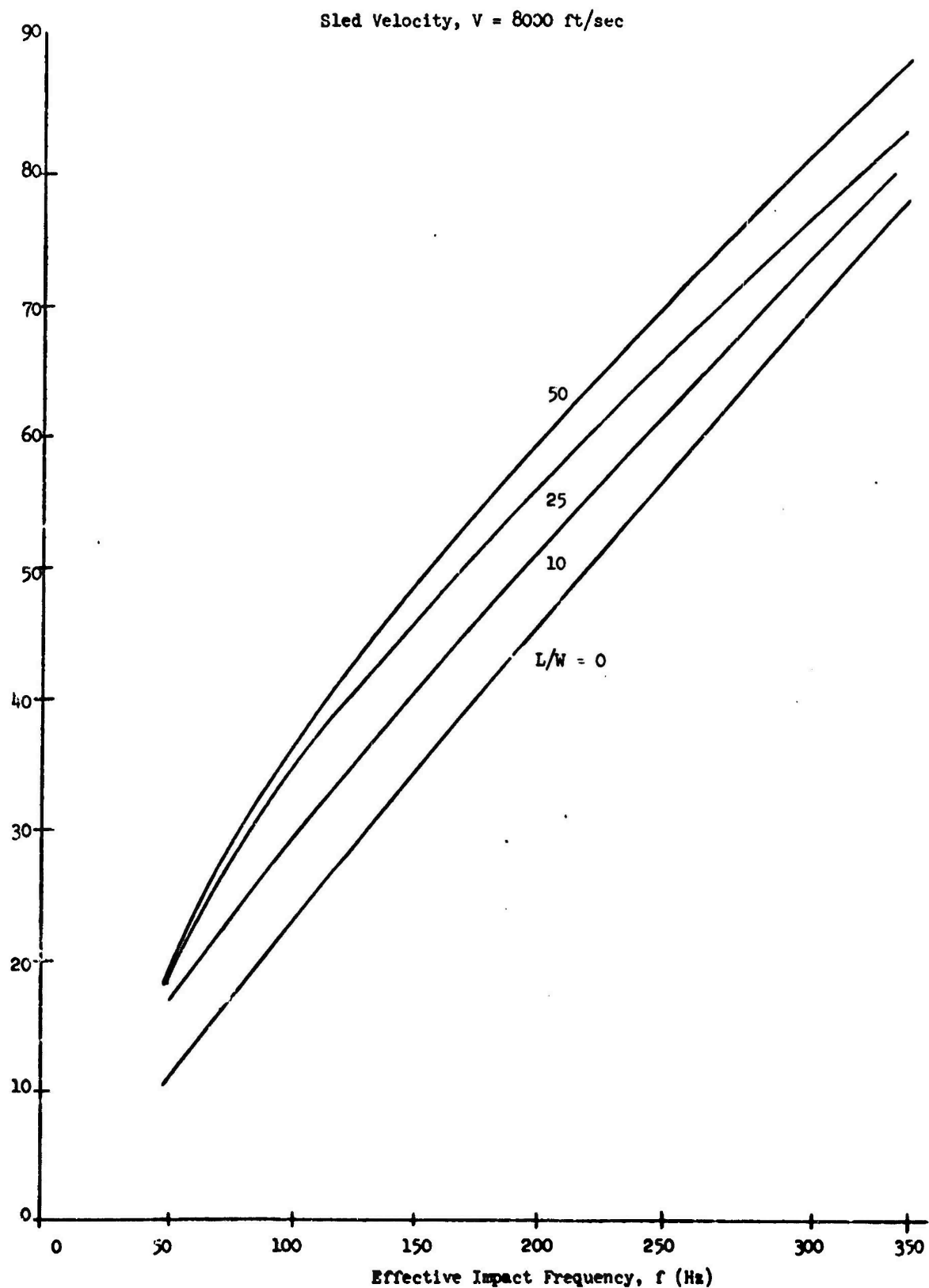


Figure 6.13. Impact Velocity for Monorail Sleds (Continued)

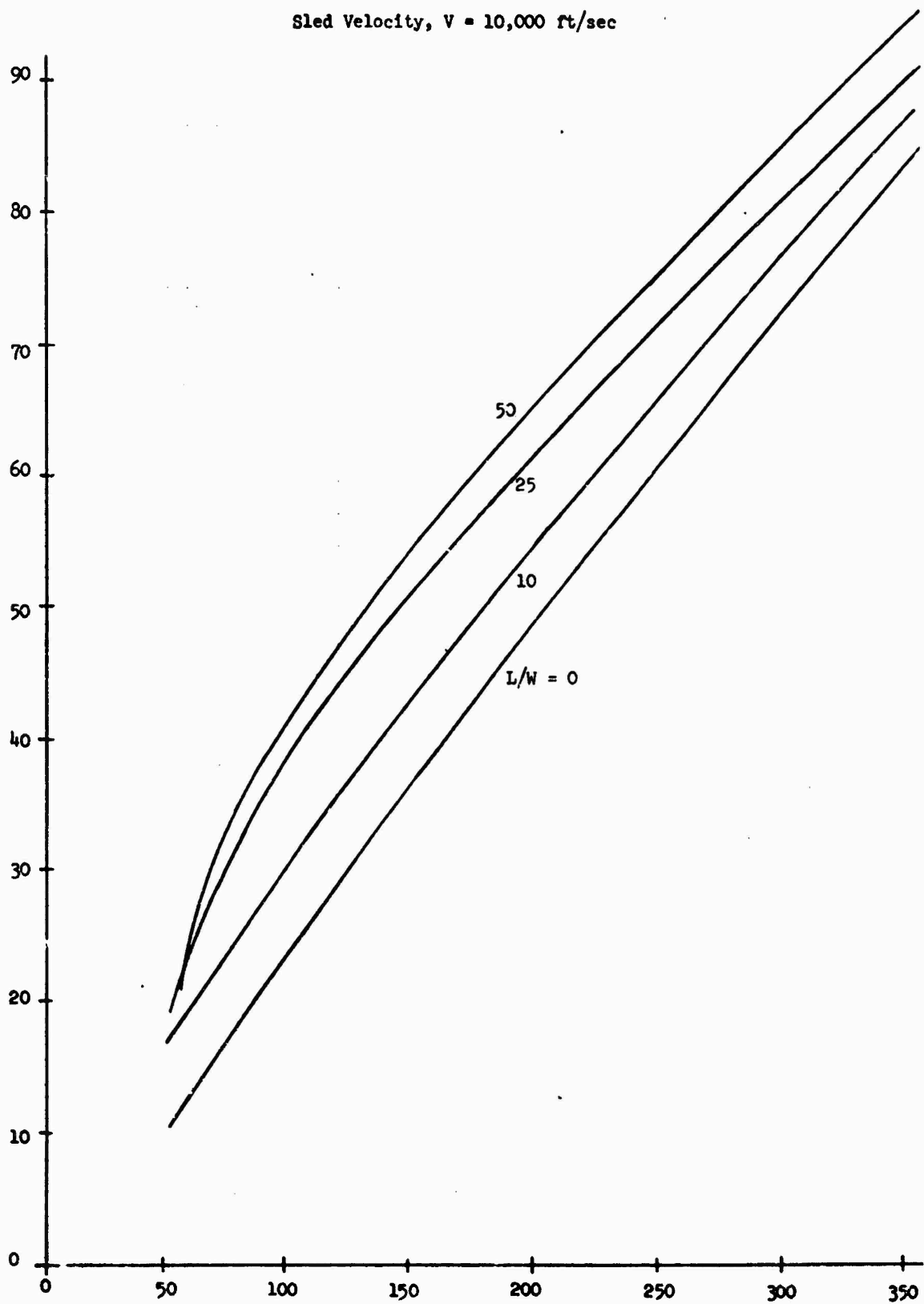


Figure 6.13. Impact Velocity for Monorail Sleds (Continued)

• Step 6

Compute the maximum slipper forces from

$$F_{FV} = 5\pi f_{FV} v_{FV} M_{eff_{FV}} \quad (1b)$$

$$F_{AV} = 5\pi f_{AV} v_{AV} M_{eff_{AV}} \quad (1b)$$

$$F_{FL} = 5\pi f_{FL} v_{FL} M_{eff_{FL}} \quad (1b)$$

$$F_{AL} = 5\pi f_{AL} v_{AL} M_{eff_{AL}} \quad (1b)$$

• Step 7

Compute the resulting acceleration responses which define four loading conditions:

a. Case FV Forward Slipper - Vertical

$$\ddot{z}_{FV} = F_{FV}/M \quad (\text{in/sec}^2)$$

$$\ddot{\theta}_{FV} = F_{FV} l_F / I_P \quad (\text{rad/sec}^2)$$

b. Case AV Aft Slipper - Vertical

$$\ddot{z}_{AV} = F_{AV}/M \quad (\text{in/sec}^2)$$

$$\ddot{\theta}_{AV} = F_{AV} l_A / I_P \quad (\text{rad/sec}^2)$$

c. Case FL Forward Slipper - Lateral

$$\ddot{z}_{FL} = F_{FL}/M \quad (\text{in/sec}^2)$$

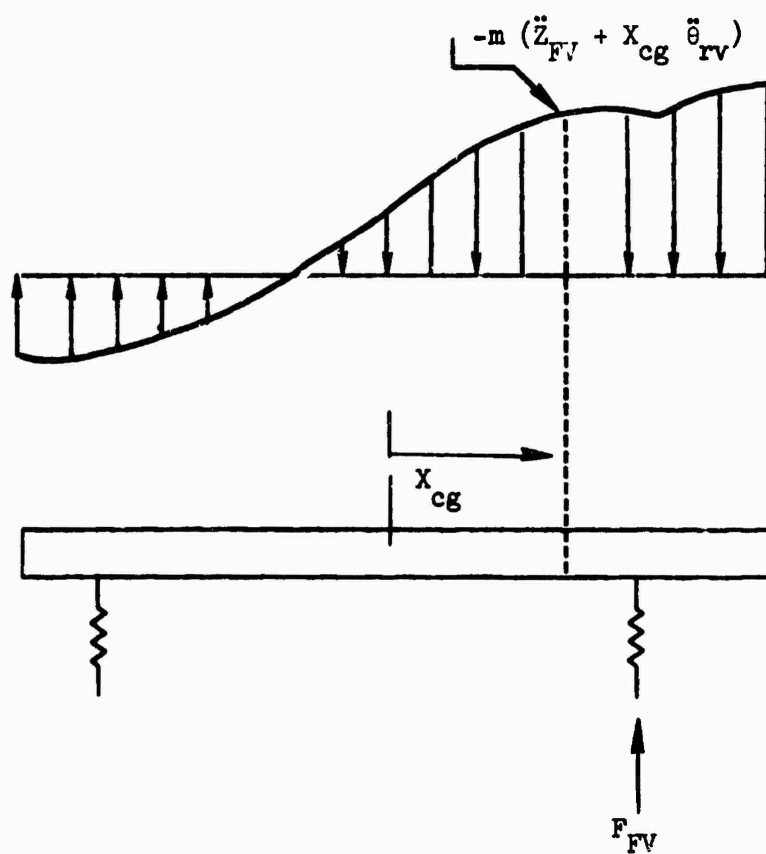
$$\ddot{\theta}_{FL} = F_{FL} l_F / I_Y \quad (\text{rad/sec}^2)$$

d. Case AL Aft Slipper - Lateral

$$\ddot{z}_{AL} = F_{AL}/M \quad (\text{in/sec}^2)$$

$$\ddot{\theta}_{AL} = F_{AL} l_A / I_Y \quad (\text{rad/sec}^2)$$

Distribution of the Case FV inertial loads over the sled is illustrated in Figure 6.14.



$m$  = distributed mass

Figure 6.14. Distribution of Case FV Preliminary Dynamic Loads

### Procedure B

This procedure is intended to provide improvement in estimating preliminary dynamic loads.

#### • Step 1

Construct preliminary simplified finite-element models of the sled with one slipper constrained (pinned for vertical; pinned and constrained against roll moment for lateral) and the other slipper free, and determine natural modes and frequencies using a program such as STARDINE.

#### • Step 2

Using a dynamic response program, such as DYNREL, applying unit step velocity inputs to the constrained slippers and, for each case, compute:

- a. The force-time history of the contacting slipper.
- b. The contact period and the associated effective impact frequency. For this calculation, assume that the slipper leaves the rail when the contact force reverses sign, as shown in Figure 6.15. The effective impact frequency is  $f = 1/2\tau$ . If the time of peak force,  $\tau_{peak}$ , is different from  $\tau/2$  (Figure 6.15), compute an effective impact frequency based on the average, i.e.,  $f = (1/2)(1/2\tau + 1/4\tau_{peak})$ .
- c. The load distribution at the time of maximum slipper force.

#### • Steps 3 and 4

Proceed with Steps 4 and 5 or Procedure A to determine the impact, velocities,  $v_{FV}$ ,  $v_{AV}$ ,  $v_{FL}$ , and  $v_{AL}$ .

#### • Step 5

Multiply the internal loads associated with the four unit-velocity impacts, determined in Step 2, by the following factors:

Case FV:  $2.5 v_{FV}$

Case AV:  $2.5 v_{AV}$

Case FL:  $5.0 v_{FL}$

Case AL:  $5.0 v_{AL}$

Note that in this procedure, the internal loads (bending moments, shears, etc.) are obtained directly. In Procedure A the external force distributions must be converted to internal loads for sizing of the structure.

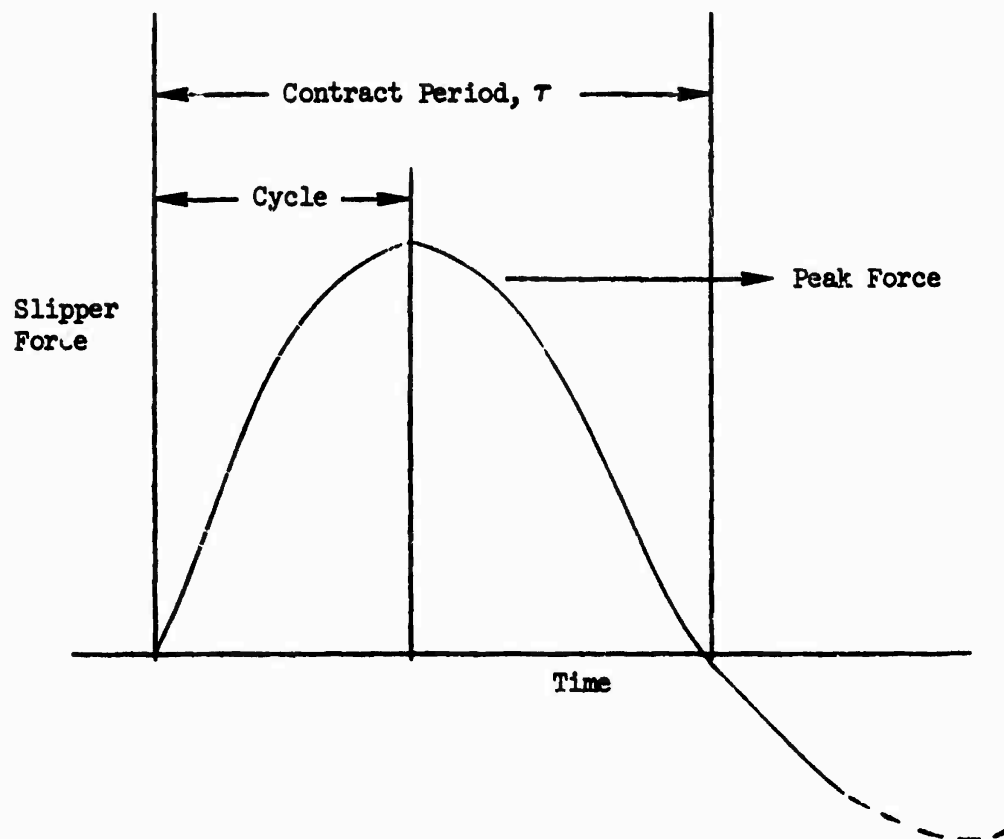


Figure 6.15. Slipper Force Time History



### Preliminary Design Loads

Preliminary design loading conditions may now be synthesized by proper combination of the quasi-steady and dynamic loads.

### Preliminary Vertical Loads

For each critical quasi-steady loading condition (except thrust ignition at zero velocity where dynamic loads are ignored), at least two loadings must be examined -- the quasi-steady loads plus each dynamic loading. The dynamic loadings must be added in the "worst" direction, i.e., so as to give worst internal loads.  $\ddot{z}_i$  and  $\ddot{\theta}_i$  ( $i = FV, AV$ ) should be both positive or both negative, depending on which gives more severe loading, but should not be of opposite sign. If it is not obvious which direction gives worst internal loads, four loadings should be examined for each quasi-steady condition in the vertical plane.

### Preliminary Lateral Loads

Lateral dynamic loads must be combined with vertical loads at every design point, except thrust ignition at rest. For preliminary design, apply the two lateral force distributions in the horizontal plane of the center of mass.

### Dynamic Braking Loads

During braking a factor of 0.7 should be applied to the vertical dynamic loads calculated by the procedures of Section 6.2.2.1.

#### 6.2.2.2 Final Dynamic Loads

When the design has progressed to a detailed configuration with structural members sized according to the preliminary design loads, a more refined dynamic analysis is necessary.

### Vertical Loads

This procedure is based on a dynamic analysis performed by SLEDYNE. The analyst proceeds as follows:

1. Make a detailed finite-element model of the sled structure including distribution of the weight. This model must be related to the  $X_1$ ,  $X_2$ , and  $X_3$  triad so that:
  - a.  $X_3$  is vertical and positive upward;
  - b.  $X_1$  and  $X_3$  lie in the sled's vertical plane of symmetry (the sled cm may be anywhere in the  $X_1 - X_3$  plane);
  - c. A positive rotation about  $X_2$  is nose up, i.e.,  $X_1$  is positive aft.

2. Restrain the model at the points where the sled body is tied to the slipper support structure. The restraints should be "displacement-only" and should not restrain rotation, especially not about the X2 axis.
3. Extract the eigenvalues and eigenvectors for the model and store them, and the geometry, on tape or punched cards.
4. Run the model at its maximum velocity over 4,000 feet of the rail in SLEDYNE, i.e., set  $TIMEF = 4000/V_{design}$ . Since, for monorail sleds, SLEDYNE calculates mean responses to rail roughness alone, the results must be scaled to adjust for peak response and to include the excitation from motor transients, transonic buffeting, etc. DFACF and DFACA are design factors which scale up the load vectors calculated by SLEDYNE. Set DFACF and DFACA equal to 2.5.
5. Transfer the scaled load vectors from SLEDYNE to the structural analysis program and combine them with the quasi-steady loads for the design stress analysis<sup>4</sup>. There will be two load vectors from SLEDYNE associated with the peak loads at the two slippers. Before running the stress analysis the analyst must examine each SLEDYNE load vector and combine with it the quasi-steady loads in the direction which will give maximum internal loads. In ambiguous cases it is best to run two solutions for a SLEDYNE vector.
6. Calculate the dynamic braking loads in SLEDYNE. A negative thrust time history is input with drag and lift tables. (The time history of lift will include the vertical braking force.) DFACF and DFACA are set to 1.6 to account for the absence of motor and pusher loads. The resulting SLEDYNE dynamic load vectors are superimposed on the quasi-steady loads which must include the quasi-steady braking loads.

#### Lateral Loads

Determine lateral dynamic loads assuming that they are a percentage of the vertical loads. The percentage depends on the distance of the cg above the rail as shown in Figure 6.16.

---

<sup>4</sup> The structural model used for step 5 is restrained only at the slippers and does not have the restraints which were imposed for the step 3 modal extraction. If lumped masses are placed along the slipper beams, their effect will be included in the load vectors from SLEDYNE.

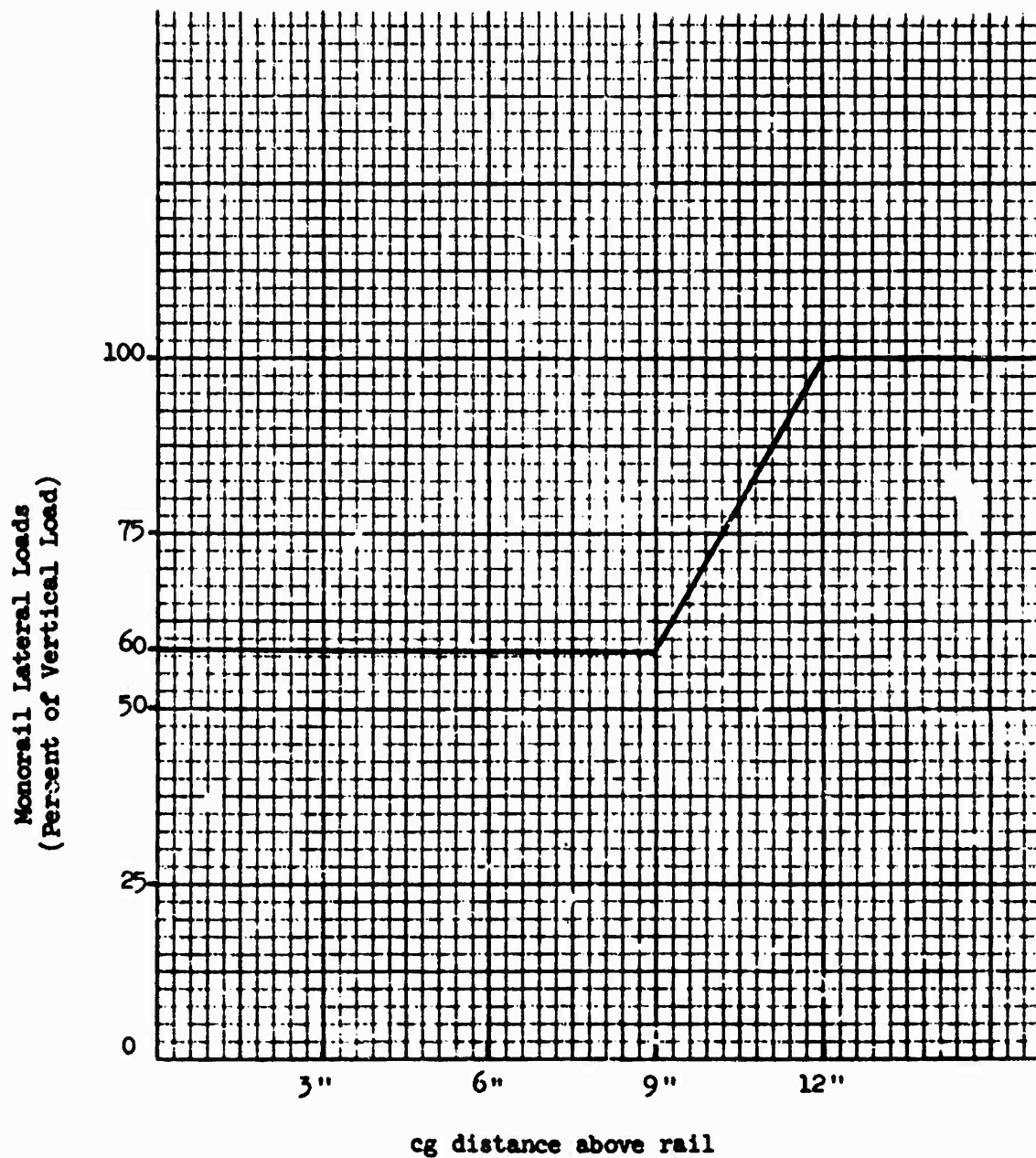


Figure 6.16. Magnitude of Lateral Loads for Monorail Sleds

## SECTION VII

### RECOMMENDATIONS

The study has identified a number of areas which deserve future considerations and investigation. These areas are described in the sections below.

#### 7.1 Measurement of Additional Sled Test Track Data

As previously mentioned in Section 2.1, there is a great lack of information on sled test data concerning the nature of the sources of dynamic excitation and limited information on the response of sled to the sources. Specifically, three major sources of dynamic excitation were identified in the study; unsteady aerodynamic forces, oscillating axial and lateral thrust forces and rail roughness. Data on the nature of these sources can only be obtained by test track measurements. Unsteady aerodynamic forces can be measured by proper placement of pressure transducers on the underside of sleds. Oscillating thrust forces can be measured by static firing tests and strain gaging the supports. Rail roughness profiles can be obtained by performing surveys and by the use of a test vehicle which has single dynamic characteristics.

The dynamic response of sleds to these sources of excitation can be measured by strain gaging the slipper support structure of dual rail sleds, and by using load transducers in monorail sleds. Of prime importance is the measurement of lateral loads in dual rail sleds, for which no test data is available, as well as the overall collection of data for a wide range of sled configurations and trajectories. The present study can serve as a basis for evaluating this test data. The proposed sled design analysis procedures can only be verified and improved by a systematic collection and analytical evaluation of additional sled test data.

#### 7.2 Rail Roughness Measurements

The only available information on rail roughness consist of 440 measurements over a 400 foot section of rail of the Holloman test track. Furthermore, they are measurements of only the height of the center of the rail. No measurements are available on horizontal roughness nor on roughness of the underside of the rail. These measurements are important to the assessment of the effect of rail roughness on sled dynamic behavior. Two methods for obtaining this data are described below:

##### 7.2.1 Survey

A survey of various portions of the Holloman track can be performed using conventional surveying practices. Two instruments are required to conduct this survey, a K & E Paragon No. 71-1010 Jig Transit and a K & E Paragon No. 71-3010 Tilting Level. The items are similar to normal surveying type instruments, but are an order of magnitude more accurate. The survey method is described below.

For establishing reference markers at approximately 100 foot intervals along the track, two instruments would be used. The first for establishing a longitudinal reference line would be a jig transit or a theodolite with an optical micrometer. The second for establishing the vertical reference manuments would be a precision tilting level with an optical micrometer with associated scales. A lateral slide mounted on a tooling fixture support would facilitate the operation. These same instruments can be used for measuring the profile and alignment of the rails.

First the longitudinal reference line is established with the jig transit by backsighting on a point, plunging the instrument and establishing the foresight point (Figure 7.1). Then the instrument is rotated  $180^\circ$  and backsighted in the plunged position, then plunged again to determine another foresight. If there is a difference in the foresight position this is split and the telescope moved in azimuth to align on the corrected foresight reference. In this case the lateral offset from the center-line of the rails must be identical.

With the jig transit set up and aligned on the longitudinal reference line the tooling bar is pushed toward the rail and measurements are read on the scale with the jig transit and optical micrometer (Figure 7.2).

For measuring vertical heights of the underside of the rail flange, the indicator is pushed up until it touches the underside of the flange and the dimensions on the scale attached to the indicator are read. To measure the rail edge vertical height, point A is aligned with the rail edge and the scale is read with the optical micrometer (Figure 7.3).

To measure vertical heights of the top of the rail, scales with pointers are used and dimensions on the scale are read with the optical micrometer (Figure 7.4).

The optical micrometer attached to the jig transit or tilting level makes it possible to read directly to .001 inches for distances up to 100 feet (Figure 7.5). First the transit, or level is aligned or leveled and the optical micrometer set to zero. The cross hair normal to the scale will read between two numbers (1.6 and 1.5 in the example). Next, the optically flat glass of the optical micrometer is turned through some angle until the line of sight is moved to bring the cross hair to coincide with the reference dimension on the scale. In the examples shown (Figure 7.5) the micrometer reads .047. Then the total measurement made is  $1.50 + .047$  or 1.547. Actually the micrometer has a vernier on its graduations so that it is possible to make readings within .0004 inches, but this is not possible over 10 - 12 feet.

These readings should be repeated several times and averaged for minimization of measurement errors.

#### 7.2.2 Test Vehicle for Measuring Rail Profile and/or Rail Roughness Excitations

As indicated previously the only data available on rail profiles for determining rail roughness excitations corresponded to measurements on a

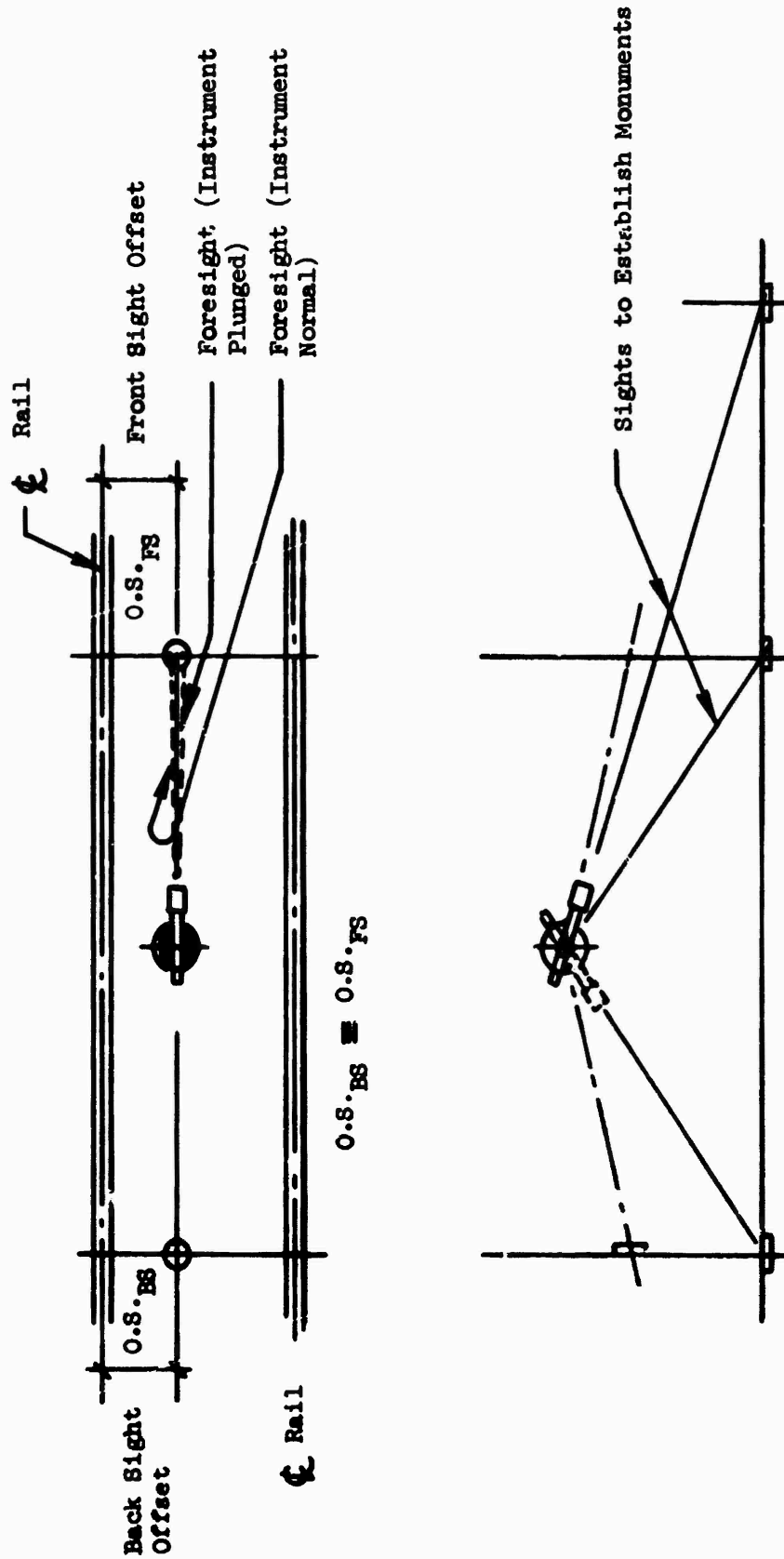


Figure 7.1(a) Establishment of Longitudinal and Vertical References

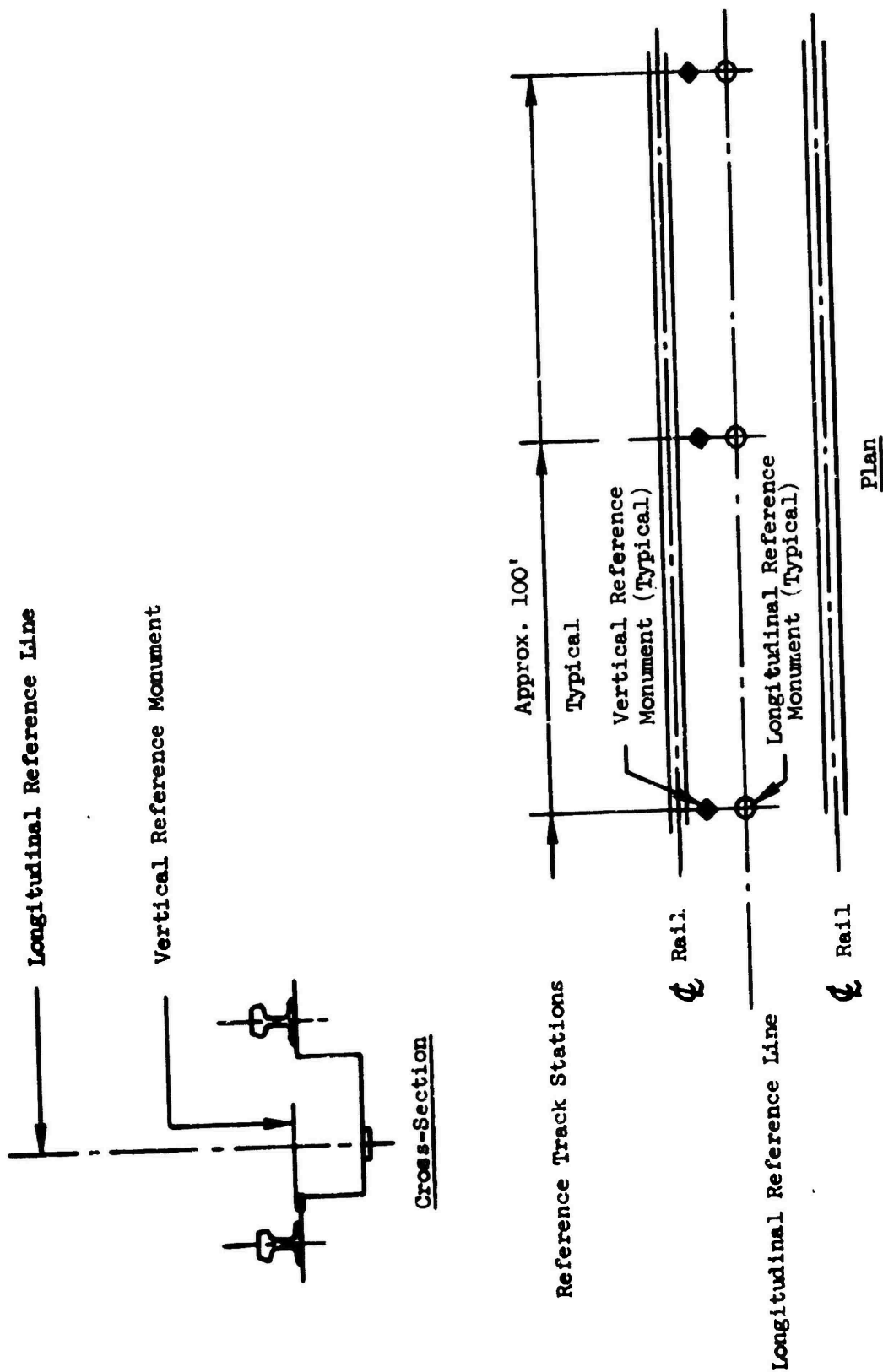


Figure 7.1(b) Establishment of Longitudinal and Vertical References

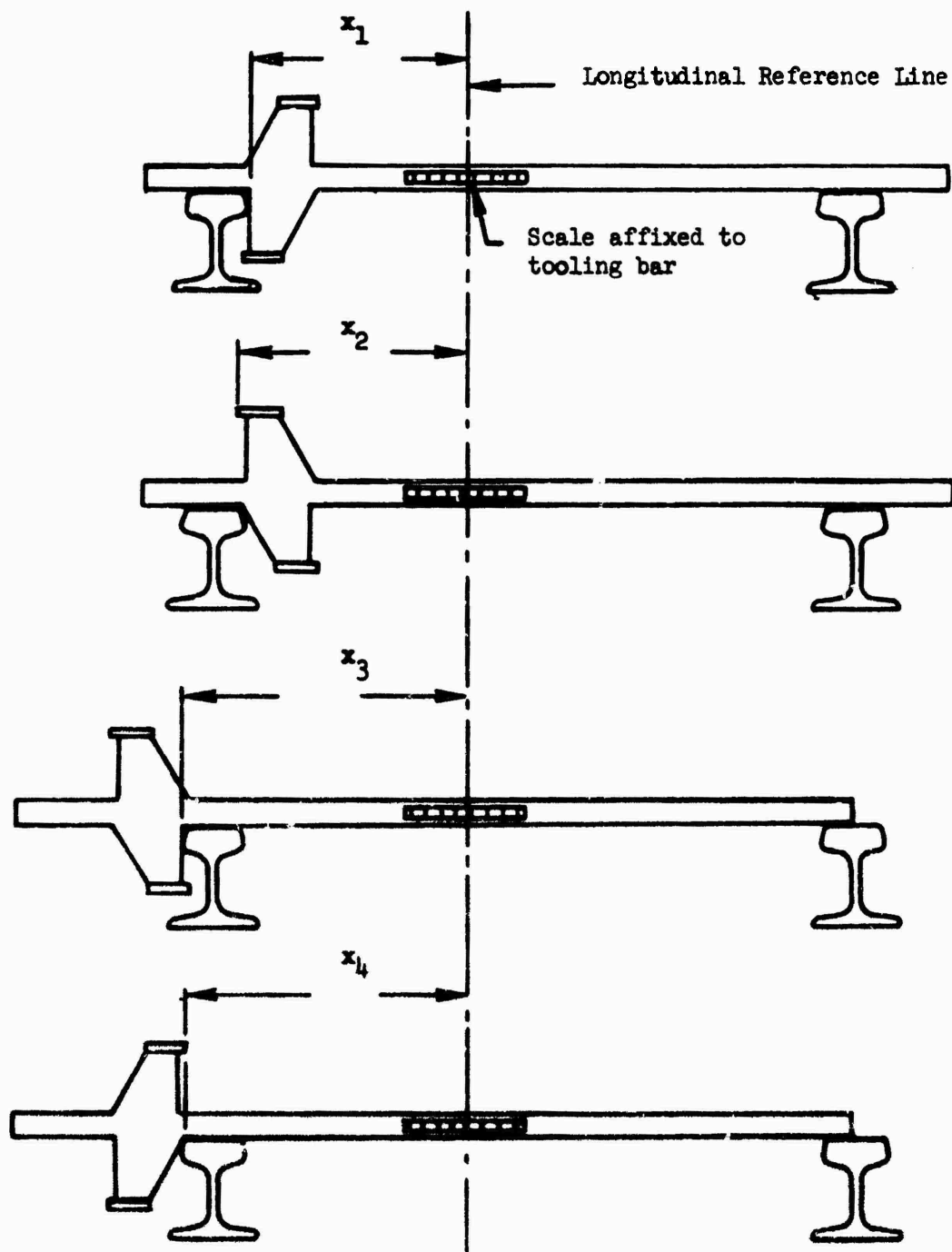


Figure 7.2 Tooling Bar



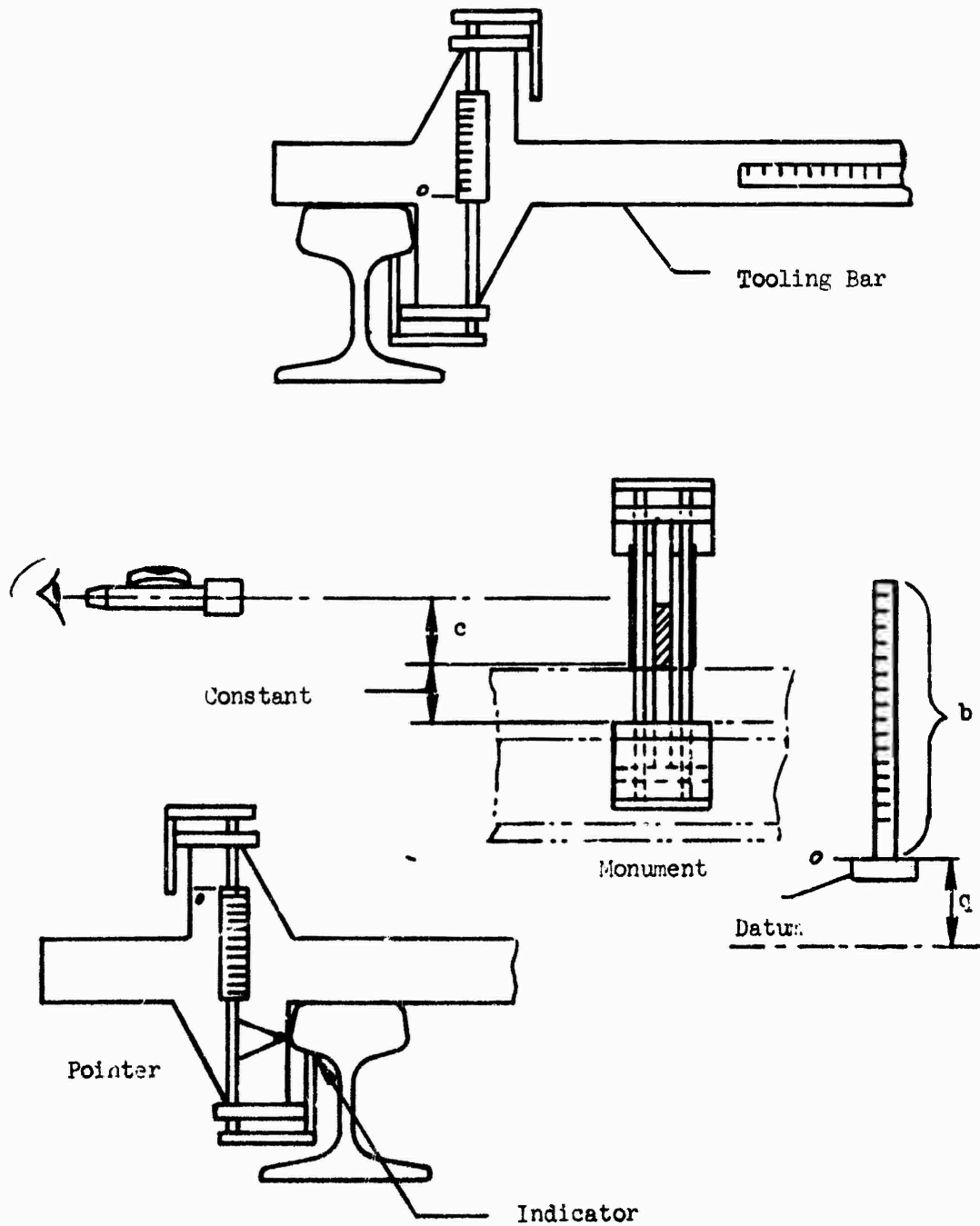


Figure 7.5 Measuring Device for Vertical Heights of the Rail Underside

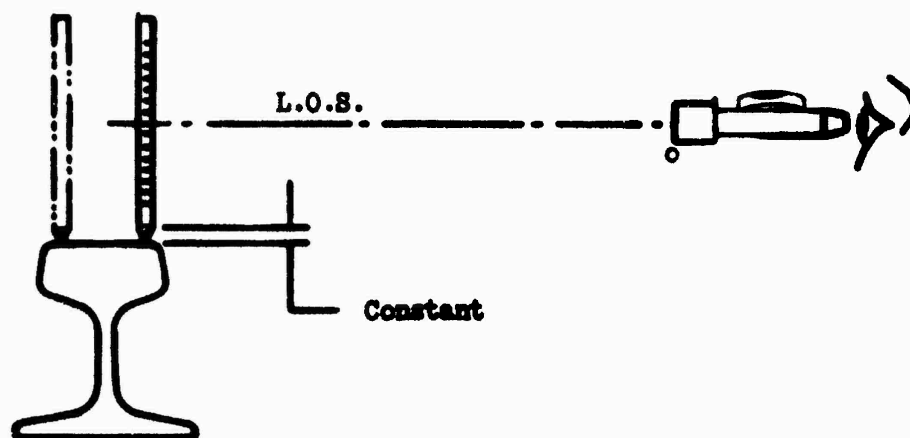
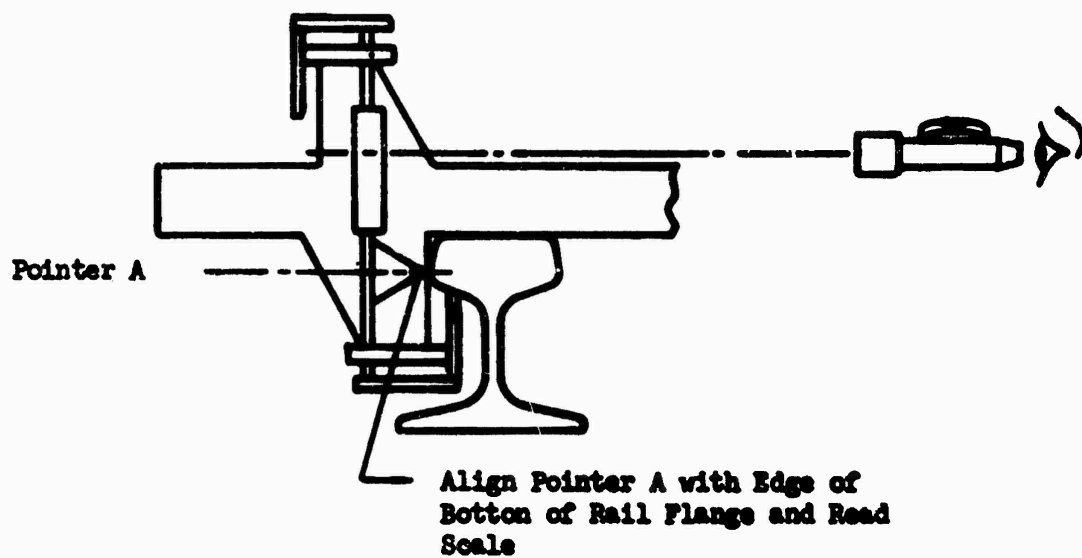


Figure 7.4. Measuring Device for Vertical Heights of the Rail Top

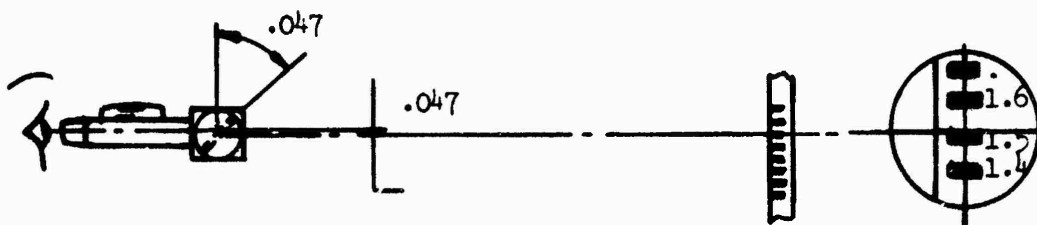
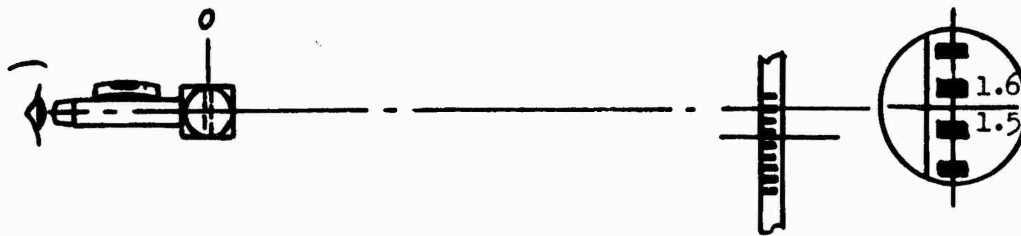


Figure 7.5. Optical Micrometer

400 foot section of rail taken at the top surface center-line. Typically, the sled rides on the bottom surface of the rail due to high lift forces. Moreover, it is important to know the rail profile at typical contact points, generally near the corners of the rail. No data was available on lateral rail profiles.

An attractive approach for determining rail profiles and/or rail roughness excitations makes use of a test vehicle having simple dynamic characteristics. The measurement technique is to infer rail profile and/or rail roughness excitations from a set of dynamic response measurements. This approach would facilitate rapid measurements over long distances of rail, and could also be used to assess rail conditions periodically for changes in profile due to wear, deterioration, etc.

Figure 7.6 shows the basic concept. It involves a towing vehicle and a test measurement vehicle. The test vehicle is towed by a long light-weight tow bar to minimize loads induced by the towing vehicle.

The test vehicle is a simple rigid structure which can be idealized by a single dynamic model. The slipper would have means for varying stiffnesses, as shown in the figure. This particular concept makes use of a set of inserts connected to the main slipper body by springs. Various measurement concepts are related to the stiffnesses of the slipper springs.

#### Approach No. 1

This approach makes use of a very compliant slipper. Instrumentation consists of a biaxial accelerometer to measure test vehicle response, and relative displacement transducers located between the main slipper structure and each insert. Displacement response of the vehicle center of mass is determined by double integration of the acceleration time history. The response at a particular insert or rail location is then determined from the geometry. Differences between these responses and those measured by the displacement transducers give the local rail profiles.

#### Approach No. 2

This approach makes use of compliant slipper springs at each location around the rail except at one location at whose profile is desired. At that location, the slipper spring is very stiff. The response will be dictated by the stiff spring, and the vehicle will respond to the desired profile. The basic approach is to determine the acceleration response history and to infer the desired rail profile through double integration.

A possible variation on the preceding approaches uses a laser beam as a fixed reference for measuring displacement response of a servo-controlled sensor on the sled body. This approach has been used successfully for measuring runway roughness. It eliminates the loss of accuracy associated with double integration of an acceleration response.

The foregoing represent possible rail measurement approaches using a special test vehicle. It is expected that other promising variations of these approaches also exist.

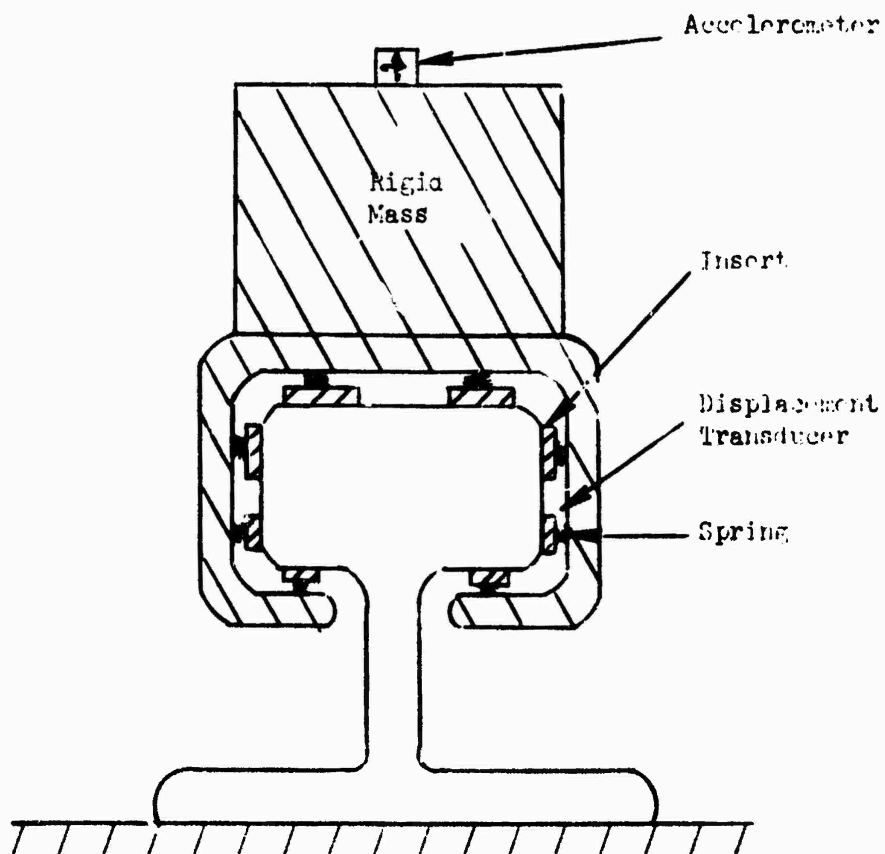
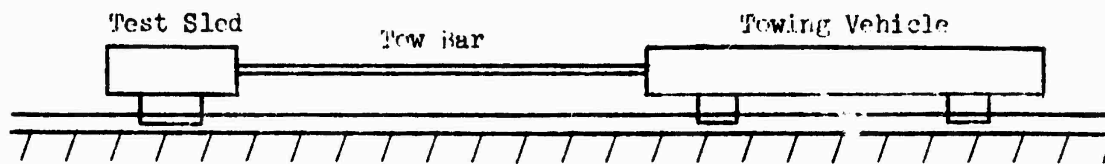


Figure 7.6. Rail Roughness Measurement Sled Concept

The previously described impact model for predicting rail roughness dynamic loads, substantiated by flight data, suggests the use of sled drop tests as a simple and useful test approach. Possible applications are as follows:

1. Development and Analysis

- a. Experimental verification of analytical models and dynamic response predictions for typical rail-induced sled loads, using improved instrumentation under laboratory conditions.
- b. Calibration of flight instrumentation.
- c. Aid in interpretation and correlation of flight data by providing a base for comparison.
- d. Development tests in conjunction with sled structure optimization and soft slipper development.

2. Acceptance Testing of New Sleds

Laboratory acceptance testing using simulated rail-induced dynamic loads provide obvious advantages over flight tests.

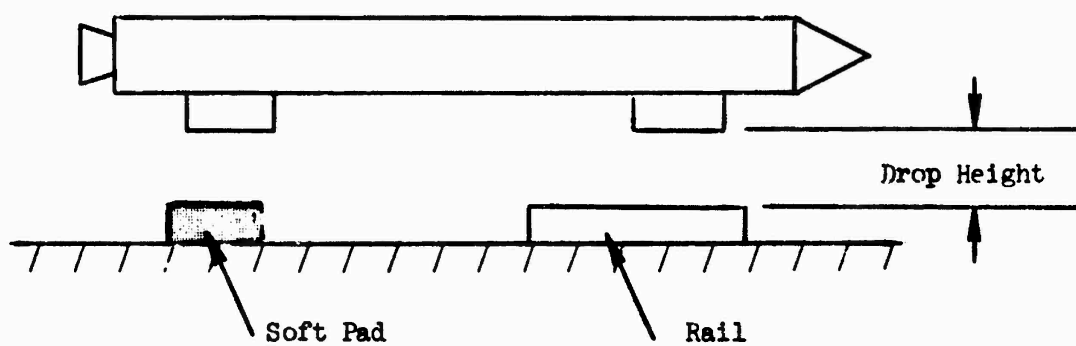
Several possible test approaches are described. Figure 7.7 shows two approaches in which the sled is dropped directly on the rail. Special slippers without lips would be required. Figure 7.7(a) corresponds to the previously described analytical impact model. The soft slipper is used to minimize loads on the "free" slipper. Figure 7.7(b), which appears to be somewhat simpler, may also be adequate, although further analysis is required to evaluate this approach.

Figure 7.8 illustrates an indirect impact approach in which the sled is mounted on a rigid support block which is dropped. Test configurations for both vertical and lateral loads are shown.

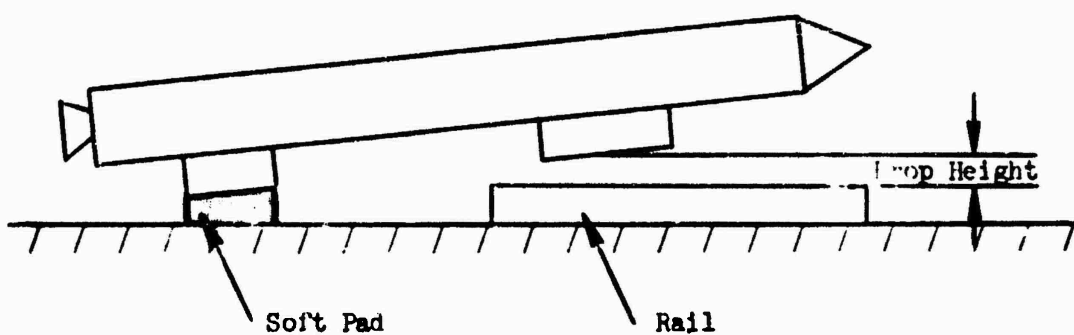
The drop heights required to simulate rail-induced dynamic loads are surprisingly small. For example, for the Instrumented Monorail sled at 4,000 fps, the impact velocity is approximately 60 in/sec, corresponding to a drop height of about five inches. A typical drop height required for dual rail sleds is one inch.

#### Soft Metal Slippers for Reducing Dynamic Loads

The previously described analytical models for predicting dynamic loads due to rail roughness, substantiated by flight data, indicate that these loads can be greatly reduced by reducing the stiffness of the slipper and/or support structure so as to reduce the effective impact frequency of the sled (Section 3.2). The small additional compliance required for substantial load reduction permits the use of "soft" metal slipper. A possible

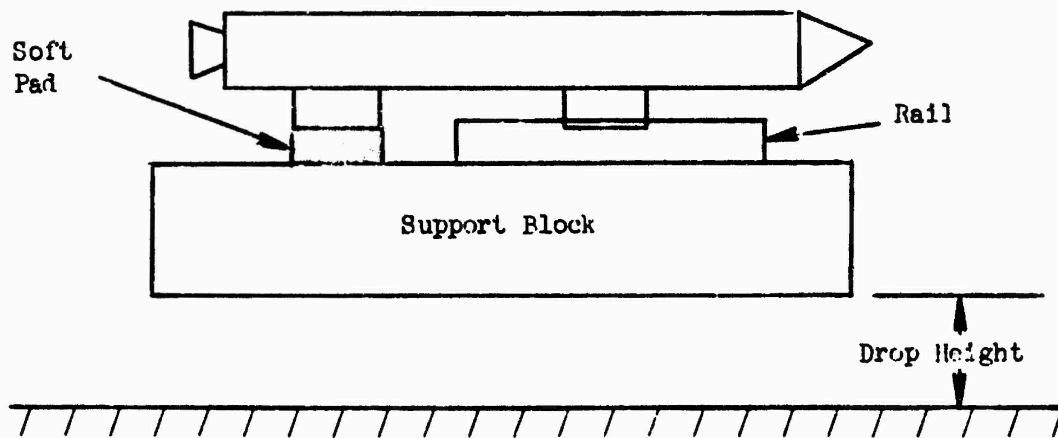


(a) Analytical Model Configuration

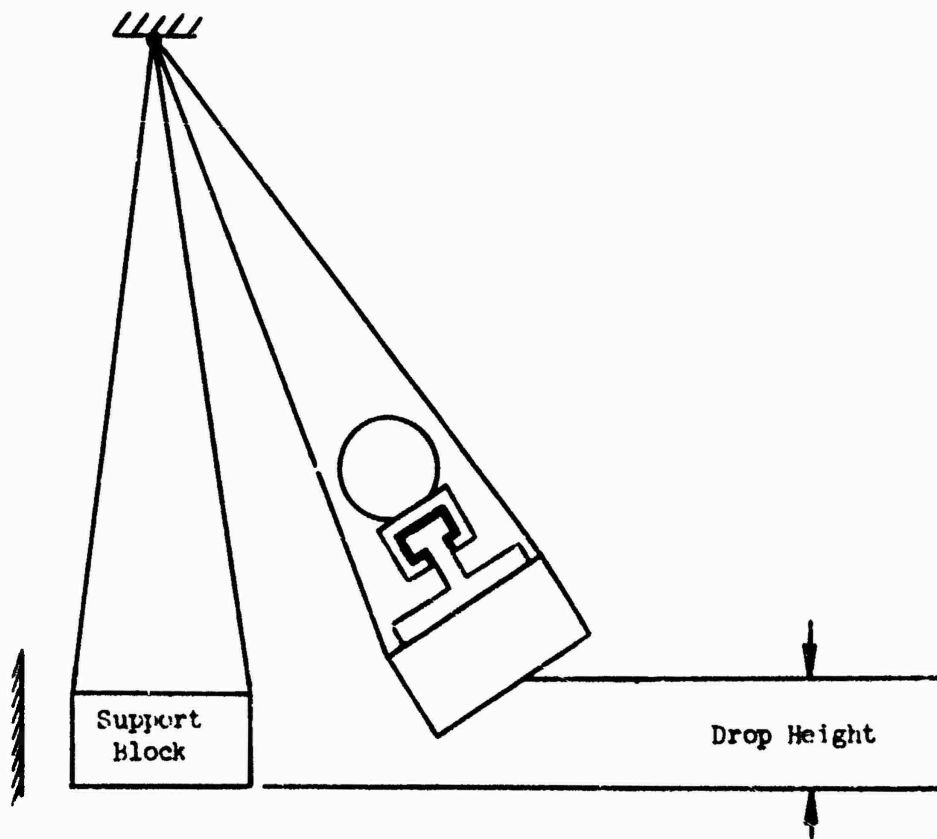


(b) Approximation to Analytical Model Configuration

Figure 7.7. Sled Drop Test Approaches -- Direct Rail Impact



(a) Vertical Loads



(b) Lateral Loads

Figure 1.8. Sled Drop Test Approaches -- Indirect Rail Impact



design approach is the use of elastic metallic devices such as Bellville springs or other compact springs between the slipper inserts and the slipper structure. Bellvilles are attractive because they would also provide beneficial damping.

A significant, and rather surprising consequence of properly designed soft metal slippers is that they would produce little, if any, increase in rail-roughness-induced dynamic deflections of the sled, although deflections due to quasi-steady loads would increase. In effect, as slipper stiffness is reduced, so also are the rail roughness loads, in such a manner that the dynamic deflections remain essentially constant.

Reduction in rail roughness loads is considerably more significant in monorail than in dual rail sleds, although the use of soft slippers would be beneficial in both. In monorail sleds, rail roughness loads have been shown to be as high as ten times quasi-steady loads; in dual rail sleds they are typically of the same magnitude. The influence of reduced sled frequencies on response to other dynamic excitations, such as oscillating aerodynamic and engine burning loads, cannot be assessed at this time, due to lack of information on these excitations.

Reduction in rail roughness dynamic loads would aid in the attainment of increased monorail sled velocities. Lower dynamic loads would permit lighter and more efficient sled structures. Also, reduced dynamic slipper loads may reduce slipper wear.

The conclusion that little, if any, increased dynamic deflection would result can be shown with the simplified impact model of Section 3.2.1. The maximum slipper force can be expressed by

$$F_{\max} = 2\pi f v M_{\text{eff}} \quad (7.1)$$

where  $f$  is the effective impact frequency,  $v$  is the impact velocity, and  $M_{\text{eff}}$  is the effective sled mass for impact on one slipper. The impact velocity curves of Figure 3.11, Section 3.2.1, indicate that, for a particular sled velocity and lift-to-weight ratio,  $v$  is approximately proportional to  $f$ , i.e.,

$$v = cf \quad (7.2)$$

where  $c$  is a constant of proportionality. Substitution of this relation into Equation (7.1), with the effective impact frequency equation,

$$f = \frac{1}{2\pi} \sqrt{\frac{K}{M_{\text{eff}}}} \quad (7.3)$$

gives the result

$$F_{\max} = 2\pi c f^2 M_{\text{eff}} = \frac{cK}{2\pi} \quad (7.4)$$

where  $K$  is the slipper and support structure stiffness.

Equation (7.4) shows that the maximum slipper force is directly proportional to K, and that the maximum slipper deflection is

$$\delta_{\max} = \frac{F_{\max}}{K} = \frac{c}{2\pi} \quad (7.5)$$

which is, indeed, approximately constant and independent of K.

The added compliance that would have to be built into a "soft" metal slipper for a substantial reduction in rail roughness loads is illustrated by the following example for the Instrumented Monorail sled:

At 4,000 fps, the average peak vertical dynamic force in the forward slipper is approximately 17,000 pounds. Consider the compliance necessary to reduce this force to 1,700 pounds, the approximate quasi-steady lift force on the forward slipper at 4,000 ft/sec. The forward slipper and support structure stiffness is, based on the finite-element model of Figure 3.12, Section 3.2,  $K = 5.53 \times 10^5$  lb/in. This would have to be reduced to  $5.53 \times 10^4$  lb/in, reducing the effective impact frequency from 312 Hz to approximately 99 Hz. The resulting maximum slipper and support structure deflection for the 1,700 pound force would be 0.031 inch, of which 0.028 inch would have to be provided by the additional compliance built into the "soft" slipper. Approximately twice this deflection capability would be required to handle both the dynamic and quasi-steady lift forces.

Soft slippers provide an attractive approach for investigating other dynamic excitations such as oscillating aerodynamic and engine burning loads. A sled subject to such excitations could be flight tested under a set of conditions differing only in slipper compliance and hence, sled frequencies. By subtracting out the known rail-induced response as a function of effective impact frequency, it would be possible to determine the response due to the other excitations. It may also be possible to reduce the rail-induced loads to such low levels that the only significant excitations would result from the other sources.

## SECTION VIII

### CONCLUSIONS

The objectives listed in Section 1.2 of this report have been achieved. The end result of the study is the establishment of new design analysis procedures for a wide range of dual rail and monorail sleds. These design procedures (Section 6.0) have been written in a manner such that they can be removed from the report and used as design criteria for future sled designs. It should be recognized that these procedures are based upon a very limited amount of test data and are not intended to be all encompassing and forever fixed. Rather, they have been formulated with the intention that they can and will be refined and improved as more sled test data and associated analyses become available. It is hoped that they will form the basis of a new rational method of designing sleds.

The study has pointed out the major areas for which more test data and supporting analyses are required. In addition, means of improving sled designs have been suggested and a method of verifying the structural adequacy of sleds, by test, has been proposed.

## REFERENCES

1. Interstation Supersonic Track Conference Structures Working Group, ISTRACON Handbook, AFMDC, Holloman AFB, New Mexico, December 1, 1961.
2. Mixon, Larry C., Sled Design Techniques, AFSWC-TR-71-3, 6586th Test Group, Holloman AFB, New Mexico, February 1971.
3. Fisher, Gary K., and Stronge, W. J., Analytical Investigations of Rocket Sled Vibrations Excited by Random Forces, U. S. Naval Ordnance Test Station, China Lake, California, July 1964.
4. Oliver, R. E., and Wu, T. Y., Final Report: Sled Track Interactions and a Rapid Method for Track-Alignment Measurements, Aeronautical Engineering Research, Pasadena, California, June 30, 1958.
5. Hasse, Hans O., Provisional Summary of a Sled Vibration Study Report, WP-MDS,66-1, AFMDC, Holloman AFB, New Mexico, February 1966.
6. Braun, Gerhard W., and Melkus, Harold A., On the Nonlinear Motion of a Rocket Sled, AFOSR/DRA-62-13, AFMDC, Holloman AFB, New Mexico, July 1972.
7. McIntyre, K. L., "Linear Aeroelastic Stability Analysis of USNOTS 8,000 FPS Third Stage Sled," General Dynamics Technical Memorandum No. 348-44. 3-2, 23 February 1967.
8. Krupovage, D., Mixon, L., and Pokorny, O., Wind Tunnel and Full-Scale Forces on Rocket Sleds, AFMDC-TR-67-12, January 1967.
9. Studies on Dynamics and Instrumentation of the Holloman Track, Holloman AFB, New Mexico, AFMDC-TR-59-8, 1959.

## APPENDIX I

### SLEDYNE USER'S GUIDE

#### I.1 Introduction

The SLEDYNE program is a tool for the structural design of rocket propelled test sleds. The program computes the time history dynamic response of a monorail or dual rail sled traveling along a track which has roughness characteristics based on test data. Input includes time histories of thrust, lift and drag. Results are in terms of slipper forces and sled accelerations.

The sled may be idealized as a lumped mass two-degree-of-freedom system or may be further defined by special mode shapes and frequencies. Their inclusion permits a more refined definition of the inertial loads and leads to more detailed internal structural loads.

SLEDYNE is compatible with the MRI/STARDYNE program and other contemporary finite-element programs. The format of the tape used for inputting the modal data is provided in Section I.3. Please refer to Figure 1 for SLEDYNE Program Flow.

The program creates a printer plot file which plots slipper forces versus time in addition to printed output.

For the sled designer, the most important SLEDYNE output is a set of force vectors. These are factored inertial forces acting on those nodes of the sled model which have lumped mass. The vectors correspond to instants of time when slipper forces are greatest. The factors by which the vectors are scaled are input by the user. In monorail sled analysis, the program also scales the force vector so that it corresponds to the average peak slipper force in .1 second intervals. This is explained in the monorail design procedure. In all cases, the load vectors include only dynamic loads even though quasi-steady loads may have been involved in the response analysis.

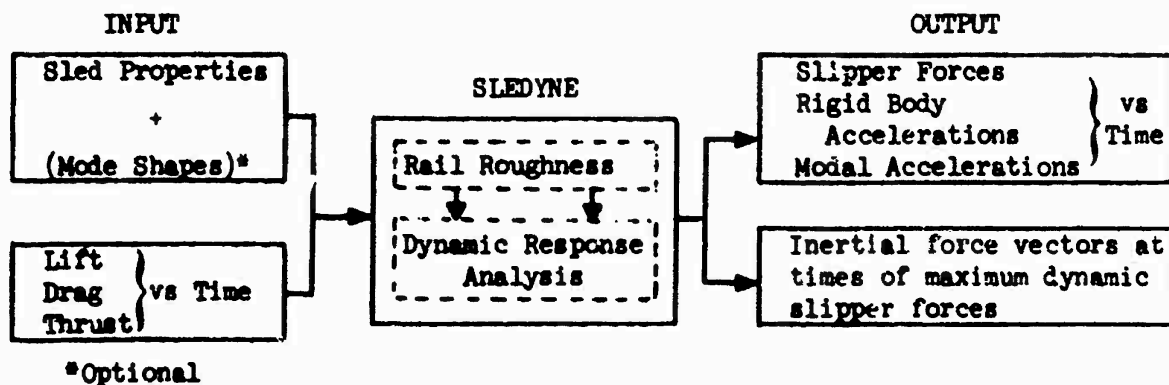


Figure 1. SLEDYNE Program Flow

# SLEDYNE USER'S GUIDE - CONTINUED

I.2

## SLEDYNE Input Format

Card Number 1: Sled Description (Up to 80 characters)

1)

USER SUPPLIED DESCRIPTION OF RUN	
----------------------------------	--

Card Number 2: Monitor Maximum Displacements, Set Symmetry Indicator

•

If a TAPE<sup>4</sup> is not available containing geometry and mode shapes, insert a blank card here and continue to card number 3.

2)

6	11	12	17	18	23	24	29	30	35	36	42	54
NNDS	N1	D1	N2	D2	N3	D3	N4	D4	N5	D5	ISYM	DTFAC
(16)	(15)	(11)	(15)	(11)	(15)	(11)	(15)	(11)	(15)	(11)	(16)	(F10.0)

NNDS = Total number of displacement variables to be monitored for maximum displacement during run. (Maximum allowed is 5.) Leave blank if none are to be checked, and look at ISYM flag.

N1-N5 = Node and DOF numbers of displacements which are to be monitored. N<sub>i</sub> is the node number. D<sub>i</sub> is the DOF which must be either three (vertical) or five (pitch).

ISYM = 1, If model on TAPE<sup>4</sup> is a symmetric half of real structure.

= 0, If full model is on TAPE<sup>4</sup>.

DTFAC = If non-zero, is multiplied by the internally calculated minimum integration time step.

# SLEDYNE USER'S GUIDE - CONTINUED

## Card Number 3: Choose Card A or B

Card A (conditional): If geometry and mode shapes are to be input, card A must be input. If mode shapes are not to be used, please ignore this card and supply only card B.

### CAUTION

The information on this card corresponds to the mode shapes picked from those available on tape. (Format of the modal data tape is described in Section I.3). The program will choose the first "NMODES" modes which have an X3 participation factor greater than X2 or X1 participation factors, i.e., the vertical modes. All "NMODES" modes are used when symmetry flag has been set = 1 (See card 2).

	6	12	18	24	30	36	40
Card A	NMODES	PCD1	PCD2	PCD3	PCD4	PCD5	PCD6
	(I6)	(F6.0)	(F6.0)	(F6.0)	(F6.0)	(F6.0)	(F6.0)

NMODES = Number of modes (vertical only) which are to be used for the response analysis. A maximum of six modes is allowed.

PCD1  
through

PCD6 = PCD<sub>i</sub> is the proportion of critical damping to be applied to the i<sup>th</sup> vertical mode. .03 gives "3 per-cent critical damping."

OR

Card B This card must be supplied only when geometry and mode shapes are not input

	12	24	36	48
	W	IYY		
	(E12.0)	(E12.0)	(E12.0)	(E12.0)

W = Sled weight (lbs.).

IYY = Pitch inertia about cg (lb.-in.<sup>2</sup>).

Card Number 4: This card indicates the type of sled being simulated, flags for printing and plotting, and design factors for output forces. This is the first card of multiple case data.

4	6	12	18	24	36	48	60	72	
TYPE	IPLØT	IPRINT	DFACF	DFACA	DFACFL	DFACAL			
(A4)	(2X)	(I6)	(I6)	(6X)	(4E12.0)				

TYPE = Punch "MØNØ" in columns 1 - 4 if this is a monorail sled.

Punch "DUAL" in columns 1 - 4 if this is a dual rail sled.

IPLØT = 1, Printer plots of slipper forces versus time will be created on TAPE8.

= 0 (or blank), No printer plots.

Note: When printer plots are created, the disk file, TAPE8 must be rewound and copied to OUTPUT -- see SCOPE control cards, Section I.3.4

IPRINT = 0 (or blank), No printout of slipper forces and modal accelerations. INPUT, maximum forces, and inertial loads will be printed always.

= 1, Slipper forces, vertical pitch and modal accelerations will be printed at each instant of time where a slipper force was a local maximum or minimum or entered or left the gap.

= 2, Only slipper forces will be printed.

DFACF  
DFACA = Design factors by which inertial force vectors are to be scaled before being output. DFACF scales vectors associated with peak forward slipper forces and DFACA, those from aft slipper peaks. (See design procedures.)

DFACFL  
DFACAL = If these factors are nonzero, lateral forces (X2 direction) will be included in the output inertial force vectors. The vertical forces corresponding to a forward slipper peak will be scaled by DFACFL and added to the output vectors in the lateral direction. DFACAL will be used similarly for vectors associated with aft slipper peak forces.



Card Number 5: This card and Card Number 6 are used to input the sled parameters. Please refer to Figure 2 on the following page for a schematic.

12	24	36	48	60	72	
EPS	$h_c$	$h_D$	$h_T$	1	$l_c$	
(E12.0)	(E12.0)	(E12.0)	(E12.0)	(E12.0)	(E12.0)	

EPS = Slipper gap (in.). Current standard value is .125.

$h_c$  = Height of cg above rail head (in.).

$h_D$  = Height of drag force.

$h_T$  = Height of thrust force.

1 = Distance between fore and aft slippers.

$l_c$  = Distance from forward slipper to cg.

Card Number 6:

12	24	36	48	60	72	
V	$K_F$	$K_A$	TIME	PCDZ	PCD $\theta$	
(E12.0)	(E12.0)	(E12.0)	(E12.0)	(E12.0)	(E12.0)	

V = Sled velocity in ft./sec.

$K_F$  = Forward slipper beam stiffness (lb./in.).

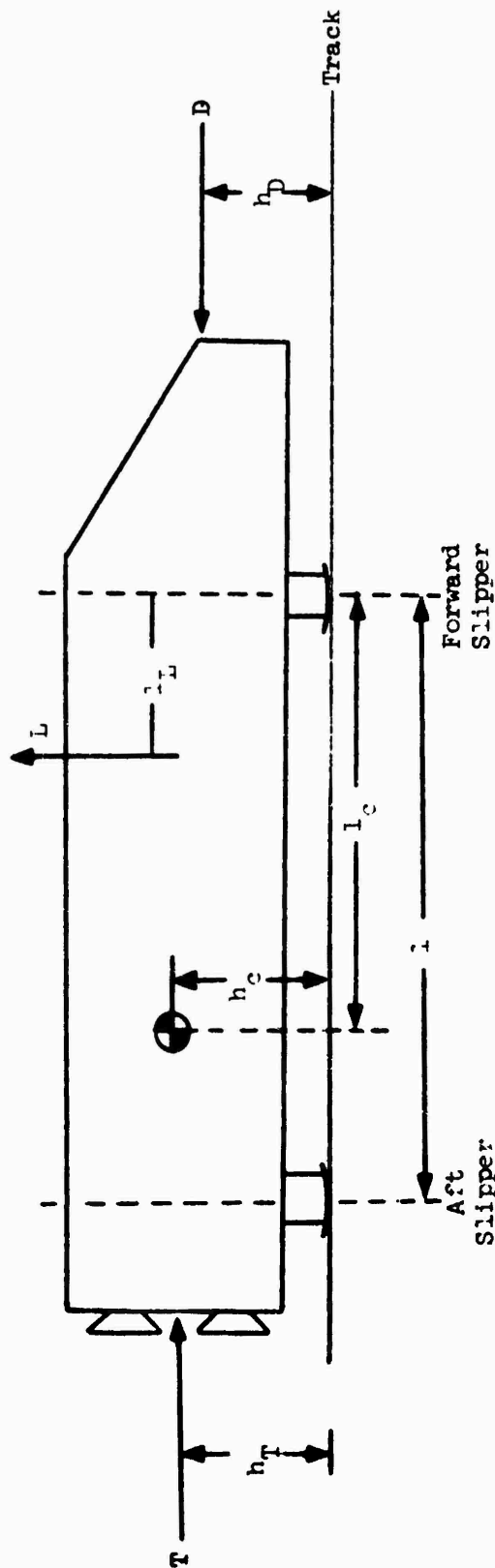
$K_A$  = Aft slipper beam stiffness (lb./in.).

Dual rail sleds:  $K_F, K_A$  should be input as twice the value of an individual forward or aft slipper.

TIME = Total time of run in seconds (time should be large enough to send the sled over a distance of at least 4,000 feet, i.e.,  $DIST = TIME \times V > 4,000$  feet).

PCDZ  
PCD $\theta$  = Proportion of critical damping for vertical and pitch "rigid body" modes. Recommended value is .03 for both.

Figure 2. Sled Geometry



Symbol	Description*	May Be Time Varying
L	Lift on Sled -----	Yes
T	Thrust -----	Yes
D	Drag -----	Yes
l	Distance Between Forward and Aft Slippers -----	No
$l_L$	Distance From Forward Slipper to Center of Lift -----	Yes
$l_c$	Distance From Forward Slipper to cg -----	No
$h_T$	Height of Center of Thrust Above Rail Head -----	No
$h_D$	Height of Center of Drag -----	No
$h_c$	Height of cg Above Rail Head -----	No

\*Units are inches or pounds

TABLES OF TIME VARIABLES

Four parameters may be input as time dependent. Linear interpolation is used. The tabular input format also allows straight line and constant inputs.

Table	Description
1	Drag versus time
2	Thrust versus time
3	Lift versus time
4	Center of lift versus time

The tables must be supplied in the above sequence. The formats of the cards in each table are described below. A blank card must follow this set of data. (See Figure 3.)

Straight Line or Constant Input

	9	12	24	36	48	60	72
NUM	/	/	0.0	QINT	SLP	/	/
(I9)	(3X)	(E12.0)	(E12.0)	(E12.0)			

NUM = Table number (must be 1, 2, 3, or 4).

QINT = Value of ordinate at time = 0.0.

SLP = Slope of line -- when slope = 0.0, the parameter is a constant with value of "QINT."

Arbitrary Input

	9	12	24	36	48	60	72
NUM	/	/	WC	QINT	0.0	T <sub>1</sub>	T <sub>2</sub>
(I9)	(3X)	(E12.0)	(E12.0)	(E12.0)	(E12.0)	(E12.0)	(E12.0)

NUM = Table number (must be 1, 2, 3, or 4).

WC = Word count required to read the table  
 $WC = 2 (NPAIRS) + 4$ .

QINT = Number of intervals in this curve  
 $QINT = NPAIRS - 1$ .

Beginning in columns 49 to 60, all the time values are input on this card and subsequent cards, followed by all the ordinates shown on the card below (-- for four pairs).

$T_1 - T_{NPAIRS}$  = Abscissa values (time points for this parameter).

$Y_1 - Y_{NPAIRS}$  = Ordinate values (values of drag or thrust, etc., at corresponding time point).

	12	24	36	48	60	72
T <sub>3</sub>	T <sub>4</sub>	Y <sub>1</sub>	Y <sub>2</sub>	Y <sub>3</sub>	Y <sub>4</sub>	

# SLEDYNE USER'S GUIDE - CONTINUED

## Card

1	1	9 12	24	36	48	60	72	ID
			0.0	0.0	0.0	0.0	0.0	
2	2		10.0	2.0	0.0	0.0	.01	ID
3		.05	0.0	20000.	30000.			ID
4	3		0.0	8000.	500.			
5	4		0.0	72.0	0.0			
6	0							

- Card 1      Table number 1: Drag force is 0.0
- Cards 2, 3   Table number 2: Thrust has three values start at time = 0.0 to time = .05
- Card 4      Table number 3: Lift is a straight line with value at time = 0.0 of 8,000 pounds and increasing at 500 pounds/second.
- Card 5      Table number 4: Center of lift is constant 72.0 over all time.
- Card 6      Blank card supplied to terminate reading of tabular data.

Figure 3. Sample Curve Data  
(Illustrative of All Curve Types Allowed)

SLEDYNE Input Formats

A SLEDYNE case will start execution after all tabular data has been read. Subsequent cases will be read starting at card number 3 of a new group.

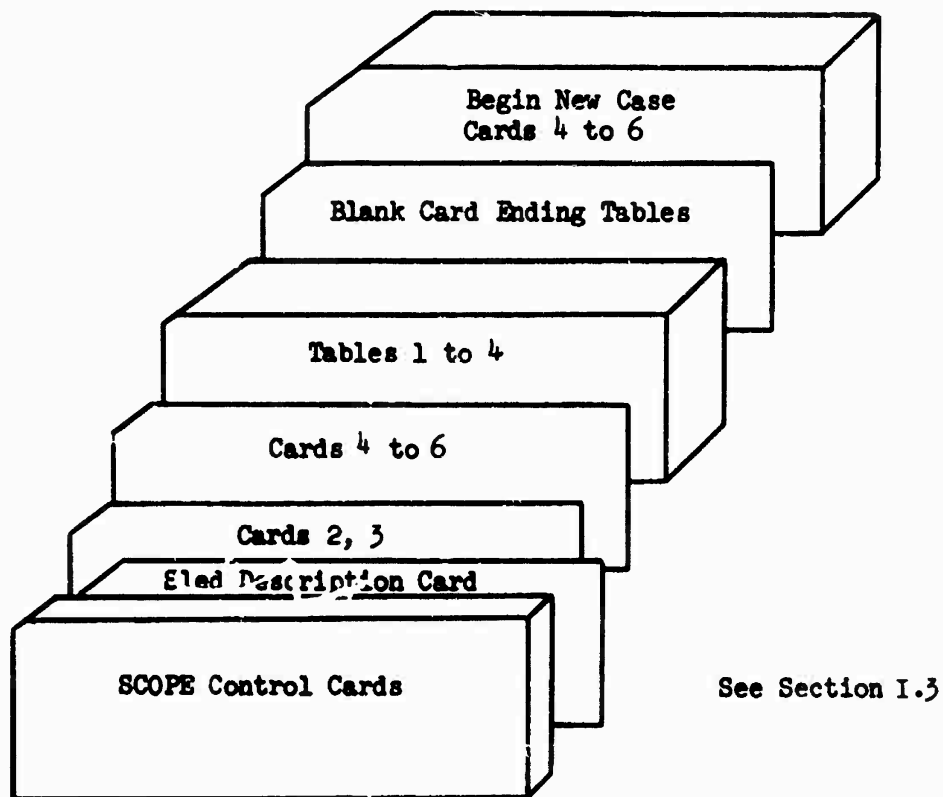


Figure 4 . SLEDYNE Deck Setup

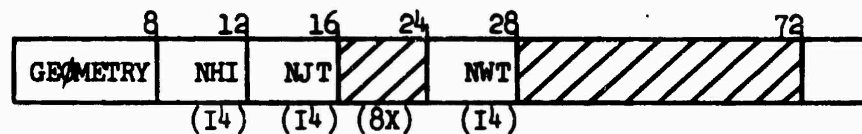
## SLEDYNE USER'S GUIDE - CONTINUED

### I.3 Geometry and Modes Tape Format

The sled finite-element model geometry, and mode shapes generated by a STARDYNE HQR run are required input to SLEDYNE. They are located on file 1 (GEOMETRY) and file 2 (MODES) of TAPE<sup>4</sup>. A description of the necessary information from those files is presented below. The user of SLEDYNE will find this information helpful if STARDYNE is not the finite-element program used to create the modes. The following data may be input on cards and copied to TAPE<sup>4</sup> prior to executing SLEDYNE. (See Section I.3.4 for necessary control cards.)

#### I.3.1 Geometry File

Card Number 1: This card is always read by SLEDYNE from TAPE<sup>4</sup>. If this card is not available, then the program does not try to read any additional information about geometry or modes.



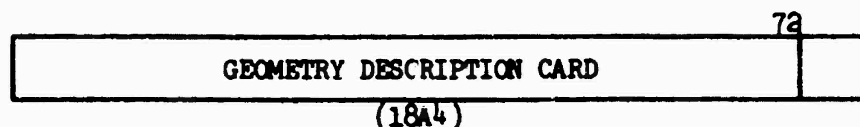
GEOMETRY = Punch GEOMETRY in columns 1 - 8.

NHI = Maximum node number.

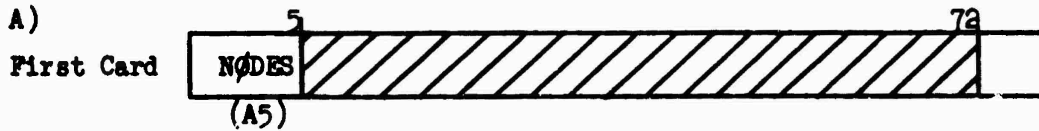
NJT = Number of defined nodes.

NWT = Number of nodes with weights.

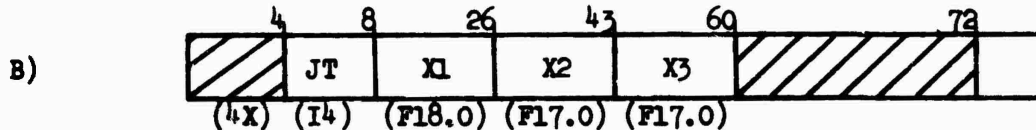
#### Card Number 2



**NODES:** The node point coordinates are read according to the formats below -- all nodes must be in a global coordinate system. Only the nodes with weights must be input to SLEDYNE.

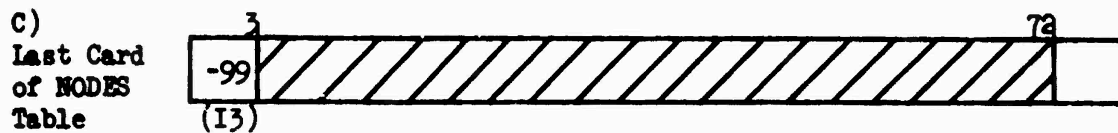


NØDES = Punch NØDES in columns 1 - 5.

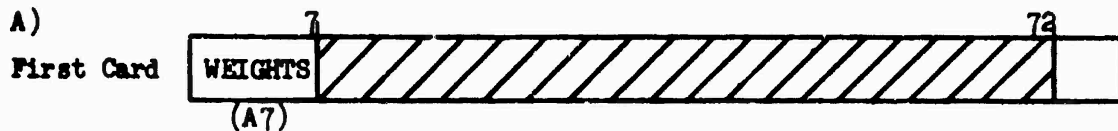


JT = Node number.

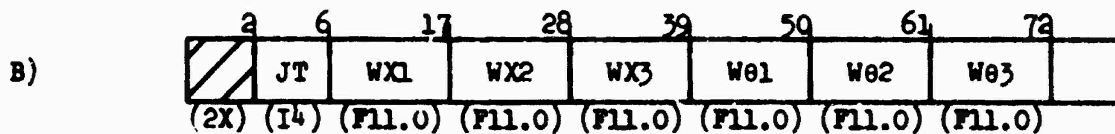
X1 } Node coordinates in global cartesian system. There  
 X2 } will be "NJT" of these cards. (See Geometry card.)  
 X3 }



-99 = Punch -99 in columns 1 - 3.



WEIGHTS = Punch WEIGHTS in columns 1 - 7.



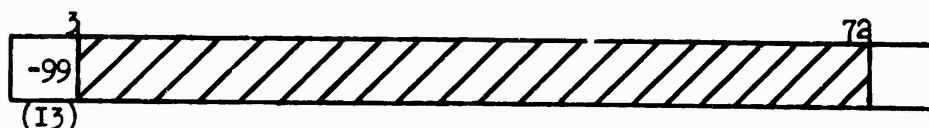
JT = Node number.

WX1 }  
 WX2 } Weights.  
 WX3 }

WØ1 }  
 WØ2 } Weight rotary inertias.  
 WØ3 }

There will be "NWT" of these cards. (See GEOMETRY card.)

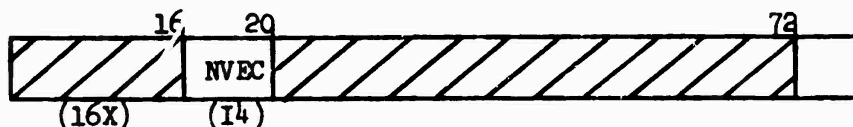
C)  
Last Card  
of WEIGHTS  
Table



-99 = Punch -99 in columns 1 - 3.

### I.3.2 Modes File

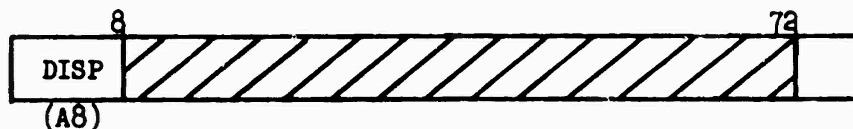
Card Number 1: This card indicates the number of mode shapes (displacement vectors) to follow.



NVEC = Number of vectors to follows.

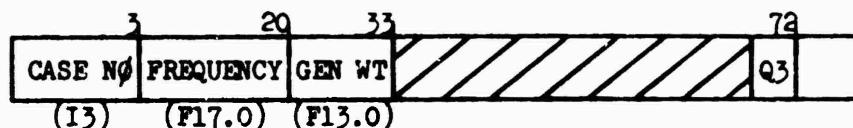
Mode Shapes: There must be "NVEC" of these tables punched.

A)  
First Card



DISP = Punch DISP in columns 1 - 4.

B)



CASE NO. = Static case number or mode number.

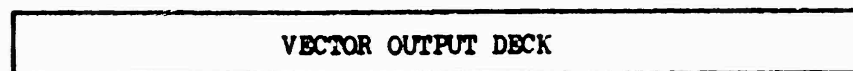
For Eigenvectors Only:

FREQUENCY = Eigenvalue in CPS.

GEN. WT. = Generalized weight.

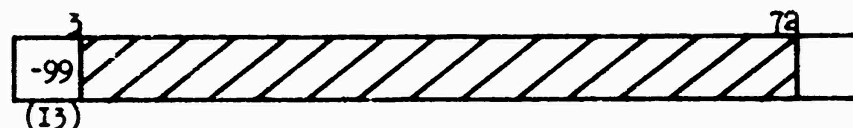
Q3 = Participation factor.

C)



This is the eigenvector/displacement array, written in the DECRDN format. All cards must have the same "DECRDN" type. (See DECRDN Description, Section I.3.3.)

Last Card  
of VECTOR



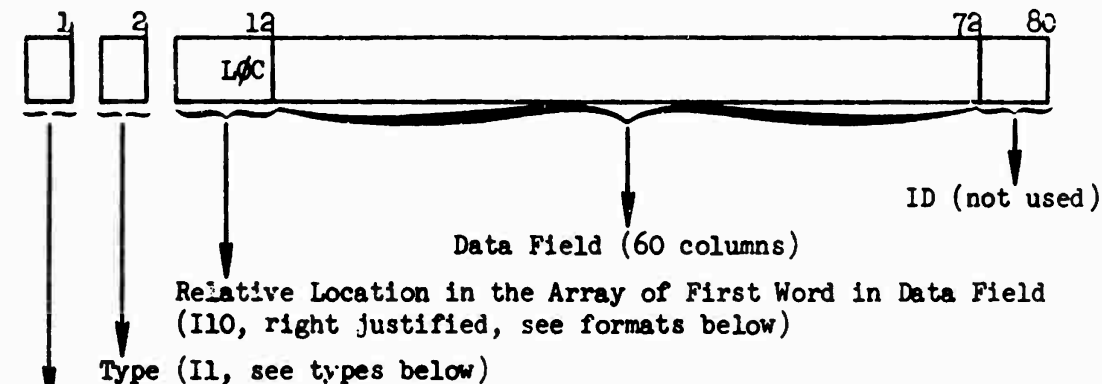


### I.3.3 DECRDN Format for Displacement Vectors

Subroutine DECRDN provides a convenient way for the user to enter floating point numbers into an array. The numbers are placed in their proper position in the array by specifying the relative array location (LOC) for the first data word of each card. The second data word on the card will be placed into array location LOC + 1, etc. Depending upon the accuracy desired, the user may select individual card formats ranging from three to six data words per card.

The relative location feature minimizes the number of cards required to enter sparse arrays and also eliminates the possibility of error due to cards being out of order. A minus punch must be placed in column 1 of the last data card in order to "terminate" the DECRDN read.

#### Acceptable Card Formats for DECRDN



A Minus in Column 1 Will Cause This Card to be "TERMINATOR" Card (11)

Type	Data Field Format	Card Columns Per Data Word
3	3F20.0	20
4	4F15.0	15
5	5F12.0	12
6	6F10.0	10
*J	6F10.0	10

#### General

- Cards may appear in any order. Card types will be read successfully even when intermixed.
- The minus sign (terminator) may be coded into either column 1, 3, 4, 5, 6, 7, 8, 9, 10, or 11.

\*Special: If type "J" is specified, the relative location (I) in the array, of the first word in data field is computed by DECRDN as:  $I = (LOC - 1) \times 6 + 1$ . In effect, LOC becomes a node number and the 6 words in the data field are: X1, X2, X3, X4, X5, and X6 terms. (See the following page for a DECRDN example.)

NAME		DATE	PAGE	OF
1	2	3	4	5
6	7	8	9	10
11	12	13	14	15
16	17	18	19	20
21	22	23	24	25
26	27	28	29	30
31	32	33	34	35
36	37	38	39	40
41	42	43	44	45
46	47	48	49	50
51	52	53	54	55
56	57	58	59	60
61	62	63	64	65
66	67	68	69	70
71	72	73	74	75
76	77	78	79	80
81	82	83	84	85
86	87	88	89	90
91	92	93	94	95
96	97	98	99	100

DECRDN EXAMPLE

The three cards shown at /ve demonstrate the manner in which the numbers shown below may be entered into the array via DECRDN. It may always be assumed that all locations in the array are initially zero.

ARRAY LOCATION	NUMBER
1	0.0
2	721.63
3	0.0
4	0.0
5	0.0
6	381.9
7	267.3
8	137.428156434
9	22.4
10	-18.0
11	0.0
12	0.0
13	0.0
14	0.0
15	3.1415926536
16	11.389

### I.3.4 Control Data SCOPE Control Cards

The SCOPE control cards, given below, will enable the user of SLEDYNE to:

- A. Create SLEDYNE program (executable absolute) from source card input. (save on tape name "SLED.")
- B. Execute SLEDYNE using a TAPE<sup>4</sup> created by a STAR HQR run. (Program on tape name "SLED.")
- C. Execute SLEDYNE using geometry and modes data input on cards. (Program on tape name "SLED.")

#### A. Create an Executable SLEDYNE Program from Source Cards

##### (A1) CDC DATA CENTERS

Card

```

1 $CHARGE, _____.
2 SLED(CM14000,CL150000,TP1,P2,T200)
3 REQUEST,SLED,HI. (SAVE,RING,PR)
4 RFL,70000.
5 FTN(ØPT=1,R=2)
6 RFL,150000.
7 SET(1)
8 MAP(PART)
9 LOAD(LGØ)
10 NØGØ.
11 UNLOAD(SLED)
12 (7/8/9) (SCOPE end of record)
    { OVERLAY(SLED,0,0) }
    { ((Above card begins in col. (7))) }
    { SLEDYNE Source Deck }
13.(6/7/8/9) (SCOPE end of file)
```

##### (A2) KIRTLAND A.F.B. 6600

Card

```

1 SLED,T200,CM150000,P2.
2 TASK(NAME,ACCT. NO.,MRI)
3 REQUEST,SLED.(a,RINGIN,MRI b,N)
    a = Tape number allocated
    b = MRI code number
    N = Name of tape requestor
4 RFL,70000.
5 FTN(ØPT=1,R=2)
6 RFL,150000.
7 MAP(PART)
8 LOAD(LGØ)
9 NØGØ.
10 (7/8/9) (SCOPE end of record)
    { OVERLAY(SLED,0,0) }
    { ((Above card begins in col. (7))) }
    { SLEDYNE Source Deck }
11 (6/7/8/9) (SCOPE end of file)
```

I.3.4 CONTROL DATA SCOPE CONTROL CARDS (CONT'D)

B. Execute SLEDYNE Using TAPE<sup>4</sup> Created by a STAR HQR Run

(B1) CDC DATA CENTERS

Card

```

1 $CHARGE, _____.
2 SLED(CM14000,CL150000,TP2,P6,T500)
3 REQUEST,SLED,HI. (xxxx,NØRING)
*4 REQUEST,TAPE4,HI. (xxxx,NØRING)
5 RFL,150000.
6 SLED.
**7 REWIND(TAPE8)
**8 CØPYSBF(TAPE8,ØUTPUT)
9 (7/8/9) (SCOPE end of record)
    { SLEDYNE Input Data }
    { (Section A.2) }
10 (6/7/8/9) (SCOPE end of file)

```

(B2) KIRTLAND A.F.B. 6600

Card

```

1 SLED,T500,CM150000,P2.
2 TASK(NAME,ACCT. NO.,MRI)
3 REQUEST,SLED.(__,RINGØUT,MRI__,N)
*4 REQUEST,TAPE4.(__,RINGØUT,MRI__,N)
5 RFL,150000.
6 SLED.
**7 REWIND(TAPE8)
**8 CØPYSBF(TAPE8,ØUTPUT)
**9 (7/8/9) (SCOPE end of record)
    { SLEDYNE Input Data }
    { (Section A.2) }
10 (6/7/8/9) (SCOPE end of file)

```

\*Card number <sup>4</sup> is optional, i.e., it is only required when inertial forces are to be calculated.

\*\*Cards 7 and 8 are needed only when printer plots of slipper forces are requested.

C. Execute SLEDYNE Using Geometry and Modes Input on Cards

(C1) CDC DATA CENTERS

Card

```

1 $CHARGE, _____.
2 SLED(CM14000,CL150000,TP2,P6,T500)
3 REQUEST,SLED,HI. (xxxx,NØRING)
4 CØPYCR(INPUT,TAPE4,2)
5 REWIND(TAPE4)
6 RFL,150000.
7 SLED.
8 REWIND(TAPE8)
9 CØPYSBF(TAPE8,ØUTPUT)
10 (7/8/9) (SCOPE end of record)
    { GEOMETRY (A.3.1) }
    { End with 7/8/9 card }
    { MODES (A.3.2) }
    { End with 7/8/9 card }
    { SLEDYNE Input Data }
    { (Section A.2) }
11 (6/7/8/9) (SCOPE end of file)

```

(C2) KIRTLAND A.F.B. 6600

Card

```

1 SLED,T500,CM150000,P2.
2 TASK(NAME,ACCT. NO.,MRI)
3 REQUEST,SLED.(__,RINGØUT,MRI__,N)
4 CØPYCR(INPUT,TAPE4,2)
5 REWIND(TAPE4)
6 RFL,150000.
7 SLED.
8 REWIND(TAPE8)
9 CØPYSBF(TAPE8,ØUTPUT)
10 (7/8/9) (SCOPE end of record)
    { GEOMETRY (A.3.1) }
    { End with 7/8/9 card }
    { MODES (A.3.2) }
    { End with 7/8/9 card }
    { SLEDYNE Input Data }
    { (Section A.2) }
11 (6/7/8/9) (SCOPE end of file)

```

## APPENDIX II

### DEVELOPMENT OF SIMULATION EQUATIONS

The motion of the sled in the vertical direction is defined as the sum of a set of displacement functions. The first two of these are a pure vertical translation ( $z$ ) and a rotation of the rigid sled about its cg ( $\theta$ ). The rest of the set is comprised of the normal modes of vibration (orthogonal to each other but not to the rigid body functions) of the sled restrained against translation at the slipper support points. So the vertical displacement,  $w$ , of the sled, at time  $t$  and station  $x$  along its longitudinal axis is:

$$w(x, t) = z + (x - x_{cg}) \theta + \sum_i \varphi_i(x) q_i(t) \quad (1)$$

The  $\varphi_i(x)$  are the normal modes of the sled pinned at the slipper supports and  $q_i(t)$  are their instantaneous amplitudes.

We will, for the moment, ignore the stiffness of the slippers (and the associated nonlinear gap effect) while we derive the equations of motion. We start with Lagrange's equation:

$$\frac{d}{dt} \left( \frac{\partial T}{\partial \dot{\eta}_i} \right) + \frac{\partial U}{\partial \eta_i} - \frac{\partial W}{\partial \eta_i} = 0 \quad (2)$$

where  $T$ ,  $U$  and  $W$  are the kinetic energy, the strain energy and the work. The  $\eta_i$  are the independent variables of motion which in this case include  $z$ ,  $\theta$ , and the  $q_i$ .

At this point we must more fully define the structure. In fact, since the structure of the sled will be idealized as a finite-element model, we convert our symbology to that of lumped parameter systems.

In matrix notation, Equation (1) becomes:

$$\{w\} = \{1.0\} z + \left\{ \begin{matrix} \vdots \\ x_j \\ \vdots \end{matrix} \right\} - x_{cg} \theta + \sum_i \{\varphi_i\} q_i \quad (3)$$

The kinetic energy is:

$$T = \frac{1}{2} \langle \dot{w} \rangle [m] \{ \dot{w} \} \quad (4)$$

We substitute Equation (3) into (4)

$$T = \frac{1}{2} \langle \dot{\eta} \rangle [M] \{ \dot{\eta} \} \quad (5)$$

Where we have defined

$$\eta = \begin{Bmatrix} z \\ \theta \\ q_1 \\ \vdots \\ q_i \end{Bmatrix}$$

We will make some observations about the elements of  $[M]$

$$M_{11} = m, \text{ the mass of the sled}$$

$$M_{22} = I, \text{ the pitch inertia of the sled}$$

$$M_{12} = M_{21} = 0$$

because we took the rotation about the sled cg.

$$M_{1i} = M_{i1} = \langle 1.0 \rangle [m] \{\varphi^n\} \quad i > 2$$

$$= \sum_j m_j \varphi_j^n \quad n = i - 2$$

Where  $m_j$  is the lumped mass at the  $j$ th node and  $\varphi_j^n$  is the vertical deflection at that node in the  $n$ th mode.

$$M_{2i} = M_{i2} = \langle \cdots x_j - x_{cg} \cdots \rangle [m] \{\varphi^n\} \quad i > 2$$

$$= \sum_j (x_j - x_{cg}) m_j \varphi_j^n \quad n = i - 2$$

$$M_{ii} = \sum_j m_j (\varphi_j^n)^2 \quad i > 2, n = i - 2$$

is the generalized mass of the  $n$ th mode.

$$M_{ij} = 0 \quad i \neq j; i, j > 2$$

because of the orthogonality of the modes.

The strain energy

$$U = \frac{1}{2} \langle w \rangle [k] \{w\} \quad (6)$$

where  $[k]$  is the sled's stiffness matrix. Substituting Equation (3)

$$U = \frac{1}{2} \langle \eta \rangle [k] \{ \eta \}$$

Due to the absence of strain energy in the rigid body functions and the orthogonality of the modes:

$$K_{11} = K_{22} = 0$$

$$K_{ij} = K_{ji} = 0 \quad i \neq j$$

$$K_{ii} = \langle \varphi^n \rangle [k] \{ \varphi^n \} \quad i > 2, n = i - 2$$

$$= M_{ii} \omega_n^2$$

where  $\omega_n$  is the natural frequency of the nth mode.

In order to define the work, we must now do business with the slipper springs. The work is a product of the force in those springs and the displacement of the attached structure. However, the attached structure was pinned in all the modes so the springs do work only on the rigid displacements,  $z$  and  $\theta$ . The forward slipper force is:

$$F_F = -k_F \delta \left( Z + l_F \theta, \frac{\epsilon}{2} + y_r (X + l) \right) - D_F$$

$$\text{where } \delta(u, v) = u - v, u > v$$

$$= 0, |u| < v$$

$$= u + v, u < -v$$

$\epsilon$  is the slipper gap and  $y_r$  is the local rail height. The aft slipper force is

$$F_A = -k_A \delta \left( Z - l_A \theta, \frac{\epsilon}{2} + y_r (X) \right) - D_A$$

$k_F$  and  $k_A$  are the slipper support stiffnesses and  $l_F$  and  $l_A$  are distances from the sled cg to the slipper supports.

$D_F$  and  $D_A$  are the damping forces and act only when the slippers are in contact.

$$D_F = C_F (\dot{Z} + l_F \dot{\theta} - v y_r' (X + l))$$

$$D_A = C_A (\dot{Z} - l_A \dot{\theta} - v y_r' (X))$$

$v$  is the sled downtrack velocity, and  $y_r'(X)$  is the local slope of the rail head. The damping coefficients are calculated as described at the end of this appendix.

The equations may now be written out by making the appropriate substitutions into Equation (2).

$$\begin{bmatrix} m & 0 & M_{13} & M_{14} & \cdots \\ & I & M_{23} & M_{24} & \cdots \\ & & M_{33} & 0 & \cdots \\ & & & M_{44} & \cdots \\ \text{Symmetric} & & & & \end{bmatrix} \begin{Bmatrix} z \\ \theta \\ q_1 \\ q_2 \\ \vdots \end{Bmatrix} + \begin{bmatrix} 0 & 0 & 0 & 0 & \cdots \\ & 0 & 0 & 0 & \cdots \\ & & 2\zeta_1 M_{33} \omega_1 & 0 & \cdots \\ & & & 2\zeta_2 M_{44} \omega_2 & \cdots \\ \text{Symmetric} & & & & \end{bmatrix} \begin{Bmatrix} z \\ \theta \\ q_1 \\ q_2 \\ \vdots \end{Bmatrix} \\
 + \begin{bmatrix} 0 & 0 & 0 & 0 & \cdots \\ & 0 & 0 & 0 & \cdots \\ & & M_{33} \omega_1^2 & 0 & \cdots \\ & & & M_{44} \omega_2^2 & \cdots \\ \text{Symmetric} & & & & \end{bmatrix} \begin{Bmatrix} z \\ \theta \\ q_1 \\ q_2 \\ \vdots \end{Bmatrix} \\
 = \begin{Bmatrix} F_F + F_A + F_S \\ F_F l_F - F_A l_A + M_S \\ 0 \\ 0 \\ \vdots \end{Bmatrix}$$

A few terms have been added which were not yet discussed. Modal damping is included where  $\zeta_n$  is the proportion of critical damping.

$F_S$  and  $M_S$  are the quasi-steady forces and moments such as lift, drag and thrust. The perceptive analyst might take exception to their being excluded from the modal equations since they do act over the whole sled body and, hence, do work on the modes. The response is:

- The modal deflections are small compared to those of the rigid body and so the work done on them by the quasi-steady loads will be as well.



- The quasi-steady loads are very low frequency (generally zero) and so are matched to the rigid body motion which is either low or zero frequency depending on whether or not the slippers are in contact.
- The output of the program is inertial load vectors.

$$\{F_I\} + -[m] \left( \{1.0\} \ddot{Z} + \begin{Bmatrix} x_j \\ \vdots \\ x_{CG} \end{Bmatrix} \ddot{\theta} + \{\varphi^n\} \ddot{q}_n \right)$$

which are unaffected by the quasi-steady forces except indirectly.

#### Damping Coefficients

Damping for the two rigid body degrees-of-freedom is not easily expressed. The critical damping ratio cannot be used because pitch and bounce are coupled and because of the nonlinear gap effect. A fairly simple approach was adopted. Since subsequent SLEDYNE results proved to be relatively insensitive to variation in damping and since they correlated with track data, the method was assumed to be adequate.

The derivation proceeds as follows. The objective is to compute damping coefficients associated with flexing of the stepper beam springs. The damping coefficient at each slipper for bounce is

$$C_b = \frac{C_Z}{4} = \frac{1}{4} (2 \zeta_Z \omega_b M)$$

$$= \frac{1}{4} (2 \zeta_Z \sqrt{(K_A + K_F) M})$$

The damping coefficient at each slipper for pitch is

$$C_p = \frac{C_\theta}{2(l_F^2 + l_A^2)} = \frac{1}{2(l_F^2 + l_A^2)} (2 \zeta_\theta \sqrt{1(k_A l_A^2 + k_F l_F^2)})$$

Now it is assumed that damping is not equal at each slipper but is proportional to the beam stiffness so, for a forward slipper

$$C_F = (C_p + C_b) \frac{2k_F}{k_A + k_F}$$

and for an aft slipper

$$C_A = (C_p + C_b) \frac{2k_A}{k_A + k_F}$$

Best correlation with track data was found for

$$\zeta_z = \zeta_\theta = .03$$

### APPENDIX III

#### BASIS OF SLED IMPACT PARAMETER

The Sled Impact Parameter (SIMP) has its origin in the idealization of a sled as a rigid body with simple springs representing the slipper beams. Without any strong basis, a postulation was made that peak slipper beam forces relate to the maximum spring force in the model shown in Figure 1 of this appendix. The test data established that there is indeed a reasonably strong correlation.

The equations of motion of the two-degree-of-freedom model of Figure 1, with the spring in contact, are:

$$m \ddot{Z} + k Z + l k \theta = 0$$

$$I \ddot{\theta} + k l^2 \theta + l k Z = 0$$

The initial conditions are:

$$\dot{Z}(0) = -v$$

$$Z(0) = \theta(0) = \dot{\theta}(0) = 0$$

A variety of methods will yield a solution to this initial value problem. The two natural frequencies are:

$$\omega^2 = 0, \quad \frac{k \left(1 + \frac{M l^2}{I}\right)}{M}$$

The associated mode shapes, in terms of  $Z$  and  $\theta$ , are

$$\begin{pmatrix} 1.0 \\ -\frac{1}{l} \end{pmatrix} \quad \text{and} \quad \begin{pmatrix} 1.0 \\ \frac{M l}{I} \end{pmatrix}$$

The first is simply a rotation of the rigid body with no deflection of the spring, hence, the zero frequency. The second mode involves bouncing of the rigid body on the spring.

The solution to the stated problem, expressed in terms of the spring force, is:

$$F_{sp} = -v \sqrt{\frac{k M}{1 + \frac{M l^2}{I}}} \sin \omega t$$

where

$$\omega = \sqrt{\frac{k \left(1 + \frac{M l^2}{I}\right)}{M}}$$

The maximum force is:

$$v \sqrt{\frac{k M}{1 + \frac{M l^2}{I}}}$$

With relation of

$$\text{SIMP} = \sqrt{\frac{k M}{1 + \frac{M l^2}{I}}}$$

$v$  becomes a design parameter, i.e., the effective impact velocity which was determined by plotting maximum slipper beam force against SIMP. (See Figure 6.5.)

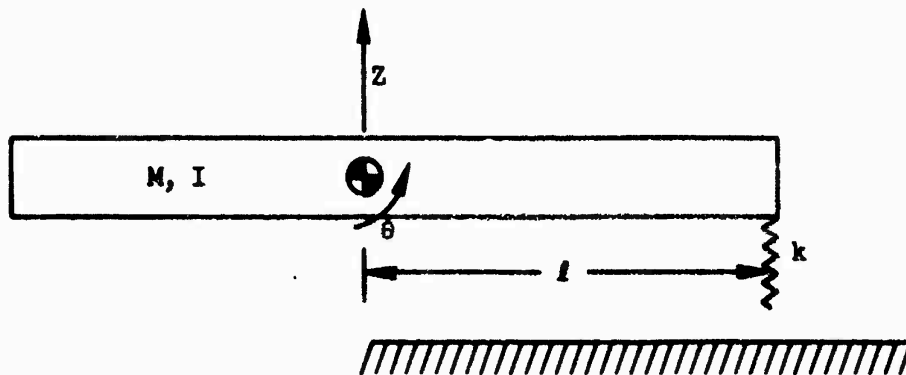


Figure 1. Model for SIMP Analysis

#### APPENDIX IV

##### SIMPLIFIED PITCH-BOUNCE RESPONSE SPECTRA MODEL FOR DUAL RAIL SLEDS

As mentioned in Section 3.1, observations of dual rail sled test data and analytical SLEDYNE results showed that their dynamic response behavior was not affected by the slipper-rail gap. This provided incentive for exploring response spectra techniques, based on the following considerations:

- The sled-rail system could be adequately analyzed using a linear model, with base excitations completely described by the rail profile and the sled forward velocity.
- Response spectra (maximum response of a single-degree-of-freedom model) could then be generated using simulated flights with a simple single-degree-of-freedom model.
- Use of these spectra to predict sled dynamic response (maximum response of each normal mode) would minimize the analysis required since the major analysis task would reduce to a modal analysis, i.e., determination of natural modes and frequencies.

Since rail roughness produces translational (bounce) and rotational (pitch) excitation of the sled, the initial response spectra approach treated these inputs separately. However, a preliminary evaluation indicated the results would be too conservative due to loss of information on phasing between the translational and rotational responses. The present method reduces this conservatism by properly treating the translational and rotational phasing, although information on phasing between modes is still lost.

The following assumptions are made:

- Motions are limited to a plane.
- Small-displacement linear elastic theory applies.
- The effect of slipper gap can be neglected.
- Response for each mode can be determined in terms of single-degree-of-freedom response spectra.
- Maximum response can be approximated by a root-sum-square combination of modes.

The sled-rail model is shown in Figure 1. Rail roughness induces translational ( $y$ ) and rotational ( $\theta$ ) motion into a rigid base. This motion is completely prescribed as a result of the rail profile and the sled velocity. It will be shown that the maximum response of the  $n$ th normal mode of the sled to the pitch-bounce input can be determined from the maximum

Table I  
COMPARISON OF PROCEDURES A AND B

Load Direction	Sled Velocity (fps)	Effective Impact Frequency, f (Hz)		Impact Velocity, v (ips)		Force Due to Unit Velocity Impact (lb)		Predicted Avg. Peak Force (lb)		Percent Deviation
		Procedure A	Procedure B	Procedure A	Procedure B	Procedure A	Procedure B	Procedure A	Procedure B	
Vertical	2000	308	312	40.5	41	285	339	11,540	13,900	-17
Vertical	4000	308	312	60	61	285	339	17,100	20,680	-17

relative displacement response  $|x_n|_{\max}$  of a single-degree-of-freedom model, subjected to an appropriate translational base input motion,  $y_n$  (Figure 1b).

### Equations of Motion

The equations of motion for the finite-element sled model, shown in Figure 2, may be written

$$[m] \{\ddot{x}\} + [k] \{x\} = -[m][T] \{\ddot{y}\} = -[m][T] \left\{ \begin{matrix} \ddot{y} \\ \ddot{y} \end{matrix} \right\} \quad (1)$$

where

$\{z\}$  = the absolute vertical displacement vector

$\{x\} = \{z\} - [T] \{y\}$  = the relative vertical displacement vector

$[m]$  = the mass matrix

$[k]$  = the stiffness matrix

$$[T] = \begin{bmatrix} 1 & l_1 \\ 1 & l_2 \\ \vdots & \vdots \\ 1 & l_n \end{bmatrix} = \text{a transformation matrix}$$

$\{y\} = \left\{ \begin{matrix} \ddot{y} \\ \ddot{y} \end{matrix} \right\}$  = the input acceleration vector

Expanding  $\{x\}$  in terms of the normal modes  $[\varphi]$  and the modal coordinates  $\{\eta\}$ ,

$$\{x\} = [\varphi] \{\eta\} \quad (2)$$

Substituting this expression into Equation (1), and premultiplying by the transpose of the nth modal vector,  $[\varphi^{(n)}]^T$ , Equation (1) becomes

$$\begin{aligned} \ddot{\eta}_n + 2\zeta_n \omega_n \dot{\eta}_n + \omega_n^2 \eta_n &= \frac{[\varphi^{(n)}]^T [m] [T] \{\ddot{y}\}}{M_n} \\ &= \frac{[\varphi^{(n)}]^T [m]}{M_n} \ddot{y} - \frac{[\varphi^{(n)}]^T [m] [l]}{M_n} \ddot{y} \\ &= -\Gamma_n \ddot{y} - \Theta_n \ddot{y} \\ &= -\Gamma_n \ddot{y}_n \end{aligned} \quad (3)$$

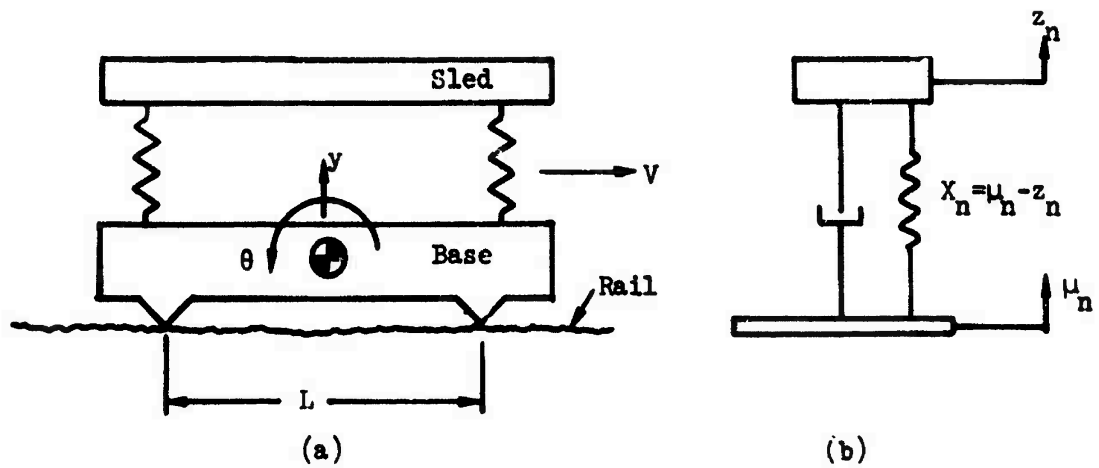


Figure 1. Sled-Rail Model

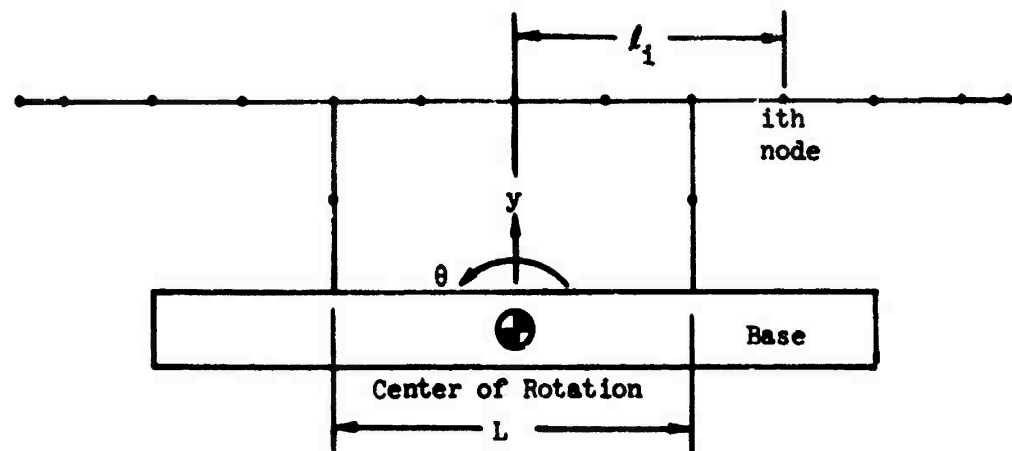


Figure 2. Finite-Element Sled Model



where  $\eta_n$  = the modal coordinate for the nth mode

$$M_n = \{\varphi^{(n)}\}^T [m] \{\varphi^{(n)}\} = \text{the generalized mass}$$

$$\Gamma_n = \frac{\{\varphi^{(n)}\}^T [m]}{M_n} = \text{the nth modal participation factor for translation (bounce)}$$

$$\Theta_n = \frac{\{\varphi^{(n)}\}^T [m] \{l\}}{M_n} = \text{the nth modal participation factor for rotation (pitch)}$$

$$\ddot{u}_n = \ddot{y} + \frac{\Theta_n}{\Gamma_n} \ddot{\theta} = \text{an equivalent base translational acceleration for the nth mode.} \quad (4)$$

Now examine the equation of motion of the single-degree-of-freedom model of Figure 3.22,

$$\ddot{x}_n + 2\zeta_n \omega_n \dot{x}_n + \omega_n^2 x_n = -\ddot{u}_n \quad (5)$$

and compare it with Equation (3). The equations are identical except for the multiplier  $\Gamma_n$  on the right of Equation (3). Thus, because of linearity, the maximum response of the nth mode is equal to  $\Gamma_n$  times the maximum response  $|x_n|_{\max}$  of the single-degree-of-freedom model, subjected to the base input  $\ddot{u}_n$  of Equation (4), i.e.,

$$|\eta_n|_{\max} = |\Gamma_n| |x_n|_{\max} \quad (6)$$

Also, the maximum contribution  $|F_n|_{\max}$  to a particular sled load  $F$ , from the nth mode is

$$|F_n|_{\max} = |F_n| |\eta_n|_{\max} = |F_n| |\Gamma_n| |x_n|_{\max} \quad (7)$$

where  $F_n$  is the corresponding modal force. The total maximum load can be estimated from a root-sum-square combination of modal contributions, i.e.,

$$|F|_{\max} = (\sum_n F_n^2)^{1/2} \quad (8)$$

### Response Spectra

A set of response spectra can be generated using the model of Figure 2b with Equation (4), and the simulated Holloman track rail (see Section 3.1.2), as a function of sled velocity, frequency, damping, slipper spacing  $L$ , and the ratio  $\Theta_n/\Gamma_n$ .

The translational and rotational inputs  $y$  and  $\theta$  are related to the rail profile by (see Figure 3)

$$y = y_1 + \frac{a}{L} (y_2 - y_1) \quad (9)$$

$$\theta = (y_2 - y_1)/L \quad (10)$$

where  $a/L$  locates the center of rotation of the base. The solution is independent of the location of the center of rotation of the base. This can be demonstrated as follows:

Expand the right side of Equation (3) in terms of  $\Gamma_n$  and  $\Theta_n$ , expressed as

$$\Gamma_n = \frac{\{\varphi^{(n)}\}^T [m]}{M_n} = \frac{1}{M_n} \sum \varphi_i^{(n)} m_i \quad (11)$$

$$\Theta_n = \frac{\{\varphi^{(n)}\}^T [m] \{l\}}{M_n} = \frac{1}{M_n} \sum \varphi_i^{(n)} m_i (l_i - a) \quad (12)$$

with  $\ddot{y}$  and  $\ddot{\theta}$  from Equations (9) and (10). The result is

$$\begin{aligned} \Gamma_n \ddot{y} + \Theta_n \ddot{\theta} &= \frac{1}{M_n} (\sum \varphi_i^{(n)} m_i) \left[ \ddot{y}_1 + \frac{a}{L} (\ddot{y}_2 - \ddot{y}_1) \right] \\ &\quad + \frac{1}{M_n} \left[ \sum \varphi_i^{(n)} m_i (x_i - a) \right] \left[ (\ddot{y}_2 - \ddot{y}_1)/L \right] \\ &= \frac{1}{M_n} \left[ (\sum \varphi_i^{(n)} m_i) \ddot{y}_1 + (\sum \varphi_i^{(n)} m_i) \frac{a}{L} (\ddot{y}_2 - \ddot{y}_1) + (\sum \varphi_i^{(n)} m_i x_i) (\ddot{y}_2 - \ddot{y}_1)/L \right. \\ &\quad \left. - (\sum \varphi_i^{(n)} m_i) \frac{a}{L} (\ddot{y}_2 - \ddot{y}_1) \right] \\ &= \frac{1}{M_n} \left[ (\sum \varphi_i^{(n)} m_i) \ddot{y}_1 + (\sum \varphi_i^{(n)} m_i x_i) (\ddot{y}_2 - \ddot{y}_1)/L \right] \quad (13) \end{aligned}$$

which is, indeed, independent of  $a/L$ .

To calculate the response spectra, it is convenient to rewrite Equation (4) as

$$\ddot{u}_n = \ddot{y} + \left( \frac{2 \Theta_n}{\Gamma_n L} \right) \left( \frac{L}{2} \ddot{\theta} \right) = \ddot{y} + \alpha_n \left( \frac{L}{2} \ddot{\theta} \right) \quad (14)$$

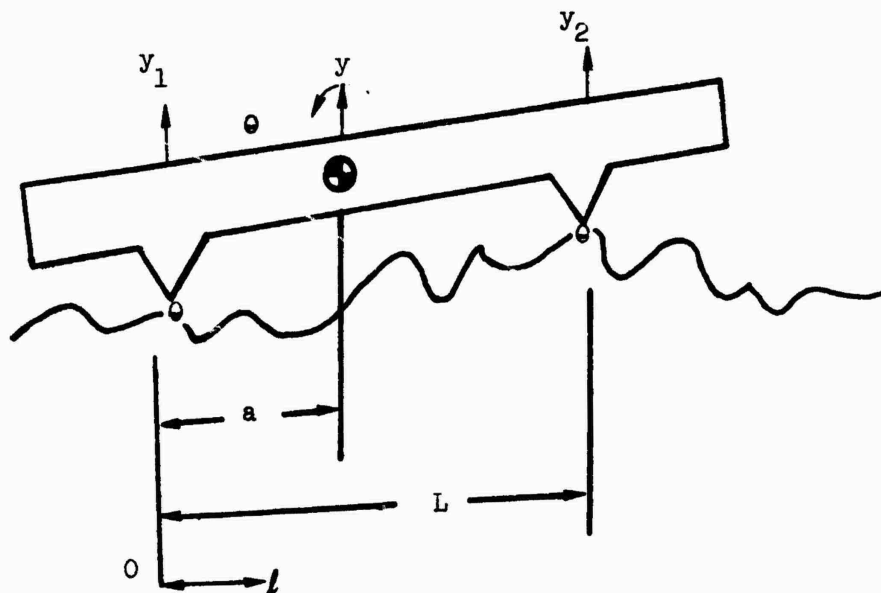


Figure 3. Model for Computing Base Inputs

$$\alpha_n \equiv \frac{2 \oplus_n}{\Gamma_n L} \quad (15)$$

The quantity  $\alpha_n$  is an input parameter to the response spectra which includes the ratio of the participation factors and the slipper spacing. The rotational input  $(L/2) \ddot{y}$  now has the same dimensions and approximate magnitude as  $\ddot{y}$ . Taking the base center of rotation as the midpoint between slippers, Equation (14) may be written,

$$\ddot{u}_n = \frac{1}{2}(\ddot{y}_1 + \ddot{y}_2) + \frac{\alpha_n}{2} (\ddot{y}_2 - \ddot{y}_1) \quad (16)$$

The response spectra can now be generated as a function of sled velocity, frequency, damping,  $\alpha_n$ , and L.

#### Application to the Single Mod Sled

The foregoing procedure was applied to the single mod sled. Forward and aft slipper forces were computed for a sled velocity of 1760 fps. Five modes were used in the analysis. Damping was taken as three percent critical. The pertinent parameters used in the calculations are summarized in Table II. Results are compared with predictions using the SLEDYNE program, as follows:

	Response Spectra	SLEDYNE Program	Deviation
Forward Slipper Force (lb)	10,618	6,884	54%
Aft Slipper Force (lb)	11,138	10,427	7%

The response spectra approach appears to give conservative results, which is generally the case for response spectra solutions. However, the response spectra used in the calculations were determined from one 1,232-foot flight simulation. It was subsequently observed that such predictions using the simulated random rail display considerable variation, which result from different rail simulations. Thus, additional runs should be made in order to provide a valid assessment of the accuracy of the response spectra approach.

#### Conclusion

The simplified pitch-bounce response spectra model for dual rail sleds appears to be one possible method for predicting dual rail sled behavior. However, work on this method was discontinued in favor of doing more work on the SLEDYNE program to make it easier to use for design analysis purposes.

Table II  
SINGLE MOD RESPONSE SPECTRA CALCULATION SUMMARY

	Mode Number					RSS
	1	2	3	4	5	
Frequency $f_n$ (Hz)	20.2	27.6	56.2	125	193	---
Generalized Weight $W_n$ (lb)	6901	1813	1525	1029	1035	---
$W_n \Gamma_n$ (lb)	7901	-246.1	533.4	-100.9	-39.21	---
$W_n \otimes_n$ ( $10^5$ lb-in)	-2.152	-3.676	0.4257	0.0097	0.0836	---
$F_n^{Fwd}$ ( $10^4$ lb/in)	6.37	-6.43	7.16	-3.71	2.89	---
$F_n^{Aft}$ ( $10^4$ lb/in)	10.1	5.48	1.44	-4.36	-10.4	---
$\alpha_n$	-0.227	12.45	0.665	-0.0798	-1.78	---
$\Gamma_n$	1.145	-0.136	0.350	-0.0981	-0.0379	---
Single DOF Max. Response $ x _{max}$ (in)	0.06754	1.064	0.05746	0.02972	0.1133	---
$ \eta_n _{max}$ (in)	0.07733	0.1446	0.0201	0.00292	0.00429	---
$ F_n^{Fwd} _{max}$ (lb)	4924	9295	1438	108	124	10,618
$ F_n^{Aft} _{max}$ (lb)	7810	7921	289	127	446	11,138